

**Heat and Mass Transfer in Regenerative  
Enthalpy Exchangers**

by

**Harald Klein**

**A thesis submitted in partial fulfillment of the  
requirements for the degree**

**Master of Science  
(Chemical Engineering)**

at the

**UNIVERSITY OF WISCONSIN-MADISON**

**1988**

---

## Abstract

---

This thesis presents the analysis of regenerative solid desiccant air-to-air enthalpy exchangers. The fundamental conservation and transfer rate equations form a set of coupled partial differential equations. Numerical solutions of the complete set of equations are available but require considerable computational effort. A method based on the  $\epsilon$ -NTU correlations for a counterflow direct type heat exchanger is presented to compute the outlet of a regenerative enthalpy exchanger within reduced CPU time limits.

The operating range where this method applies is investigated as well as the effect of the system parameters on the performance of an enthalpy exchanger. It is shown that unfavorable adsorbent characteristics can be eliminated by operating the device at higher rotational speeds.

Air-to-air enthalpy exchangers transfer water vapor in adsorbed phase and are therefore less susceptible to freezing than sensible heat exchangers. At very cold winter conditions, however, ice builds up at the matrix and the flow channels for the air streams are blocked after a defined number of rotations, depending on the adsorptive capacity of the hygroscopic matrix.

---

## Acknowledgments

---

After completing this thesis and writing about all the sophisticated scientific and engineering problems, it is a pleasure to write about people; people who contributed to this work, people who made my stay here at the University of Wisconsin-Madison an unforgettable experience in my life.

I am deeply indebted to Professor Zeitz whose personal effort opens the possibility every year to engineering students of the University of Stuttgart to study two or more semesters at the Chemical Engineering Department of the University of Wisconsin-Madison. Thanks to all German tax payers and the German Academic Exchange Service (DAAD) for the financial support during the first period of this project. The support was continued by the Department of Energy (DOS).

My stars were lucky when Jack Duffie took me out of his solar class and offered me this project. Thank you, Jack, for showing interest in both my research and my personal life. Thanks to Sandy Klein who was the main advisor and a constant source of new ideas. Sandy, I think it is not only the last name that we share but also a never ending curiosity in thermodynamics and transport phenomena. Thanks also for canceling some of the weekly advisor meetings in times when I considered myself as being too busy to do any research. John Mitchell contributed to this work after returning from good 'old' Europe. Thank you, John, for asking critical questions and leading me to the right answers. Thanks also to Bill Beckman, the new director of the

Lab and known for tough questions during the weekly seminars. The already legendary pre-Christmas dinners at the Beckman's made me feel almost like being at home. I would like to thank Erik van den Bulck for introducing me into the strange (at least at the beginning!) world of combined heat and mass transfer potentials.

Without my fellow graduate students of the Solar Lab it would have been impossible for me to go through all the 'hoops' of research and class work. Thanks to Diane, Blake, Doug, Frank, Manni, Mark and Tim, you made even the well known 'all-nighters' enjoyable. Thanks to all of you for many fruitful discussions about serious problems in our research topics as well as the life outside the Lab.

I would like to thank all my housemates I had throughout my stay here in Madison. Living with you at the 'Brooks Street Zoo' was the best way for me to see 'how Americans live like'. Thanks to all of you for being patient with the 'Kraut', especially during the time I was writing this thesis and too busy to do the dishes after a fast 'Macaroni Cheese' dinner.

It was a great experience living in a foreign country and meeting people from all over the world. Especially, I would like to thank Willi for the 'Introduction to Madison' and Albrecht for providing me with the most recent German soccer scores (usually right after the American football Sunday!). Thanks to Rogerio and all the friends in Brazil for the hospitality during the time Manni and I were travelling through your gorgeous country.

Thanks to all my pals back home in Germany. It helped a lot having there a letter after coming home late at night. I have to apologize for not answering all of them, partially because I was too busy, partially because I was too lazy.

I am deeply indebted to my parents and my sister Bettina. Without their support

the entire stay here in the United States would not have been possible. It was always a good feeling to know that things back home are going well.

Mama, Papa und Bettina, vielen Dank Euch Allen für die Unterstützung während des gesamten Aufenthaltes hier in den Staaten. Ich liebe Euch.

Last, but probably most important I would like to thank the most important person in my life. Without the mental support of my girlfriend Ute I would never have had the energy to go through all the hassle of the life as a graduate student. Ute, I thank you for being so patient with me. Your letters and the phone calls gave me confidence in the things I was doing here and your two visits here in Wisconsin gave me the energy to complete this work. Thanks a lot for waiting for me back home. *I love you.*

---

## Table of Contents

---

Abstract	ii
Acknowledgments	iii
List of Figures	ix
List of Tables	xiv
Nomenclature	xv
<b>Chapter 1 Introduction</b>	<b>1</b>
1.1 The Nature of Regenerative Heat and Mass Exchangers	2
1.2 Applications of Rotary Regenerators in Air Conditioning Systems	4
1.2.1 The Ventilation Desiccant Cooling Cycle	5
1.2.2 Ventilation Systems with Energy Recovery	7
1.3 Thesis Objectives	13
<b>Chapter 2 Theory of Rotary Regenerators</b>	<b>15</b>
2.1 Coordinate System, Assumptions and Nomenclature of Rotary Regenerators	15
2.2 Model of the Rotary Sensible Heat Exchanger	19
2.2.1 Fundamental Equations	19
2.2.2 Solution of the Model Equations	22

2.3	Model of Regenerative Heat and Mass Exchangers	27
<b>Chapter 3</b>	<b>Thermodynamic Relationships</b>	<b>32</b>
3.1	Properties of Humid Air	32
3.2	Matrix Properties	34
3.2.1	Jurinak's Generic Isotherm Model	35
3.2.2	Dubinin-Polanyi Theory for Silica Gel	39
3.2.3	Enthalpy of the Matrix	41
<b>Chapter 4</b>	<b>Solutions of the Model Equations</b>	<b>45</b>
4.1	Numerical Solution of the Model Equations	46
4.1.1	Finite Difference Equations	46
4.1.2	Solution Procedure and Convergence	50
4.1.3	Determination of the Step Size	53
4.2	Equilibrium Model and Wave Analysis	54
4.2.1	Combined Transfer Potentials for Equilibrium Systems	54
4.2.2	$F_1$ - $F_2$ Charts and Wave Diagrams	63
4.3	Analogy Method	69
4.4	Method Based on Uncoupled Transfer Rate Equations	74
4.4.1	The Case of Infinite Rotation Speed	74
4.4.2	Wave Diagram and Infinite Rotation Speed	80
<b>Chapter 5</b>	<b>Model Comparison and Parametric Studies</b>	<b>82</b>
5.1	Model Parameters and Inlet Conditions	82

5.2	Effect of Rotation Speed and Number of Transfer Units	84
5.3	Effect of Matrix Parameters	98
5.3.1	Specific Heat Capacity	98
5.3.2	Adsorption Isotherm Correlation	104
5.4	Effect of Non-Unity Lewis Number	113
<b>Chapter 6</b>	<b>Condensation and Freezing in Rotary Regenerators</b>	<b>118</b>
6.1	Mass Transfer in Non-Hygroscopic Energy Recovery Regenerators	118
6.1.1	Van Leersum's Model of Combined Heat and Mass Transfer	120
6.2	Freezing in Hygroscopic Enthalpy Exchangers	124
6.2.1	Modification of the Finite Difference Method for Hygroscopic Matrices	126
6.2.2	Simulations of Transient Behavior	129
<b>Chapter 7</b>	<b>Conclusions and Recommendations</b>	<b>140</b>
7.1	Conclusions	140
7.2	Unresolved Issues	142
Appendix A	Derivation of the Energy Balance	144
Appendix B	Analysis of the Combined Potentials	148
	Bibliography	153

---

## List of Figures

---

Figure 1.1	Schematic and Psychrometric Chart of the Ventilation Solid Desiccant Cooling Cycle	6
Figure 1.2	Conventional Space Conditioning System	7
Figure 1.3	Air Cooling without Energy Recovery	8
Figure 1.4	Air Heating without Energy Recovery	9
Figure 1.5	Space Conditioning System with Regenerative Energy Recovery Unit	10
Figure 1.6	Air Cooling Using a Sensible Heat Exchanger	10
Figure 1.7	Air Cooling Using an Enthalpy Exchanger	11
Figure 1.8	Air Heating Using a Sensible Heat Exchanger	12
Figure 1.9	Air Heating Using an Enthalpy Exchanger	13
Figure 2.1	Coordinate System and Nomenclature of a Rotary Regenerator	16
Figure 2.2	Effect of $C_r^*$ on the Rotary Sensible Heat Exchanger Effectiveness	26

Figure 3.1	Adsorption Isotherm for a Molecular Sieve	38
Figure 3.2	Adsorption Isotherm for Brunauer Type 3 Adsorbents	39
Figure 3.3	Adsorption Isotherm for Silica Gel	40
Figure 4.1	MOSHMX Finite Difference Grid	48
Figure 4.2	Dehumidifier Inlet States with Lines of Constant F-potential	64
Figure 4.3	Wave Diagram for Period 1 of a Regenerative Dehumidifier	65
Figure 4.4	Wave Diagram with Breakthrough of the Second Wave	67
Figure 4.5	Wave Diagram for Period 1 of an Enthalpy Exchanger	68
Figure 4.6	Wave Diagram for Period 1 of an Enthalpy Exchanger with Infinite Rotation Speed	81
Figure 5.1	Outlet States of Stream 1 as Computed by MOSHMX for High NTU	85
Figure 5.2	Outlet States of Stream 1 as Computed by MOSHMX for Medium NTU	87
Figure 5.3	Outlet States of Stream 1 as Computed by MOSHMX for Low NTU	87
Figure 5.4	Enthalpy Effectiveness as Computed by MOSHMX as a Function of $\bar{\gamma}_1 \Gamma$ and the Number of Transfer Units	88
Figure 5.5	Wave Diagram with Broadened Wave Fronts	90

Figure 5.6	Absolute Errors in Outlet States Computed with Counterflow Heat Exchanger Correlations Compared to MOSHMX	92
Figure 5.7	Outlet States of an Enthalpy Exchanger Computed Using Counterflow Heat Exchanger Correlations	93
Figure 5.8	Enthalpy Effectiveness as a Function of the Number of Transfer Units	94
Figure 5.9	Comparison of MOSHMX and the Linear Analogy Solution	95
Figure 5.10	Dimensionless Wave Speeds as a Function of the Specific Heat Capacity of the Matrix	99
Figure 5.11	Outlet States of Stream 1 as Computed by MOSHMX for Different Specific Heat Capacities of the Matrix	102
Figure 5.12	Enthalpy Effectiveness as Computed by MOSHMX as a Function of $\Gamma$ and the Specific Heat Capacity of the Matrix	103
Figure 5.13	Enthalpy Effectiveness as Computed by MOSHMX as a Function of $\bar{\gamma}_1 \Gamma$ and the Specific Heat Capacity of the Matrix	104
Figure 5.14	Outlet States of Stream 1 as Computed by MOSHMX for Different Isotherm Correlations	106
Figure 5.15	Enthalpy Effectiveness as Computed by MOSHMX as a Function of $\Gamma$ for Silica Gel and a Molecular Sieve	107
Figure 5.16	Enthalpy Effectiveness as Computed by MOSHMX as a Function of $\bar{\gamma}_1 \Gamma$ for Silica Gel and a Molecular Sieve	109
Figure 5.17	Outlet States of Stream 1 as computed by MOSHMX for Different Isotherm Correlations	110
Figure 5.18	Enlargement of Figure 5.17 Showing the Intersection Points	110

Figure 5.19	Enthalpy Effectiveness as Computed by MOSHMX as a Function of $\Gamma$ for Silica Gel and the Type 3 Isotherm	111
Figure 5.20	Enthalpy Effectiveness as Computed by MOSHMX as a Function of $\bar{\gamma}_1 \Gamma$ for Silica Gel and the Type 3 Isotherm	113
Figure 5.21	Outlet States of Streams 1 and 2 as Computed by MOSHMX for Different Lewis Numbers	114
Figure 5.22	Errors in the Outlet States Using the Linear Analogy Method and the Counterflow Heat Exchanger Correlations	117
Figure 6.1	Inlet Conditions with Condensation on a Non-Hygroscopic Matrix	119
Figure 6.2	Inlet Conditions with Freezing on a Non-Hygroscopic Matrix	120
Figure 6.3	Inlet Conditions with Freezing on a Hygroscopic Matrix	125
Figure 6.4	Transient Matrix Profiles of a Regenerative Dehumidifier at the Beginning of the First Period with Convergence to Steady State	130
Figure 6.5	Variation of the Air Outlet Temperature of Stream 1 with the Rotation Angle	131
Figure 6.6	Variation of the Air Outlet Humidity Ratio of Stream 1 with the Rotation Angle	132
Figure 6.7	Transient Matrix Profiles of an Enthalpy Exchanger at the Beginning of the First Period with Convergence to Steady State	133
Figure 6.8	Variation of the Air Outlet Temperature of Stream 1 with the Rotation Angle for an Enthalpy Exchanger	134

Figure 6.9	Variation of the Air Outlet Humidity Ratio of Stream 1 with the Rotation Angle for an Enthalpy Exchanger	135
Figure 6.10	Transient Matrix Temperature Profiles of an Enthalpy Exchanger with One Cold Inlet Stream at the Beginning of the First Period	136
Figure 6.11	Transient Matrix Water Content Profiles of an Enthalpy Exchanger with One Cold Inlet Stream at the Beginning of the First Period	137

---

## List of Tables

---

Table 4.1	Parametric Sensitivity Coefficients at the Outlet of an Enthalpy Exchanger with Infinite Rotation Speed	78
Table 5.1	Comparison of Required CPU Times for the Solution Methods Used in this Study for Medium Number of Transfer Units	96
Table 5.2	Comparison of Required CPU Times for the Solution Methods Used in this Study for High Number of Transfer Units	96
Table 5.3	Dimensionless Wave Speeds and Slope of the Isotherm for Silica Gel and a Molecular Sieve Evaluated at the Average of Inlet Pair 1	108
Table 5.4	Dimensionless Wave Speeds and Slope of the Isotherm for Silica Gel and a Type 3 Isotherm Evaluated at the Average of Inlet Pair 2	112
Table 6.1	Simulation Summary Using Inlet Pair 3 and Different Isotherm Correlations	139

---

## Nomenclature

---



---

### English Letter Symbols

---

Symbol	Definition	SI-Units
a	derivative of a thermodynamic state property function as defined in Equations (4.16)-(4.17)	
$A_j$	heat and mass transfer area at period j	[m <sup>2</sup> ]
A	adsorption potential	[kJ/kmol]
$c_{Lw}$	specific heat capacity of liquid water	[kJ/kg°C]
$c_{pw}$	specific heat capacity of water vapor	[kJ/kg°C]
$c_{pA}$	specific heat capacity of dry air	[kJ/kg°C]
$c_A$	specific heat capacity of humid air	[kJ/kg°C]
$c_m$	specific heat capacity of the matrix	[kJ/kg°C]
$C_{min}$	minimum air capacitance rate	[kJ/°C s]
$C_{max}$	maximum air capacitance rate	[kJ/°C s]
$C^*$	ratio of minimum to maximum air capacitance rate	
$C_r^*$	ratio of matrix to minimum air capacitance rate	
$F_1$	first combined heat and mass transfer potential	
$F_2$	second combined heat and mass transfer potential	

Symbol	Definition	SI-Units
$G$	integrating factor as used in Equation (4.24)	
$h^*$	ratio of specific differential heat of adsorption to specific heat of vaporization	
$h_t$	heat transfer coefficient	[ kW/m <sup>2</sup> °C ]
$h_w$	mass transfer coefficient	[ kg/m <sup>2</sup> s ]
$i_f$	specific enthalpy of humid air	[ kJ/kgDA ]
$I_m$	specific enthalpy of the matrix	[ kJ/kgDM ]
$i_w$	specific enthalpy of water vapor	[ kJ/kgW ]
$i_v$	specific heat of vaporization	[ kJ/kg ]
$i_s$	specific differential heat of adsorption	[ kJ/kg ]
$\bar{i}_s$	specific integral heat of adsorption	[ kJ/kg ]
$I_{ad}$	enthalpy of adsorbed water	[ kJ/kgDM ]
$L$	axial flow length of a rotary regenerator	[ m ]
$Le$	Lewis number	
$\dot{m}_f$	mass flow rate of dry air	[ kgDA/s ]
$M_m$	mass of the dry matrix	[ kgDM ]
$NTU_t$	number of transfer units for sensible heat transfer	
$NTU_w$	number of transfer units for mass transfer	
$NTU_0$	number of transfer units for the counterflow direct type heat exchanger effectiveness correlations	

Symbol	Definition	SI-Units
$NTU_i$	number of transfer units for the $i^{\text{th}}$ combined heat and mass transfer potential	
$N_m$	number of space steps of the finite difference solution	
$N_f$	number of time steps of the finite difference solution	
$P_{\text{tot}}$	total ambient pressure	[kPa]
$p_w$	partial pressure of water vapor	[kPa]
$P_{\text{wsat}}$	water vapor saturation pressure	[kPa]
$R$	gas constant for water vapor	[ kJ/kg °K ]
$R$	universal gas constant	[ kJ/kmol °K ]
$t_f$	temperature of humid air	[°C]
$t_m$	temperature of the matrix	[°C]
$t_{\text{DP}}$	dewpoint temperature of humid air	[°C]
$T$	thermodynamic temperature	[°K]
$T$	time required for one complete regenerator rotation	[s]
$w_f$	humidity ratio of humid air	[ kgW/kgDA ]
$w_m$	humidity ratio of humid air in equilibrium with the matrix	[ kgW/kgDA ]
$w_{\text{sat}}$	humidity ratio of humid air at saturation	[ kgW/kgDA ]
$W_m$	water content of the matrix	[ kgW/kgDM ]
$W_{\text{max}}$	maximum water content of the matrix	[ kgW/kgDM ]
$W^*$	ratio of actual to maximum water content of the matrix	

---

Symbol	Definition	SI-Units
W	parametric sensitivity coefficient	
x	axial flow coordinate	[m]
z	dimensionless axial flow coordinate	

---



---

### Greek Letter Symbols

---

Symbol	Definition	SI-Units
$\alpha_i$	negative reciprocal of a line of constant $F_i$ -potential in a psychrometric chart	
$\beta_j$	period fraction of period j	
$\gamma_i$	combined capacitance ratio of the $i^{\text{th}}$ combined potential	
$\bar{\gamma}_i$	averaged combined capacitance ratio	
$\Gamma$	ratio of "matrix flow rate" to air flow rate	
$\epsilon_t$	heat transfer effectiveness	
$\epsilon_w$	mass transfer effectiveness	
$\epsilon_i$	enthalpy transfer effectiveness	
$\epsilon_{\text{direct}}$	effectiveness of a direct type counterflow heat exchanger	

---

Symbol	Definition	SI-Units
$\epsilon_{ij}$	effectiveness of the $i^{\text{th}}$ combined potential at period $j$	
$\Theta$	time coordinate	[s]
$\Phi$	dimensionless time coordinate	
$\lambda_i$	dimensionless wave speed of the $i^{\text{th}}$ transfer wave	
$\sigma$	ratio of specific heat capacity of the matrix to the specific heat capacity of humid air	
$\tau$	dimensionless time coordinate as defined in Equation (4.18)	
$\phi$	relative humidity of humid air	

---

### Subscripts

---

Symbol	Definition
f	fluid or air state
m	matrix state
j	1 or 2, index for stream or period
3-j	index for "the other" stream or period
in	inlet state

Symbol	Definition
--------	------------

---

out	outlet state
-----	--------------

i	1 or 2, index for the two combined heat and mass transfer potentials
---	--

IP	intermediate state or intersection point
----	--

sat	saturated state
-----	-----------------

---

---

**Miscellaneous**

---

Symbol	Definition
--------	------------

---

W	water
---	-------

DA	dry air
----	---------

DM	dry matrix
----	------------

n	iteration step
---	----------------

$\Delta$	difference
----------	------------

---

---

Chapter 1  
**Introduction**

---

Many unit operations in engineering are based on the transfer of heat and mass from one fluid stream to another. In chemical engineering, unit operations which change compositions of mixtures are significant and are referred to as mass transfer operations. Treybal [1] classifies these operations and cites many examples such as fractional distillation, liquid extraction or gas absorption.

Air conditioning, as used in this study, refers to the conditioning of buildings and spaces in general and involves both heating and cooling. Since thermal comfort is determined by both the temperature and humidity of the air, both heat and mass transfer operations are involved in air conditioning operations. These processes are cooling and dehumidification or heating and humidification of air streams.

In many air conditioning devices referred to as regenerators, coupled heat and mass transfer mechanisms determine the thermodynamic state of the outlet streams. The fluid streams can be considered as binary mixtures of dry air and water vapor. This chapter presents a brief introduction into the terminology of regenerators and their applications in air conditioning systems.

## 1.1 THE NATURE OF REGENERATIVE HEAT AND MASS EXCHANGERS

A heat exchanger can be defined as a device to transfer energy between fluid streams which do not mix. There are several approaches to achieve high heat transfer coefficients and prevent mixing of the heat exchanging streams.

If the two fluid streams can be considered as immiscible (or a slight mass carry-over is permitted) the most efficient way to transfer heat is to bring the two fluids into direct contact. An example of this type of heat exchanger is a cooling tower where water is cooled with an air stream.

In recuperative heat exchangers, a metal plate or pipe separates the hot and cold fluid streams and the transfer mechanisms involve both convective and conductive heat transfer. Since the driving potential for the heat transfer in recuperators is the local temperature gradient between the fluids, Kays and London [2] refer to recuperators as direct type heat exchangers.

Finally, in regenerative heat exchangers, also called periodic flow heat exchangers [2], heat is transferred from the hot fluid during the first period to a solid heat carrier and during the second period from the solid to the cold stream. Neglecting the conductive resistance into the matrix perpendicular to the flow direction, the governing heat transfer mechanism is of convective nature. The metallurgical regenerators as described by Nußelt [3], probably one of the first applications of regenerators, used high temperature resistant bricks as heat storing material. The solid also can consist of a metal matrix.

Two different combinations of regenerator type and flow arrangement are used to accomplish the alternating heating and cooling of the matrix. The valved type alternates

the two streams flow through a fixed bed. Continuous operation is only possible using two regenerators. The rotary type permits continuous operation using only one matrix by rotating the matrix cyclically from one stream to the other. An early example of a rotary device is the Ljungström air preheater [4]. These heat exchangers are very compact in terms of effectiveness and required space and are therefore useful in vehicular gas turbine applications as described by Mondt [5].

Unless the fluid streams separating material consists of a permeable membrane, recuperative heat exchangers usually do not permit any mass transfer between the fluid streams. Regenerative heat exchangers can, however, turn into heat and mass exchangers if phase changes of one or more components of the fluid streams occur within the thermodynamic operating conditions.

There are two possible mass transfer mechanisms that can occur in heat exchange operations: condensation/evaporation and sorption/desorption. Both mechanisms can be described with the same differential equations, but with different thermodynamic relationships. Condensation and evaporation can occur using any kind of matrix. The sorption processes require a matrix carrying sorptive particles such as silica gel or lithium chloride crystals. For this kind of matrix, the components are transferred in an adsorbed rather than a condensed phase and the regenerator therefore shows a different behavior.

In chemical engineering applications, cyclic operations in stationary fixed beds of adsorptive materials are important [6] whereas in air conditioning systems compact rotary devices carrying hygroscopic materials are used in air dehumidification and energy recovery.

There is no unique terminology in textbooks and research papers for the various devices used in air conditioning systems. The term *rotary sensible heat exchanger* is used here for exchangers with non-sorptive matrix and inlet conditions such that no condensation can occur. The term *regenerative heat and mass exchanger* is used throughout this thesis for rotary regenerators with mass transfer in either the condensed or adsorbed phase.

## 1.2 APPLICATIONS OF ROTARY REGENERATORS IN AIR CONDITIONING SYSTEMS

In the United States, space heating and cooling add up to 21% of all energy used nationwide [7]. Much effort has been put into the investigation of alternatives to the traditional vapor compression air conditioning systems. In the vapor compression cycle, a refrigerant cools humid air below its dew point in order to condense water vapor on a cooling coil [8]. For thermal comfort, the air must be reheated which makes the vapor compression system inefficient in a thermodynamic sense although the heating can in some cases be provided inexpensively using condenser waste heat.

A variety of desiccant cooling cycles have been proposed and investigated extensively by Jurinak [9]. The potential use of a low temperature heat source, such as solar energy, originally initialized the interest of the Solar Energy Laboratory of the University of Wisconsin in desiccant cycles. As an example, the ventilation desiccant cooling cycle is discussed in Section 1.2.1 as described by Duffie and Beckman [10].

In order to provide a healthy indoor environment the concentration of pollutants must not exceed a specified level. The easiest way to maintain high air quality is to supply a fresh outdoor stream and discard the same amount of exhaust air. Since

ventilation can impose a significant load on heating and cooling equipment, energy recovery from exhaust streams is often considered to reduce the energy consumption of space conditioning systems [7]. Section 1.2.2 describes the use of regenerators in an energy recovery system in combination with a conventional air conditioning system.

### 1.2.1 The Ventilation Desiccant Cooling Cycle

Figure 1.1 shows the schematic and psychrometric chart of the ventilation solid desiccant cooling cycle with two regenerative components. The rotary sensible heat exchanger consists of a non-hygroscopic matrix whereas the regenerative heat and mass exchanger contains a solid desiccant material.

As can be seen from the psychrometric chart, humid ambient air at state 1 is dehumidified and heated. The temperature rise is due to both the heat of adsorption released as the water vapor is adsorbed by the desiccant and heat transfer from the matrix. The matrix would be saturated after one period of operation if a regenerating stream, which has to be hot at state 8, were not provided to desorb the water from the desiccant.

The desired outlet state of the supply stream leaving the desiccant wheel is a state of low absolute humidity at state 2 which can be achieved by operating the device at about 10 rev/hr [11]. A regenerative heat and mass exchanger operating at this medium rotation speed with the outlet at low humidity is referred to as *regenerative dehumidifier* throughout this thesis.

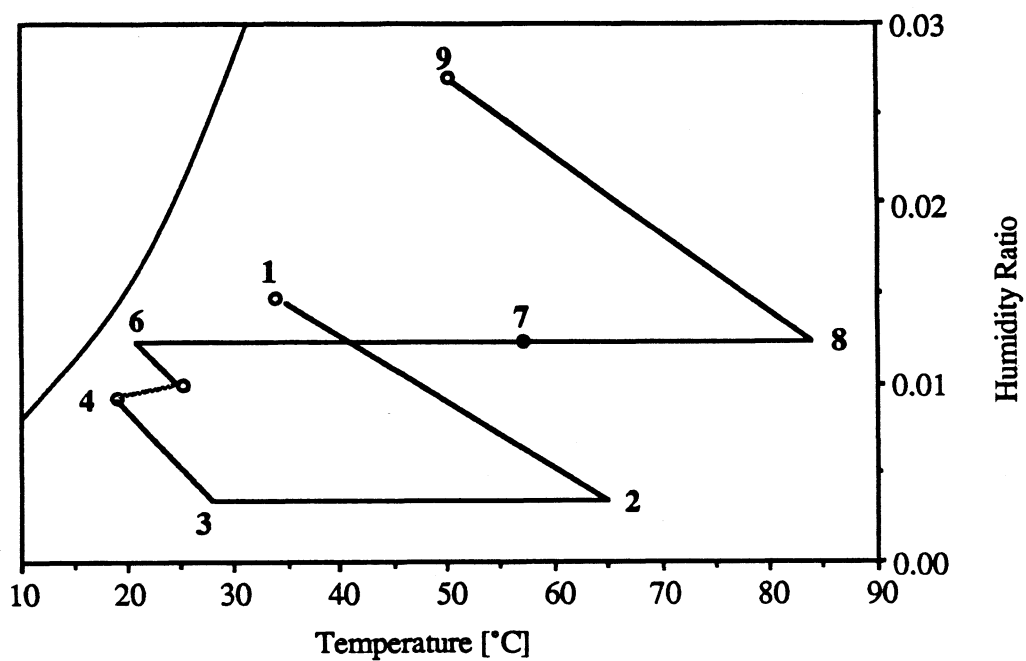
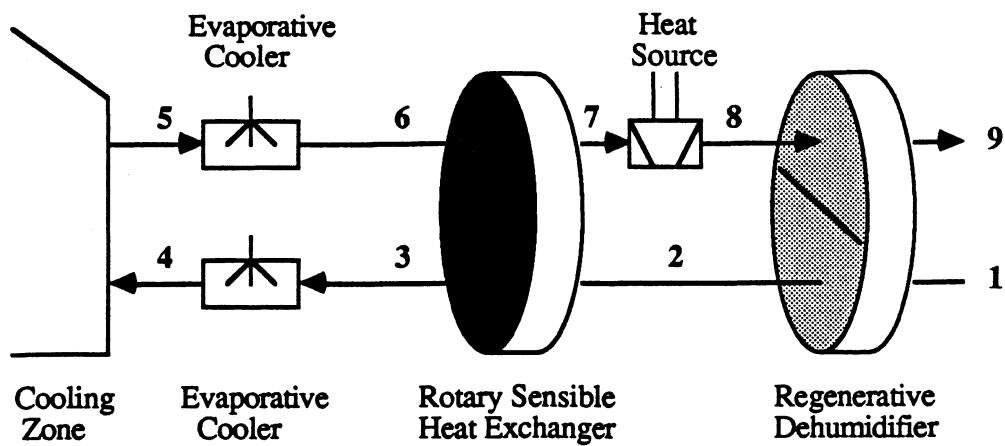


**Figure 1.1** Schematic and Psychrometric Chart of the Ventilation Solid Desiccant Cooling Cycle

In order to achieve high heat transfer rates between the air streams at state 2 and state 6 the rotary sensible heat exchanger must be operated at higher rotation speeds.

Rearrangement of the basic components results in other cycles as described by Jurinak [9]. The recirculation cycle uses the same components as the ventilation cycle and the indoor air is not discarded but recirculated. The Dunkle cycle [12] requires one more heat exchanger and can be considered as a combination of the cycles described above.

### 1.2.2 Ventilation Systems with Energy Recovery

Figure 1.2 shows a conventional space conditioning system without energy recovery. The supply air to the building is made up of 100% fresh outdoor air, as required in a hospital for example.

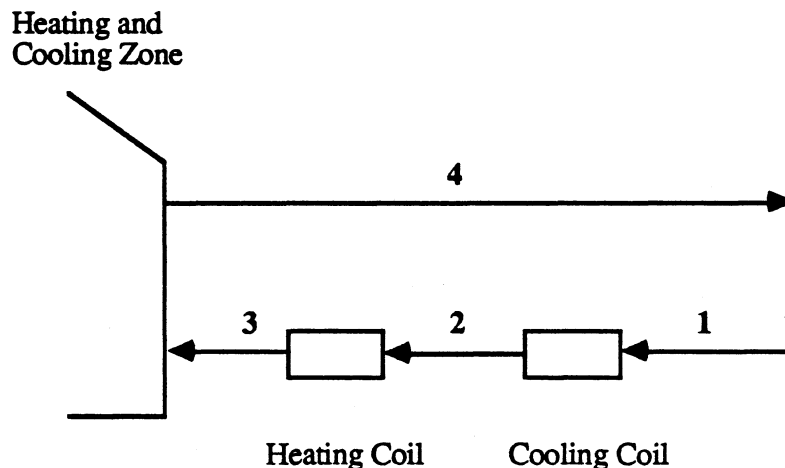
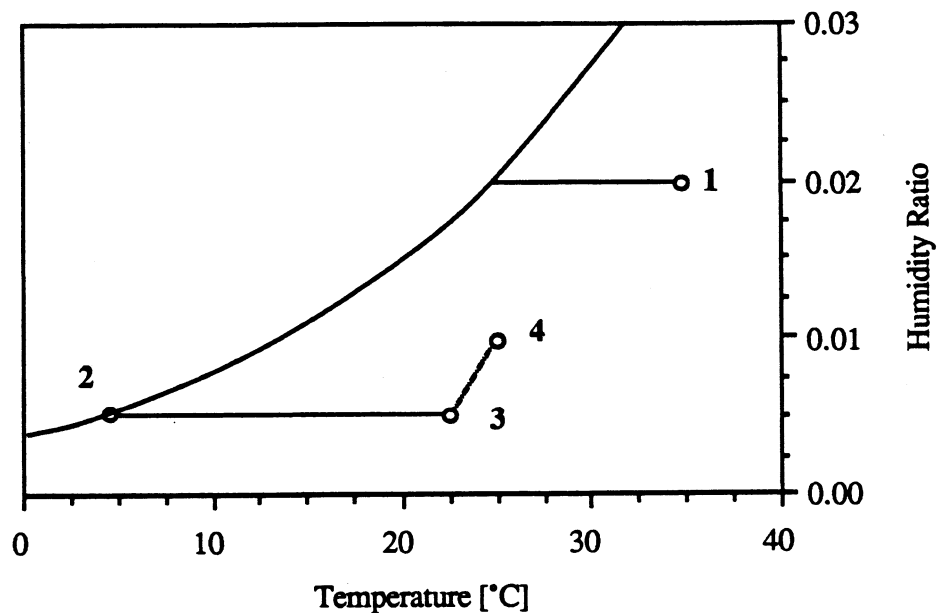


Figure 1.2 Conventional Space Conditioning System

For hot and humid summer days, the air conditioning process is shown in the psychrometric chart in Figure 1.3. Outdoor air is passed through the cooling coil and thereby cooled and dehumidified as soon as the temperature goes below the dew point temperature of the air-water mixture. The outlet state of the coil is saturated and represented by state 2. The cold air must be reheated to state 3 and is then blown into the building with the indoor conditions represented at state 4.



**Figure 1.3** Air Cooling without Energy Recovery

In winter applications shown in Figure 1.4, the cooling coil is by-passed, i.e. state 1 is the same as state 2, and the air is heated up to state 3 and supplied to the zone. This air must be humidified in the building since it is too dry and out of the thermal comfort range.

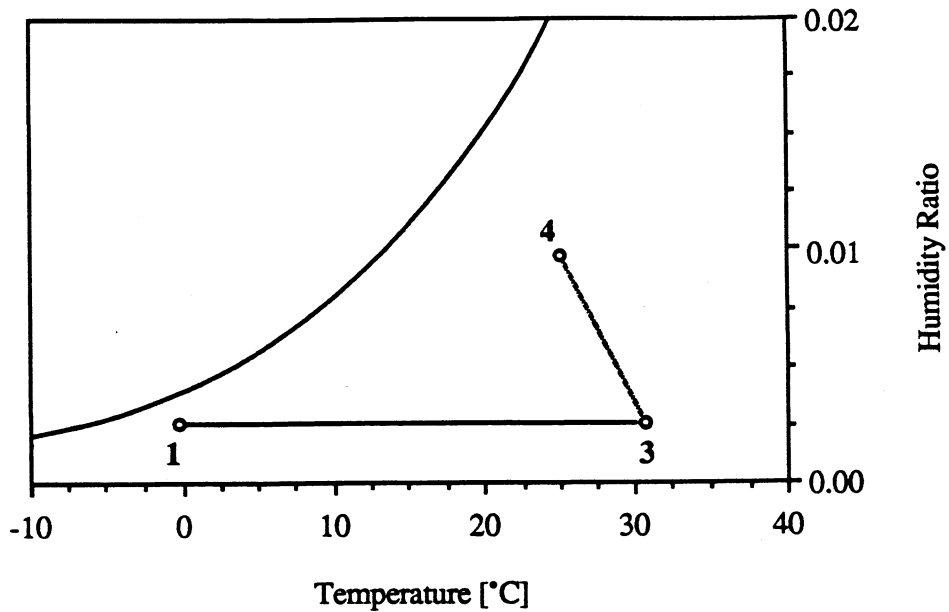


**Figure 1.4** Air Heating without Energy Recovery

Using an energy recovery regenerator as shown in Figure 1.5 reduces the energy consumption and improves the performance of the space conditioning system. In summer applications with a rotary sensible heat exchanger, the incoming air of state 1 is pre-cooled by the exhaust air stream which is warmed up from state 5 to state 6. As shown in Figure 1.6, the amount of energy savings depends on the effectiveness of the heat exchanger, i.e. how much one outlet state approaches the temperature of the other stream.

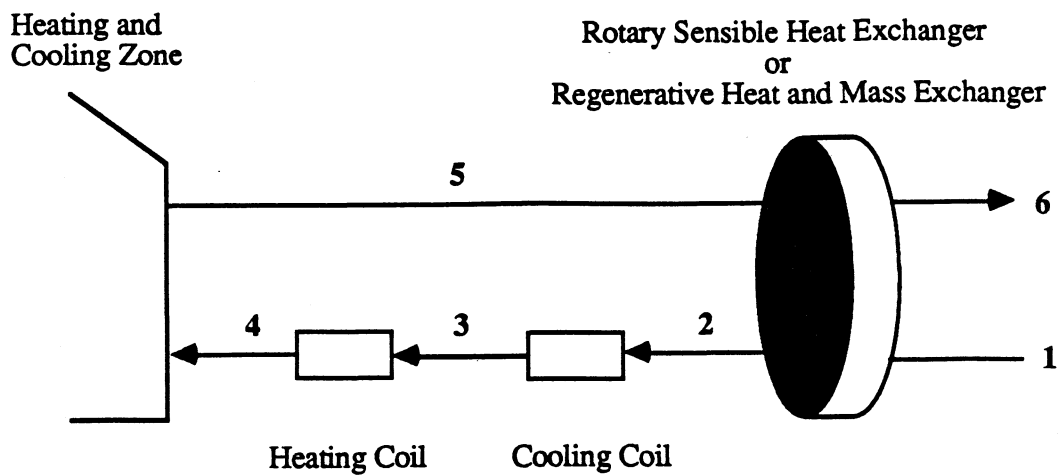


Figure 1.5 Space Conditioning System with Regenerative Energy Recovery Unit

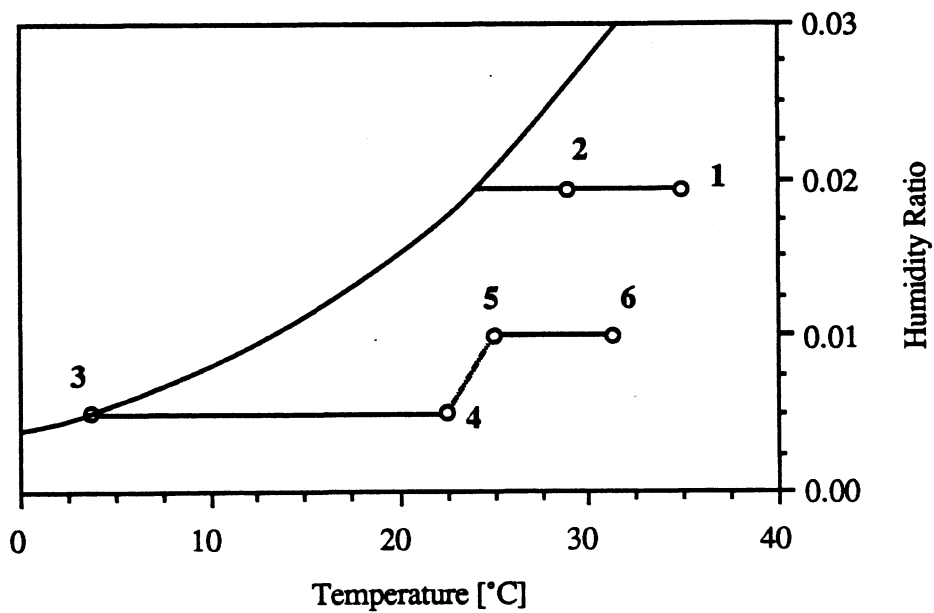
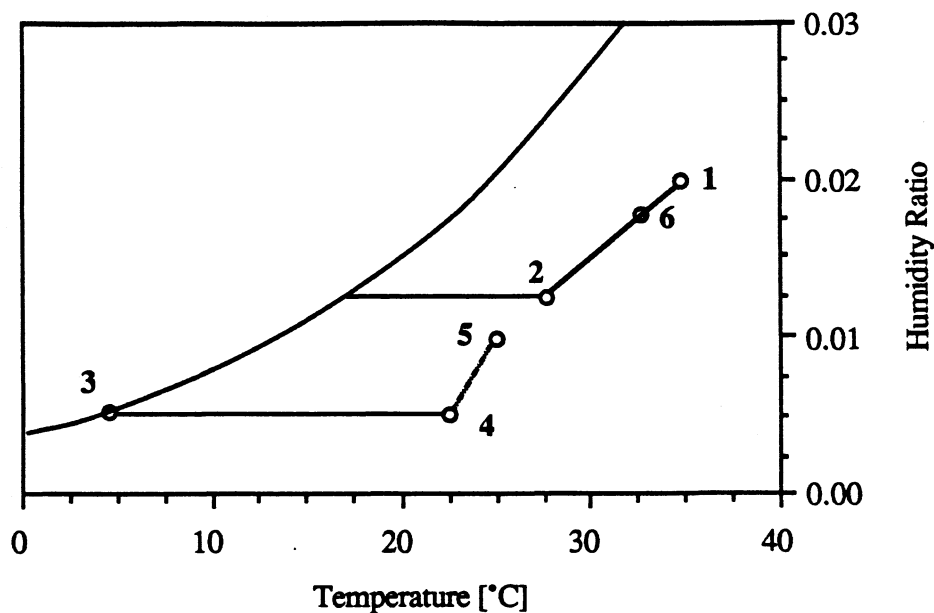


Figure 1.6 Air Cooling Using a Sensible Heat Exchanger

If the regenerator matrix is adsorptive, the outdoor air is both cooled and dehumidified from state 1 to state 2 as indicated in Figure 1.7.



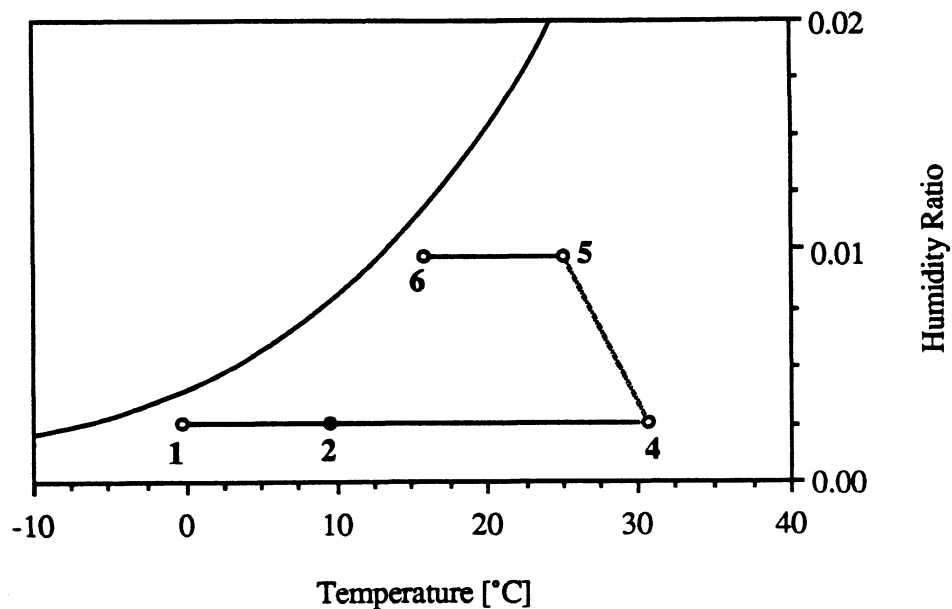
**Figure 1.7** Air Cooling Using an Enthalpy Exchanger

In this application of a regenerative heat and mass exchanger, the desired outlet is not a point of minimum humidity as in the desiccant cycle applications as described in Section 1.2.1 but rather the "state of the other stream". This approach towards the state of the other stream is equivalent to an exchange of the enthalpies of the air streams and can be achieved by operating the hygroscopic regenerator at higher rotation speed as shown in Chapter 4.

Fast rotating regenerative heat and mass exchangers are called total heat or enthalpy exchangers. The author prefers the term *enthalpy exchanger* since it

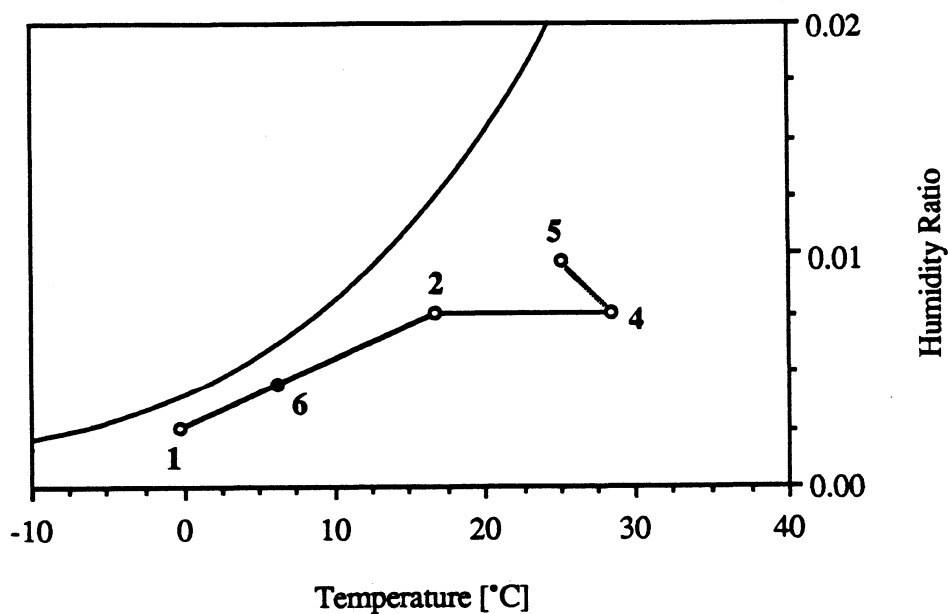
describes the thermodynamic process. The same is true for the regenerative dehumidifier with the outlet at low absolute humidity. The transfer of water vapor in enthalpy exchangers reduces both the latent and sensible load of the cooling coil whereas rotary sensible heat exchangers usually transfer only sensible heat.

Figure 1.8 shows an energy recovery application in cold winter climates using a sensible heat exchanger. Again, the cooling coil is by-passed and state 2 is the same as state 3. Sensible heat exchange as shown in Figure 1.8 preheats the cold outdoor air from state 1 to state 2 whereas the exhaust stream is cooled to state 6. For this example, the heat exchanger effectiveness is low in order to avoid condensation and freezing of water vapor as the exhaust air of state 6 moves further left across the saturation line.



**Figure 1.8** Air Heating Using a Sensible Heat Exchanger

Using an enthalpy exchanger can improve the performance of an energy recovery system also in winter applications as illustrated in Figure 1.9. The incoming outdoor air is humidified and preheated from state 1 to 2 whereas the state of the exhaust changes from state 5 to 6. Since water vapor transferred in an adsorbed phase, enthalpy exchangers can be operated at a high effectiveness even for inlet conditions where condensation would occur using a sensible heat exchanger.



**Figure 1.9** Air Heating Using an Enthalpy Exchanger

### 1.3 THESIS OBJECTIVES

The goal of this study is the development of a numerical model for a regenerative heat and mass exchanger operating at high rotation speed and therefore accomplishing enthalpy exchange between the two flow streams. Since regenerators are applicable in

air conditioning systems, as described in Chapter 1.2, the analysis of the following chapters emphasizes the mixture air-water vapor. The model should be suitable for the use in system simulations and show characteristics such as accuracy and computational simplicity.

Several models have been developed for adsorptive heat and mass exchangers [9,13,14,15,16] as well as for non-hygroscopic devices with mass transfer in the condensed phase [17,18,19]. Most of the previous studies on adsorptive regenerators have excluded the extensive analysis of enthalpy exchangers; investigations focused on the analysis of the various solid desiccant cycles using rotary sensible heat exchangers as well as regenerative dehumidifiers.

Chapter 2 provides an introduction of the theory of rotary sensible heat exchangers as well as regenerative heat and mass exchangers and presents the governing equations. Since even the most simple models results in a distributed parameter system, partial differential equations are required to describe the exchangers.

The thermodynamic property relationships of the system air-water-desiccant are described in Chapter 3. The numerous solution techniques for the differential equations are reviewed in Chapter 4. Chapter 5 presents a comparison of the solutions as well as a parametric study in order to examine the effect of mass flow rate, rotation speed, heat and mass transfer coefficients and the desiccant properties on the performance of an enthalpy exchanger.

Finally, the case where condensation or freezing of water vapor on the matrix occurs is investigated in Chapter 6.

---

## Chapter 2

# Theory of Rotary Regenerators

---

This chapter presents the theory of rotary regenerators and describes the underlying assumptions of the fundamental conservation and transfer rate equations. The rotary sensible heat exchanger, as the most simple example of a rotating regenerator, is described first, including the techniques to solve the equations. An empirical solution based on finite differences results is presented. The equations of regenerative heat and mass exchangers are more complicated to solve and their solutions are presented in following chapters.

### 2.1 COORDINATE SYSTEM, ASSUMPTIONS AND NOMENCLATURE OF ROTARY REGENERATORS

Figure 2.1 illustrates a rotary regenerator with a matrix which is cyclically exposed to physically separated air streams in counterflow arrangement. Real regenerator wheels are constructed with a hub and spokes with the actual matrix, either adsorptive or non-sorbent, between them. An excellent overview of the various matrix and regenerator geometries, such as drum-type or parallel plate matrix design, has been given by Schultz [20]. In each case, the regenerator is rotating in a duct which is separated by a wall in order to prevent mixing of the two air streams. The two streams

are referred to as stream or period 1 (in this study the stream with the lower temperature) and stream or period 2.

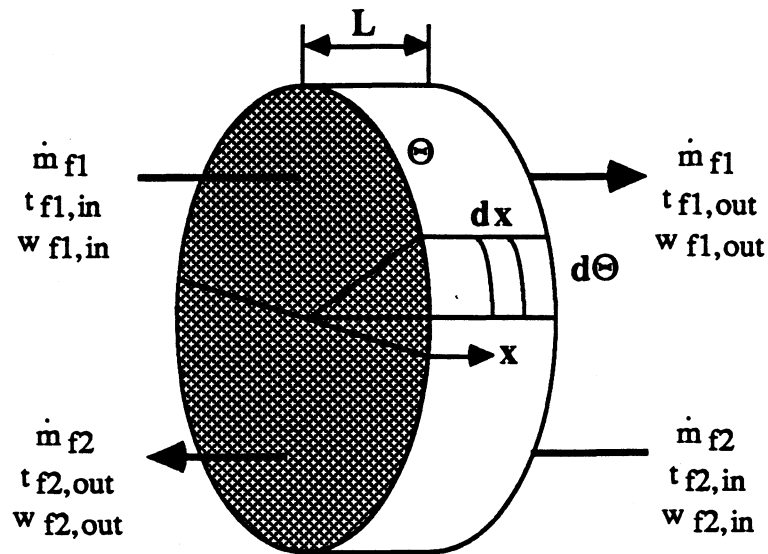


**Figure 2.1** Coordinate System and Nomenclature of a Rotary Regenerator

The inlet states are known and the objective is to determine the outlet states for a specified set of system parameters. Since there are four unknown outlet states in the overall mass and energy balance, these conservation laws cannot yield the solution alone. Therefore the fundamental equations have to be derived using an infinitesimal small segment of the regenerator and the following conventional assumptions:

1. The state properties of the inlet streams are uniform in time.
2. The state properties of the streams are uniform in radial and angular position

when entering the regenerator at the inlet face.

3. There is only a small pressure drop along the axial flow length compared to the total pressure; the changes of thermodynamic properties of the fluid and matrix are not affected by this small pressure drop.
4. The mass of air entrained in the matrix is small compared to the mass of the matrix. Therefore the energy storing effect of the air is neglected as well as the carry-over of air when switching from one period to the other.
5. The mixing of the fluid streams through leaking radial sealing strips which are attached on the spokes of the wheel is neglected.
6. The fluid and matrix states are considered to be uniform in the radial coordinate.
7. Angular and axial heat conduction and water diffusion due to gradients in temperature and concentration, respectively, are neglected.
8. The matrix is considered to be a homogeneous solid with constant matrix characteristics and porosity, as illustrated in Figure 2.1.
9. The heat and mass transfer between the air streams and the matrix can be described by convective transfer coefficients which are constant throughout the system.
10. The regenerator operates adiabatically.

Before the governing equations are derived, a brief discussion of the preceding model assumptions is helpful to understand the limitations of the model.

The assumption of time independent inlet conditions limits the analysis to the case of steady state operation. The method used to solve the governing differential equations

in this study permits dynamic considerations to some extent as described in Chapter 6.

The assumption of uniform inlet states of the air streams at the regenerator inlet in the radial and angular position is acceptable in energy recovery applications since the incoming streams can be considered to be well mixed. Brandemuehl [21] has considered spatially non-uniform inlet conditions which may be significant in desiccant cooling cycle applications where the non-uniform outlet of one regenerator may be the inlet of another one.

Fluid carry-over, leakage and pressure drop are characteristics of the actual device and do not affect the nature of the fundamental equations. Depending on the regenerator characteristics these assumptions may cause differences in predicted and experimental performance.

Assumption 6 reduces the dimensionality of the problem such that it can be described with partial differential equations in the axial and angular coordinates. Without assumption 7, second derivatives would appear in the equations, resulting in a dramatic increase in the numerical effort required to solve the equations.

The crucial assumptions are the homogeneous matrix and the negligible conductive and diffusive resistance into the matrix. One way to take into account for these effects is to replace the convective transfer coefficients by lumped overall transfer coefficients which can be obtained only experimentally. The matrix is usually non-homogeneous and therefore parameters such as the effective matrix mass and heat capacity must be selected very carefully, as shown by Schultz [20].

As described above, the problem becomes two dimensional and the governing equations can be derived using a pie-shaped infinitesimal control volume of the size  $dx$  and  $d\theta$ . The chosen coordinate system is not fixed in space but rotating with the

matrix through the flow streams. Thus, the apparently angular coordinate  $\Theta$  is not a dimensionless angle but a time from the view point of an observer rotating with the matrix. The axial flow coordinate  $x$  is chosen to be always positive in the flow direction and varies from zero at the inlet to the thickness  $L$  of the matrix at the outlet.

In steady state operation, the outlet states of a rotary regenerator vary with the angular position. This variation is analogous to the time dependence of the outlet state of a fixed bed regenerator. The equations are derived using the rotating coordinate system but are the same for both the fixed bed and rotary regenerator. The two models differ, however, in the initial conditions which are more complicated for the rotary device.

## **2.2 MODEL OF THE ROTARY SENSIBLE HEAT EXCHANGER**

### **2.2.1 Fundamental Equations**

A regenerator with non-sorptive matrix usually transfers sensible heat only. However, if the inlet temperature of the cold stream is below the dew point temperature of the hot and more humid stream, water may be transferred in condensed phase. This case is excluded here such that the humidities of the air streams do not change during the whole process. Therefore the system can be described with an energy balance and a energy transfer rate equation. The rigorous derivation is given in Appendix A and the resulting equations are consistent with Maclaine-cross' equations for negligible energy storage of the air entrained in the matrix [13].

### Energy Conservation

$$\frac{\partial i_f}{\partial z} + \Gamma_j \beta_j \frac{\partial I_m}{\partial \Phi} = 0 \quad (2.1)$$

where

- $z$  =  $\frac{x}{L}$  dimensionless axial flow coordinate  
 $\Phi$  =  $\frac{\Theta}{T}$  dimensionless time coordinate  
 $i_f$  = specific enthalpy of the air stream [ kJ/kgDA ]  
 $I_m$  = specific enthalpy of the matrix [ kJ/kgDM ]  
 $M_m$  = mass of the dry matrix [kgDM]  
 $\dot{m}_{fj}$  = air mass flow rate of stream j [ kgDA/s ]  
 $T$  = time required for one complete rotation [s]  
 $\Gamma_j$  =  $\frac{M_m}{\dot{m}_{fj} T}$  ratio of "matrix flow rate" to air flow rate  
 $\beta_j$  =  $\frac{T_j}{T}$  time fraction of period j  
 $j$  = 1,2 stream or period index

The specific enthalpy of the air is based on the mass of dry air (DA) since the flow rate of dry air is constant, no matter if water vapor is transferred or not. The same holds for the specific enthalpy of the matrix which is based on the constant mass of dry matrix (DM).

### Energy Transfer Rate

$$\frac{\partial i_f}{\partial z} = c_A NTU_{tj} (t_m - t_f) \quad (2.2)$$

where

$t_f$  = temperature of the air stream [ $^{\circ}\text{C}$ ]

$t_m$  = temperature of the matrix [ $^{\circ}\text{C}$ ]

$c_A$  = specific heat capacity of humid air [kJ/kg $^{\circ}\text{C}$ ]

$NTU_{tj} = \frac{A_j h_{tj}}{\dot{m}_f c_A}$  number of transfer units for heat transfer

$A_j$  = transfer area of period j

$h_{tj}$  = heat transfer coefficient of period j [kW/m $^2$  $^{\circ}\text{C}$ ]

Assuming ideal gas behavior of the air the enthalpies can be replaced by the fluid and matrix temperatures as the independent variables:

$$\frac{\partial t_f}{\partial z} + \sigma \Gamma_j \beta_j \frac{\partial t_m}{\partial \Phi} = 0 \quad (2.3)$$

$$\frac{\partial t_f}{\partial z} = NTU_{tj} (t_m - t_f) \quad (2.4)$$

where

$\sigma = \frac{c_m}{c_A}$  ratio of matrix heat capacity to humid air heat capacity

Equations (2.3)-(2.4) form a pair of coupled partial differential equations with boundary and inlet conditions:

$$\text{at } z = 0 \quad t_f(z = 0, \Phi) = t_{f,j, \text{in}} \quad j = 1,2 \quad (2.5)$$

$$\text{at } \Phi = \beta_j \quad \lim_{\Phi \rightarrow \beta_j^-} t_m(z, \Phi) = \lim_{\Phi \rightarrow \beta_j^+} t_m(z, \Phi) \quad j = 1,2 \quad (2.6)$$

Equation (2.6) is called reversal condition and implies that at steady state operation, the matrix state at the end of one period must be equal to the matrix state at the beginning of the other period. The reversal condition is the reason for the substantial difference in the solution techniques of the fixed bed and the rotary regenerator since iterative methods are required in order to find a solution which matches the reversal condition.

### 2.2.2 Solution of the Model Equations

The heat transfer effectiveness  $\epsilon_t$  is a convenient way to present the solution of Equations (2.3)-(2.6);  $\epsilon_t$  is defined as the ratio of the actual heat transfer rate to the thermodynamically limited maximum possible heat transfer rate [2].

In energy recovery applications of regenerators, both flow streams are air streams and the value of the specific heat capacity is approximately the same for both streams within the temperature range of interest.

For the remainder of this chapter the index  $j$  refers to the stream with the smaller flow rate and for convenience "3-j" indicates "the other stream". The ratio of minimum to maximum air capacitance rate can be expressed independent of the heat capacity of

the air:

$$C^* = \frac{C_{\min}}{C_{\max}} = \frac{\dot{m}_{fj}}{\dot{m}_{f3-j}} = \frac{\Gamma_{3-j}}{\Gamma_j} \quad (2.7)$$

The dimensionless parameter  $\Gamma$ , defined as the ratio of the "matrix flow rate" to the air flow rate, is an important parameter for rotary regenerators. The matrix as a solid "does not flow" but the mass of the matrix  $M_m$  divided by the rotation time  $T$  required for one complete rotation can be treated as a "flow stream" of matrix material. Rather than air flow ratios, the ratio of  $\Gamma_j$  and  $\Gamma_{3-j}$  appears in the following equation for the rotary sensible heat exchanger effectiveness:

$$\varepsilon_t = \frac{t_{fj,\text{out}} - t_{fj,\text{in}}}{t_{f3-j,\text{in}} - t_{fj,\text{in}}} = \frac{\Gamma_j (t_{f3-j,\text{in}} - t_{f3-j,\text{out}})}{\Gamma_{3-j} (t_{f3-j,\text{in}} - t_{fj,\text{in}})} \quad (2.8)$$

The effectiveness can be calculated using the outlet state of any period and both calculations must yield the same result, otherwise the first law of thermodynamics would not be satisfied.

Hausen [22,23] provided a solution for regenerators using series of eigenfunctions. Lambertson [24] gave the first comprehensive solution for rotary regenerators. He divided the matrix up into small cross flow heat exchangers where sensible heat exchange occurs between the "matrix stream" and the air stream. The ratio of the specific heat capacities  $\sigma$  was assumed to be independent of the temperature. Then the system of Equations (2.3)-(2.4) becomes a linear system of hyperbolic

differential equations. Maclaine-cross [13] derived the same finite difference equations by applying central difference techniques to the governing differential equations. He investigated the linear variation of  $\sigma$  with the temperature and the numerical stability of numerical solutions of regenerators.

Kays and London [2] provide  $\epsilon$ -NTU charts for rotary sensible heat exchangers for a wide range of system parameters which are based on the results of Lambertson [24] and Bahnke and Howard [25]. The effect of  $\Gamma_j$  and  $\sigma$  can be described using the empirical correlation

$$\epsilon_t = \epsilon_{\text{direct}} \left[ 1 - \frac{1}{9 (C_r^*)^{1.93}} \right] \quad (2.9)$$

where

$$\begin{aligned} \epsilon_{\text{direct}} &= \text{counterflow direct type heat exchanger effectiveness} \\ C_r^* &= \sigma \Gamma_j \text{ ratio of matrix capacitance rate to minimum fluid} \\ &\quad \text{capacitance rate} \end{aligned}$$

The direct counterflow heat exchanger effectiveness can be computed as a function of  $C^*$  and  $NTU_{tj}$  using the following formulas:

$$\epsilon_{\text{direct}} = \frac{1 - \exp[-NTU_0(1-C^*)]}{1 - C^* \exp[-NTU_0(1-C^*)]} \quad (2.10)$$

where

$$\frac{1}{NTU_0} = \frac{1}{NTU_{tj}} + \frac{C^*}{NTU_{t3-j}} \quad (2.11)$$

The rigorous derivation of Equation (2.10) is given in [2] and applies only for unbalanced flow arrangement, i.e. the value of  $C^*$  must be less than one. In energy recovery applications the two flow rates of the air streams are usually equal in order to supply the same amount of air as is removed and discarded with the exhaust stream. The regenerator is then called balanced and  $\Gamma_1$  is equal to  $\Gamma_2$ . In this case, the correlations for the counterflow direct heat exchanger effectiveness simplify to

$$\epsilon_{\text{direct}} = \frac{NTU_0}{1 + NTU_0} \quad (2.12)$$

where

$$NTU_0 = \frac{NTU_{tj}}{2} \quad (2.13)$$

Figure 2.2 illustrates the effect of  $C_r^*$  on the heat transfer effectiveness of a rotary sensible heat exchanger. The effectiveness of a direct counterflow heat exchanger is approached with increasing values of  $C_r^*$ . Since  $\sigma$  is assumed to be a physical property constant, the approach to counterflow direct type performance can be achieved only by increasing  $\Gamma_j$ . The effect of  $\Gamma_j$  and other non-dimensional parameters on the regenerator performance is discussed in Chapters 4 and 5.

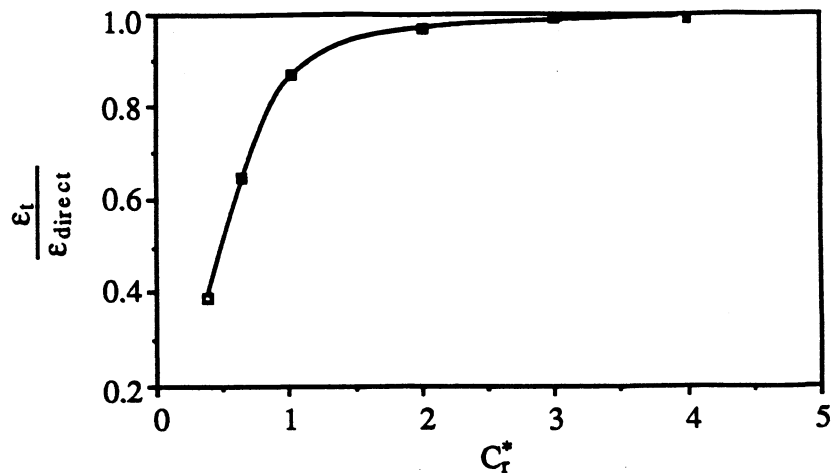


**Figure 2.2** Effect of  $C_r^*$  on the Rotary Sensible Heat Exchanger Effectiveness

Equation (2.9) cannot be used for very low rotation speeds, which is equivalent to low values of  $\Gamma_j$  or  $C_r^*$ . Maclaine-cross [13] showed that for  $C_r^* \leq 0.4$  the following effectiveness correlation holds:

$$\epsilon_t = C_r^* \quad (2.14)$$

Many investigators have dropped one or more of the assumptions and more refined models have been developed. Hausen [4] studied the effect of heat conduction into the matrix, which is important in metallurgical regenerators with thick bricks as heat storing matrix. Bahnke and Howard [25] considered longitudinal conduction in the matrix whereas Jeffreson [26] modified the number of transfer units to take into account the thermal capacity of the air entrained in the matrix.

### 2.3 MODEL OF REGENERATIVE HEAT AND MASS EXCHANGERS

In order to transfer a chemical component in a regenerator from one stream to the other, the phase of this component must be changed from the gaseous state in the air to a state where it can be carried by the rotating matrix to the other period. In air conditioning applications considered here, the component which must be transferred is water vapor. The water can condense on the matrix or it can be adsorbed by a hygroscopic material. In both cases, the humidity of the air streams changes and a mass balance and mass transfer rate equation must be added to the energy equations which were required to describe the rotary sensible heat exchanger. The derivation of the mass conservation and mass transfer rate equation is analogous to the derivation presented in Appendix A.

#### Mass Conservation

$$\frac{\partial w_f}{\partial z} + \Gamma_j \beta_j \frac{\partial W_m}{\partial \Phi} = 0 \quad (2.15)$$

where

$w_f$  = humidity ratio of the air stream [kg W/kg DA]

$W_m$  = water content of the matrix [kg W/kg DM]

$\Gamma_j, \beta_j$  as defined in Equation (2.1)

### Mass Transfer Rate

$$\frac{\partial w_f}{\partial z} = NTU_{w_j} (w_m - w_f) \quad (2.16)$$

where

$w_m$  = humidity of air in equilibrium with the matrix [ kgW/kgDA ]

$NTU_{w_j} = \frac{A_j h_{w_j}}{\dot{m}_{f_j}}$  number of transfer units for mass transfer

$h_{w_j}$  = mass transfer coefficient of period j [ kg/m<sup>2</sup> s ]

The fundamental mass equations are analogous to the energy equations of the rotary sensible heat exchanger. The humidity ratio is based on the mass of dry air (DA) and the water content of the matrix on the mass of dry matrix (DM). The driving force for the water vapor transfer is the difference between the humidity ratio of the air stream  $w_f$  and  $w_m$ , which can be considered as the humidity ratio of a thin layer of air above the matrix surface in equilibrium with the matrix. To be in equilibrium with the matrix does not imply to have the same water concentration as the matrix but rather the same chemical potential. Mass transfer by itself never occurs since energy effects are always involved. Therefore the energy equations from Section 2.2.1 must also be considered.

### Energy Conservation

$$\frac{\partial i_f}{\partial z} + \Gamma_j \beta_j \frac{\partial I_m}{\partial \Phi} = 0 \quad (2.17)$$

### Energy Transfer Rate

$$\frac{\partial i_f}{\partial z} = c_A NTU_{tj} (t_m - t_f) + i_w NTU_{wj} (w_m - w_f) \quad (2.18)$$

where

$$i_w = \text{specific enthalpy of the transferred water [ kJ/kgW ]}$$

The energy conservation equation is identical to that for the rotary sensible heat exchanger whereas the energy transfer rate contains an extra term which indicates that energy is transferred in two different ways. As in the sensible case there is an energy transport due to the temperature gradient between the air stream and the matrix. Energy is also transferred with the water vapor. This energy stream is called latent energy and is due to the enthalpy  $i_w$  of the water vapor.

Equations (2.15)-(2.18) form a set of coupled hyperbolic differential equations. The coupling is a result of two different effects. First, as described above, there is both a sensible and a latent term in the energy transfer rate equation. Furthermore, the equations are coupled through the following thermodynamic relationships:

$$i_f = i_f(t_f, w_f) \quad (2.19)$$

$$I_m = I_m(t_m, W_m) \quad (2.20)$$

$$W_m = W_m(t_m, w_m) \quad (2.21)$$

$$i_w = i_w(t_f) \quad (2.22)$$

Equations (2.15)-(2.22) form a set of differential and algebraic equations with 8 thermodynamic state properties as the dependent variables and the non-dimensional axial flow direction  $z$  and time  $\Phi$  as the independent variables. The boundary conditions of the system are the inlet conditions of the air streams. As for the rotary sensible rotary heat exchanger, the reversal conditions at the period switches are the initial conditions.

$$\text{at } z = 0 \quad w_f(z = 0, \Phi) = w_{f,j,\text{in}} \quad j = 1,2 \quad (2.23)$$

$$t_f(z = 0, \Phi) = t_{f,j,\text{in}} \quad j = 1,2 \quad (2.24)$$

$$\text{at } \Phi = \beta_j \quad \lim_{\Phi \rightarrow \beta_j^-} W_m(z, \Phi) = \lim_{\Phi \rightarrow \beta_j^+} W_m(z, \Phi) \quad j = 1,2 \quad (2.25)$$

$$\lim_{\Phi \rightarrow \beta_j^-} t_m(z, \Phi) = \lim_{\Phi \rightarrow \beta_j^+} t_m(z, \Phi) \quad j = 1,2 \quad (2.26)$$

The coupled non-linear system of Equations (2.15)-(2.26) cannot be solved analytically and therefore numerical and approximate analytical solution techniques

must be used to determine the outlet states as well as the state property distributions of the fluid and the matrix.

---

Chapter 3

**Thermodynamic Relationships**

---

This chapter presents the thermodynamic relationships used in this study to solve Equations (2.15)-(2.26). All equations described below are for conventional SI units and the temperatures are in °C.

### 3.1 PROPERTIES OF HUMID AIR

Following ASHRAE [27], humid air at ambient pressure is treated as an ideal gas mixture of dry air and water vapor. There are many parameters used to specify the amount of water vapor in the air, such as mass fraction, mole fraction, relative humidity or wet bulb temperature. In this study, the humidity ratio and relative humidity are used along with the following conversions:

$$w_f = \frac{m_w}{m_{DA}} = 0.622 \frac{\phi}{\frac{P_{tot}}{P_w} - \phi} \quad (3.1)$$

$$\phi = \frac{P_w}{P_{wsat}} = \frac{w_f}{0.622 + w_f} \frac{P_{tot}}{P_{wsat}} \quad (3.2)$$

where

- $m_w$  = mass of water in the air [kgW]
- $m_{DA}$  = mass of dry air [kgDA]
- $p_{tot}$  = total ambient pressure [kPa]
- $p_w$  = partial pressure of water vapor in the air [kPa]
- $p_{wsat}$  = partial pressure of water vapor at saturation [kPa]
- $\phi$  = relative humidity

The water vapor saturation pressure over ice or liquid water, depending on the temperature, is calculated using polynomial expressions presented in ASHRAE [27].

The enthalpy of water vapor in humid air is calculated using saturated liquid water at 0 °C as reference state, as suggested in [1]:

$$i_w = c_{Lw} t_{DP} + i_v(t_{DP}) + c_{pw} (t_f - t_{DP}) \quad (3.3)$$

where

- $t_f$  = temperature of the air [°C]
- $t_{DP}$  = dew point temperature of the air-water mixture [°C]
- $c_{Lw}$  = specific heat capacity of liquid water [ kJ/kg°C ]
- $c_{pw}$  = specific heat capacity of water vapor [ kJ/kg°C ]
- $i_v$  = specific heat of vaporization at the dew point [ kJ/kg ]

Using the heat of vaporization at the reference state, Equation (3.3) simplifies to

$$i_w = i_v + c_{pw} t_f \quad (3.4)$$

Since humid air is treated as an ideal gas, the enthalpy is the sum of the dry air and water vapor enthalpy:

$$i_f = c_{pA} t_f + w_f (i_v + c_{pw} t_f) \quad (3.5)$$

where

$$c_{pA} = \text{specific heat capacity of dry air [ kJ/kg}^\circ\text{C ]}$$

The specific heat capacity of humid air can be defined as

$$c_A = c_{pA} + w_f c_{pw} \quad (3.6)$$

The effect of the variation of  $c_A$  with the humidity ratio on the number of transfer units for heat transfer as defined in Equation (2.2) is in the range of one percent and is neglected in this study.

### 3.2 MATRIX PROPERTIES

For non-hygroscopic matrices and sensible heat exchange only, i.e., no condensation occurs, the only thermodynamic parameter of the matrix is the specific heat capacity of the matrix material. In this case, the regenerator can completely be

described with Equations (2.3)-(2.4) along with the initial and boundary conditions and the value of  $\sigma$ , which is assumed to be independent of the temperature in this study.

In the case of hygroscopic matrices with the capability to adsorb water from humid air streams, the thermodynamic behavior of the matrix is highly non-linear and cannot be described by a single "mass capacity" parameter.

Equation (2.21) is the equilibrium relation between the water content of the matrix and the humidity ratio of the air and is known as adsorption isotherm correlation. The enthalpy of the matrix in Equation (2.20) is determined in part by the adsorption isotherm correlation, the specific heat capacity of the matrix material and the energy effect involved in the adsorption process, referred to as heat of adsorption.

The mechanisms of adsorption are not fully understood and there does not exist a unique adsorption isotherm correlation which can be used for all solid desiccants, such as micro-porous silica gel or molecular sieves for example. In this study two different models for the adsorption isotherm correlations are used in order to investigate the effect of the solid desiccant characteristics on the performance of a regenerative heat and mass exchanger which is operating at conditions such that enthalpy exchange between the air streams occurs.

### **3.2.1 Jurinak's Generic Isotherm Model**

The basis for Jurinak's generic adsorption isotherm model is the Clausius-Clapeyron equation [9]. Adsorption is the transition from gaseous phase to an adsorbed phase with one or more molecular layers of adsorbate on the adsorbent. It is believed that this state shows different thermodynamic characteristics than a condensed

layer of bulk phase water.

Using the Clausius-Clapeyron equation with the assumption of ideal gas behavior and negligible specific volume of the liquid, the differential heat of adsorption and the heat of vaporization can be written as

$$i_s = R T^2 \frac{d \ln p_w}{dT} \quad (3.7)$$

$$i_v = R T^2 \frac{d \ln p_{wsat}}{dT} \quad (3.8)$$

where

$i_s$  = differential heat of adsorption [ kJ/kg ]

$i_v$  = specific heat of vaporization [ kJ/kg ]

$R$  = gas constant for water [ kJ/kg °K ]

$T$  = thermodynamic temperature [°K]

From equations (3.7)-(3.8) it can be seen that vaporization/condensation occurs only if the air is saturated whereas a change from water vapor to adsorbed phase can occur in unsaturated air.

It is convenient to use condensation as a reference process for adsorption. The following definition is helpful and relates the energy effects of the two phenomena:

$$h^* = \frac{i_s}{i_v} = \frac{d \ln p_w}{d \ln p_{wsat}} \quad (3.9)$$

The ratio  $h^*$  is approximately independent of the temperature and a function of the matrix water content only [9]. Integration of Equation (3.9) yields a relation between the relative humidity and the water content of the matrix in equilibrium with humid air. This relation is not unique but contains undetermined expressions which depend on the water content of the matrix. These expressions have been used to fit available experimental data for a variety of desiccants. Jurinak [9] used the following empirical correlations which allows to reproduce the features of the five so called *Brunauer adsorption isotherm types*:

$$h^* = 1 + \Delta h^* \frac{e^{kW^*} - e^k}{1 - e^k} \quad (3.10)$$

$$\phi = \frac{s W^*}{1 + s W^* - W^*} \left[ \frac{p_{wsat}(t_m)}{p_{wsat}(t_0)} \right]^{h^* - 1} \quad (3.11)$$

where

$$W^* = \frac{W_m}{W_{max}} \quad \text{ratio of actual matrix water content to}$$

maximum matrix water content

$$\Delta h^*, s, k, t_0 \quad \text{empirical scaling parameters}$$

For the case where the matrix water content reaches its maximum value, the differential heat of adsorption becomes the same as the heat of vaporization. This maximum water content is reached if the matrix is in equilibrium with saturated air.

Equations (3.10)-(3.11) can be used to iteratively compute the matrix water

content as a function of the relative humidity. Figure 3.1 shows the adsorption isotherm for 20 °C of a molecular sieve as an example for a Brunauer Type 1 isotherm [9].

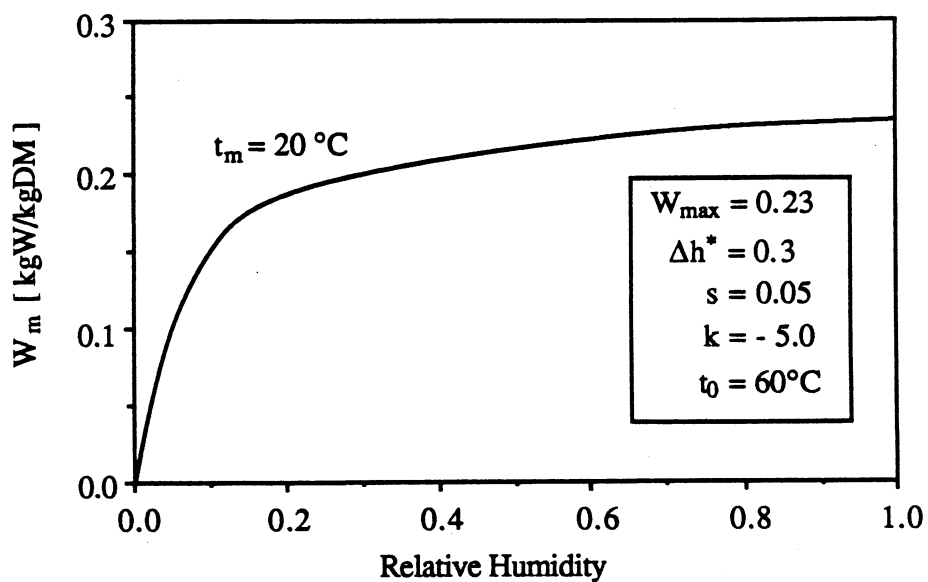


**Figure 3.1** Adsorption Isotherm for a Molecular Sieve

An example for a Brunauer Type 3 isotherm is given in Figure 3.2. Adsorbents of this type have a differential heat of adsorption which is less than the heat of vaporization [9]. Therefore the scaling parameter  $\Delta h^*$  was chosen to be negative.

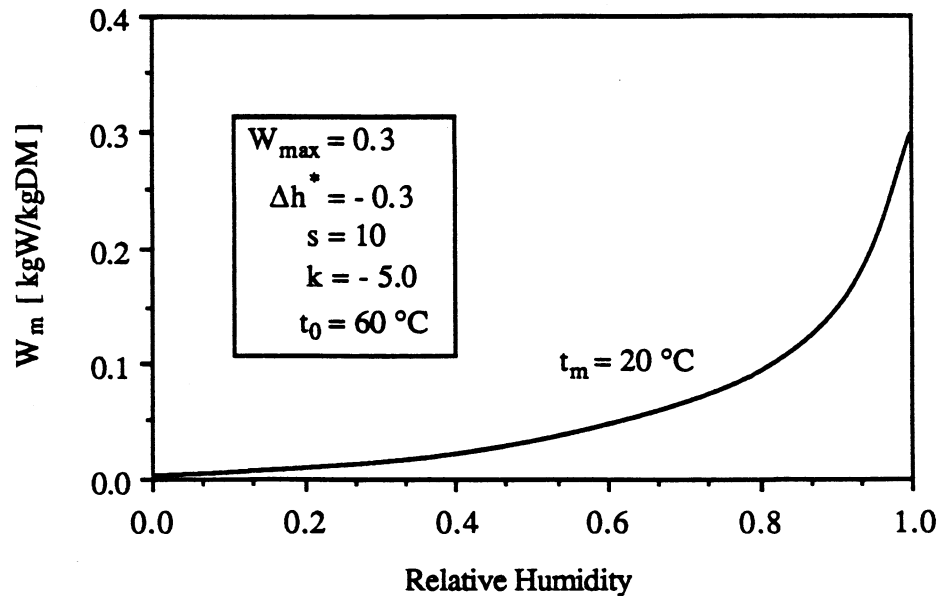


**Figure 3.2** Adsorption Isotherm for Brunauer Type 3 Adsorbents

### 3.2.2 Dubinin-Polanyi Theory for Silica Gel

The Dubinin-Polanyi theory for micro-porous adsorbents is based on the adsorption potential which has been originally proposed by Polanyi and is defined as follows [28]:

$$A = -RT \ln \frac{p_w}{p_{wsat}} \quad (3.12)$$

where

**A** = adsorption potential [ kJ/kmol ]

**R** = universal gas constant [ kJ/kmol °K ]

Using the Clausius-Clapeyron equation, it can be shown that the defined adsorption potential is essentially the difference in the enthalpy between water in adsorbed phase and saturated bulk phase liquid water:

$$A = (i_s - i_v) M_w \quad (3.13)$$

where

$$M_w = \text{molecular weight of water [ kg/kmol ]}$$

Van den Bulck [29] showed that for regular density silica gel, the characteristic curve of the matrix water content as a function of the adsorption potential is independent of the temperature. He correlated available data using the following two-sited expression:

$$W_m = W_{01} \exp\left[-\left(\frac{A}{E_{01}}\right)^2\right] + W_{02} \exp\left[-\left(\frac{A}{E_{02}}\right)^2\right] \quad (3.14)$$

The parameters used in this study are for Davison silica gel Type 11 as used by Schultz in his experimental studies of regenerative dehumidifiers [20]:

$$W_{01} = 0.117 \quad \text{kgW/kgDM}$$

$$E_{01} = 7.74 \times 10^3 \quad \text{kJ/kmol}$$

$$W_{02} = 0.237 \quad \text{kgW/kgDM}$$

$$E_{02} = 2.50 \times 10^3 \quad \text{kJ/kmol}$$

The maximum water content of the matrix is reached if it is in equilibrium with saturated air. The adsorption potential becomes zero and

$$W_{\max} = W_{01} + W_{02} \quad (3.15)$$

Figure 3.3 shows the adsorption isotherm for silica gel using Equation (3.14) and the parameters described above.

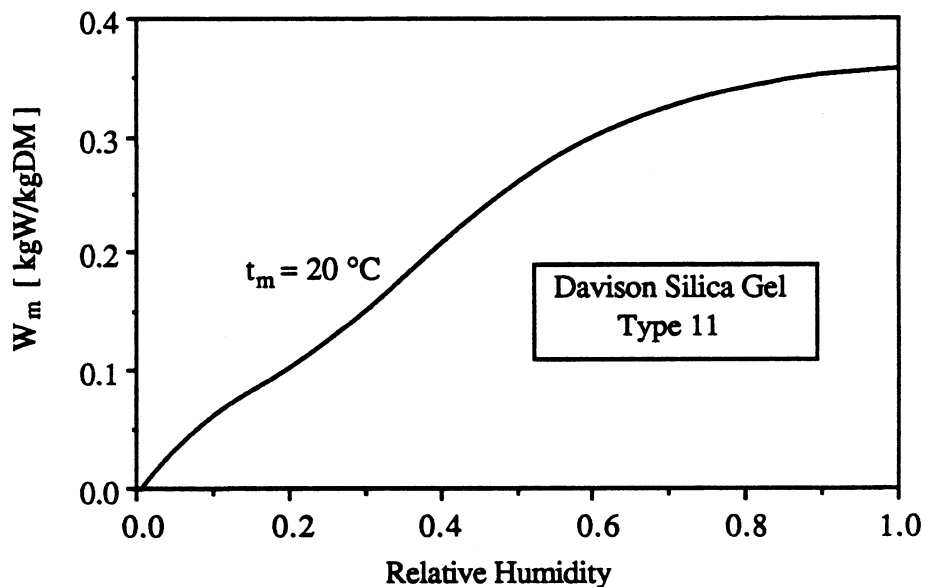


**Figure 3.3** Adsorption Isotherm for Silica Gel

### 3.2.3 Enthalpy of the Matrix

The specific differential heat of adsorption can be defined as the heat which is liberated when a unit quantity of water vapor is adsorbed such that the temperature and the water content of the matrix does not change, i.e., the mass of the matrix is large

compared to the mass of adsorbed water vapor.

The enthalpy of the matrix can be computed as the sum of the enthalpies of the dry matrix and the adsorbed phase.

$$I_m = c_m t_m + I_{ad} \quad (3.16)$$

where

$$c_m = \text{specific heat capacity of the dry matrix [ kJ/kg°C ]}$$

$$I_{ad} = \text{specific enthalpy of adsorbed water [ kJ/kgDM ]}$$

The enthalpy of adsorbed water is the enthalpy of the water vapor at the same temperature reduced by the heat liberated heat during the adsorption process, called the integral heat of adsorption, which can be written as

$$\bar{i}_s = \int_0^{W_m} i_s dW \quad (3.17)$$

Neglecting the last term in Equation (3.3) which takes into account superheating the enthalpy of water vapor at matrix temperature can be expressed as the sum of saturated liquid water and the heat of vaporization at the matrix temperature rather than at the reference state:

$$i_w(t_m) = c_{Lw} t_m + i_v(t_m)$$

After substitution into Equation (3.16), the matrix enthalpy can be computed as a function of the temperature and the water content of the matrix:

$$I_m = c_m t_m + c_{Lw} t_m W_m + \int_0^{W_m} (i_v - i_s) dW \quad (3.18)$$

The last term is called the *integral heat of wetting* and depends on the correlation for the adsorption isotherm.

For Jurinak's isotherm correlation the integral heat of wetting depends on the temperature because of the temperature dependence of the heat of vaporization [27]:

$$i_v(t_m) = 2502.4 - 2.4302 t_m \quad [ \text{kJ/kg} ]$$

The ratio of differential heat of adsorption and heat of vaporization, as defined in Equation (3.9), is assumed to be a function of the matrix water content only and independent of the temperature so the enthalpy of the matrix can be computed as

$$I_m = c_m t_m + c_{Lw} t_m W_m + i_v \int_0^{W_m} (1 - h^*) dW \quad (3.19)$$

For the Dubinin-Polanyi adsorption models the matrix enthalpy can be obtained by integrating over the adsorption potential from the state of dry matrix to the actual matrix water content. Substitution of Equation (3.13) in to (3.18) gives an expression

for the matrix enthalpy with a temperature independent integral heat of wetting:

$$I_m = c_m t_m + c_{Lw} t_m W_m - \frac{1}{M_w} \int_0^{W_m} A dW \quad (3.20)$$

The evaluation of the integral heat of wetting causes some difficulties. The differential in the integral can be substituted such that the integral which must be solved can be written as

$$\int_{-\infty}^A A \frac{\partial W_m}{\partial A} dA$$

This integral has an "analytical" solution which includes terms of the error function, and therefore tables are required to compute the matrix enthalpy.

---

Chapter 4

**Solutions of the Model Equations**

---

This chapter presents the solution techniques used in this study to solve the governing conservation and transfer rate equations introduced in Chapter 2. Equations (2.15)-(2.22) describe the coupled heat and mass transfer mechanisms which occur in a regenerative heat and mass exchanger. The solution techniques for these coupled equations may be classified in the following manner:

1. Numerical solution of the coupled equations.
2. Transformation of the equations to uncoupled form along with analytical and analogy solutions.

The first part of this chapter describes the numerical solution used in this study as a reference solution for the models which are based on uncoupling the differential equations. Van den Bulck's equilibrium model [14] gives insight into the transport phenomena which occur in the hygroscopic matrix of a regenerative heat and mass exchanger. The linearized analogy method [9,13] uses the analogy to rotary sensible heat exchangers where heat transfer only occurs. Finally, a technique is presented to uncouple the equations which can be used for regenerative heat and mass exchangers

operating at high rotational speed and accomplishing enthalpy exchange between the two air streams.

#### 4.1 NUMERICAL SOLUTION OF THE MODEL EQUATIONS

A numerical solution of the governing model equations has been developed by Maclaine-cross [13] and is based on a finite difference scheme. The reason for selecting this numerical solution was because most of the FORTRAN code called MOSHMX<sup>1</sup> was available to the author and the second order accuracy of the finite difference equations. Since the model was extensively used throughout this study and modified for the problems encountered in Chapter 6 the theory of MOSHMX is presented here.

##### 4.1.1 Finite Difference Equations

The total differentials of the enthalpies of humid air and the matrix can be obtained from equations (2.19)-(2.20) and expressed as

$$di_f = \left( \frac{\partial i_f}{\partial t_f} \right)_{w_f} dt_f + \left( \frac{\partial i_f}{\partial w_f} \right)_{t_f} dw_f \quad (4.1)$$

$$dI_m = \left( \frac{\partial I_m}{\partial t_m} \right)_{W_m} dt_m + \left( \frac{\partial I_m}{\partial W_m} \right)_{t_m} dW_m \quad (4.2)$$

---

<sup>1</sup>MOSHMX stands for Method Of Solving Heat and Mass X(transfer)

The coefficients can be obtained as the partial derivatives of the state property relations in Equations (3.5) and (3.18).

Equations (4.1)-(4.2) are substituted into the energy conservation and transfer rate equations such that the temperatures and water concentrations are the dependent variables of a new set of equations:

$$\frac{\partial w_f}{\partial z} + \Gamma_j \beta_j \frac{\partial W_m}{\partial \Phi} = 0 \quad (4.3)$$

$$\frac{\partial w_f}{\partial z} = NTU_{w,j} (w_m - w_f) \quad (4.4)$$

$$\left( \frac{\partial i_f}{\partial t_f} \right)_{w_f} \frac{\partial t_f}{\partial z} + \left( \frac{\partial i_f}{\partial w_f} \right)_{t_f} \frac{\partial w_f}{\partial z} + \Gamma_j \beta_j \left( \frac{\partial I_m}{\partial t_m} \right)_{w_m} \frac{\partial t_m}{\partial \Phi} + \Gamma_j \beta_j \left( \frac{\partial I_m}{\partial W_m} \right)_{t_m} \frac{\partial W_m}{\partial \Phi} = 0 \quad (4.5)$$

$$\frac{\partial t_f}{\partial z} = NTU_{t,j} (t_m - t_f) \quad (4.6)$$

To obtain the finite difference equations the matrix is divided up into a grid of discrete space and time steps as illustrated in Figure 4.1. Each grid is treated as a small heat and mass exchanger with an air stream and a "matrix stream" in crossflow arrangement.

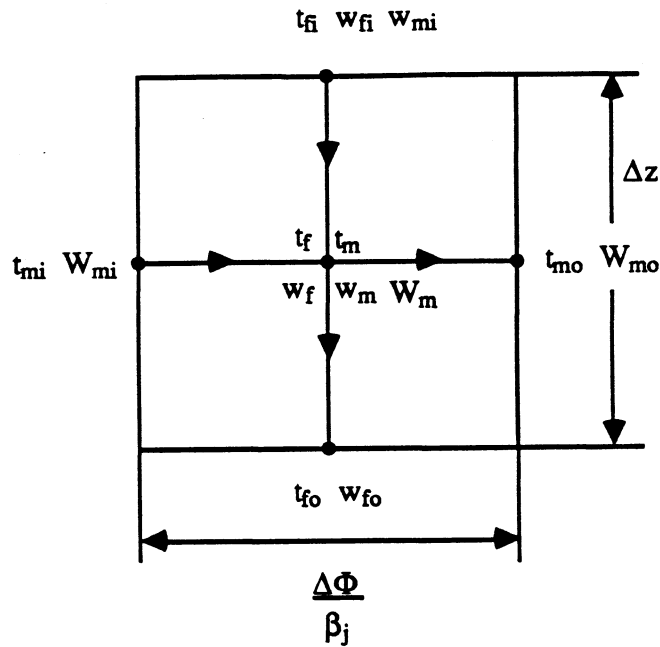


**Figure 4.1** MOSHMX Finite Difference Grid

A first order Taylor series expansion about the center of the grid yields a second order accurate approximation of the outlet state:

$$w_{fi} = w_f - \frac{\partial w_f}{\partial z} \frac{\Delta z}{2} + \frac{\partial^2 w_f}{\partial z^2} \frac{\Delta z^2}{8} \quad (4.7)$$

$$w_{fo} = w_f + \frac{\partial w_f}{\partial z} \frac{\Delta z}{2} + \frac{\partial^2 w_f}{\partial z^2} \frac{\Delta z^2}{8} \quad (4.8)$$

Similar equations can be obtained for all other fluid and matrix properties. The difference of Equation (4.7) and (4.8) gives a second order accurate approximation for

the derivative of the air and matrix properties whereas the sum approximates the state at the center of the grid:

$$\frac{\partial w_f}{\partial z} = \frac{w_{fo} - w_{fi}}{\Delta z} \quad (4.9)$$

$$w_f = \frac{w_{fo} + w_{fi}}{2} \quad (4.10)$$

The humidity ratio of air in equilibrium with the matrix is approximated by a first order Taylor series:

$$w_m = w_{mi} + \left( \frac{\partial w_m}{\partial t_m} \right)_{W_m} (t_m - t_{mi}) + \left( \frac{\partial w_m}{\partial W_m} \right)_{t_m} (W_m - W_{mi}) \quad (4.11)$$

These approximations for the state properties and their derivatives are substituted into Equations (4.3)-(4.6) and the resulting finite difference equations can be expressed conveniently using the following matrix notation:

$$A \begin{bmatrix} w_{fo} - w_{fi} \\ t_{fo} - t_{fi} \\ W_{mo} - W_{mi} \\ t_{mo} - t_{mi} \end{bmatrix} = \begin{bmatrix} 0 \\ 0 \\ -2(w_{fi} - w_{mi}) \\ -2(t_{fi} - t_{mi}) \end{bmatrix} \quad (4.12)$$

where

$$A = \begin{bmatrix} \frac{1}{\Delta z} & 0 & \frac{\Gamma_j \beta_j}{\Delta \Phi} & 0 \\ \frac{1}{\Delta z} \frac{\partial i_f}{\partial w_f} & \frac{1}{\Delta z} \frac{\partial i_f}{\partial t_f} & \frac{\Gamma_j \beta_j}{\Delta \Phi} \frac{\partial I_m}{\partial W_m} & \frac{\Gamma_j \beta_j}{\Delta \Phi} \frac{\partial I_m}{\partial t_m} \\ 1 + \frac{2}{NTU_{wj} \Delta z} & 0 & -\frac{\partial w_m}{\partial W_m} & -\frac{\partial w_m}{\partial t_m} \\ 0 & 1 + \frac{2}{Le NTU_{wj} \Delta z} & 0 & -1 \end{bmatrix}$$

$$Le = \frac{NTU_{tj}}{NTU_{wj}} \quad \text{overall Lewis number}$$

For a given set of values for  $t_{mi}$  and  $W_{mi}$  as well as  $t_{fi}$  and  $w_{fi}$ , which are referred to as matrix and fluid inlet states of a discrete element, respectively, the outlet states of this element can be computed using Equation (4.12).

#### 4.1.2 Solution Procedure and Convergence

The first step of the finite difference algorithm is the initialization of the matrix states. The values have to be guessed and are chosen to be between the inlet states of the two air streams. Starting at the inlet of the regenerator the procedure of computing the outlet states of the grids marches down the flow direction until the outlet is reached. This is repeated for all time steps until one complete rotation is accomplished.

The fluid outlet states of the regenerator vary with the rotation angle and therefore change from one time step to another. The average outlet states are calculated using the weighted sum of the outlet states of the last element at the regenerator outlet. The derivative of the state properties in Equation (4.12) are evaluated at the inlet states of the element and a first estimate of the four outlet states is computed. Using the average of the inlet and the first estimate the coefficients of the matrix are evaluated again and the fluid and matrix outlet states are recalculated. This technique maintains the second order accuracy of the finite difference equation and is analogous to a second order Runge-Kutta method [13].

In steady state operation the matrix and fluid states do not vary in time and the reversal conditions in Equations (2.25)-(2.26) are satisfied. The finite difference scheme reaches this steady state solution if the matrix and air states do not vary for two complete consecutive numerical cycles. MOSHMX uses two different algorithms to achieve fast convergence to the steady state solution. There is also a variety of possible convergence criteria to check whether the steady state solution has been reached or more iterations are required.

The *transient method* for convergence is a successive substitution of the matrix states. It uses the computed matrix properties from one iteration step as the initial value for the next numerical cycle. The most obvious criteria for convergence is to determine the changes of state properties for a certain discrete element. It is more efficient to compare a single quantity at each iteration step, for example the enthalpy effectiveness.

Convergence criteria

$$|(\varepsilon_i)^n - (\varepsilon_i)^{n+1}| \leq 10^{-6} \quad (4.13)$$

where

$$\varepsilon_i = \frac{i f_{j,\text{out}} - i f_{j,\text{in}}}{i f_{3-j,\text{in}} - i f_{j,\text{in}}} \quad \begin{array}{l} \text{enthalpy effectiveness using the stream} \\ \text{with the minimum flow rate} \end{array}$$

Whereas the coefficients in Equation (4.3) are constant, the coefficients in Equation (4.5) vary in a highly non-linear manner with the state properties and the finite difference equations do not conserve energy. However, Maclaine-cross [13] found that for the convergence criteria described above the overall mass balance is satisfied to an accuracy of  $10^{-8}$  whereas the accuracy of the overall energy balance is  $10^{-4}$ . This is accurate enough considering the underlying assumptions of the models described in Chapter 2.

The successive substitution method describes essentially the transient behavior of the matrix from its initially assumed state to steady state operation. The convergence to steady state is very slow for fast rotating devices and enthalpy exchangers. Therefore Maclaine-cross [13] developed a second iteration scheme which is basically a modified Newton-Raphson method and referred to as *matrix method*. A combination of the transient and the matrix method is suggested to achieve an optimum rate of convergence.

### 4.1.3 Determination of the Step Size

Through numerical experiments and wave analysis, Maclaine-cross [13] determined the number of space and time steps required to achieve high accuracy in the computed outlet states as well as computations within reasonable CPU time.

The number of space steps depends on the number of transfer units since a high transfer rate causes steep state property profiles and therefore a smaller discretization of the finite difference grid is required:

$$N_m = \text{INT} \left( 0.85 \sqrt{\max(\text{NTU}_{w_j}, \text{NTU}_{t_j})} + 1.6 \right) \quad (4.14)$$

where

$$N_m = \text{number of space steps}$$

The wave theory presented in Chapter 4.2 shows that, in the case of infinite transfer coefficients, two distinct transfer waves move through the matrix at each period. The faster wave propagates with the speed  $\lambda_1$  which is about 10 -100 times faster than the second wave. In order to follow the fast wave front, the required number of time steps  $N_{fj}$  can be related to the number of space steps:

$$\beta_j \frac{\Delta z}{\Delta \Phi} = \frac{N_{fj}}{N_m} \approx \frac{\lambda_1}{\Gamma_j} \quad (4.15)$$

The version of MOSHMX used in this study also allows the user to specify the number of space and time steps explicitly.

In addition to the grid size determined as described above MOSHMX computes the outlet states using two smaller grid sizes and a Richardson extrapolation to zero grid size is performed. The analysis of numerical stability and the theory of the extrapolation has been discussed in detail by Maclaine-cross [13] and reviewed by Jurinak [9].

## 4.2 EQUILIBRIUM MODEL AND WAVE ANALYSIS

The finite difference solution described in Chapter 4.1 yields an accurate solution of the governing model equations but does not give further insight into the transport phenomena occurring in a regenerative heat and mass exchanger. Van den Bulck [30] derived, for the case of infinite transfer coefficients, a wave theory which is a powerful tool to explain the difference in the performance of a regenerative dehumidifier and an enthalpy exchanger.

### 4.2.1 Combined Transfer Potentials for Equilibrium Systems

In the case of infinite transfer coefficients, the air streams and the solid desiccant matrix are in equilibrium at each point throughout the entire regenerator:

$$w_m ( z, \Phi ) = w_f ( z, \Phi )$$

$$t_m ( z, \Phi ) = t_f ( z, \Phi )$$

The system can be described using a reduced set of the equations derived in Chapter 2.

### Mass Conservation

$$\frac{\partial w_f}{\partial z} + \Gamma_j \beta_j \frac{\partial W_m}{\partial \Phi} = 0 \quad (2.15)$$

### Energy Conservation

$$\frac{\partial i_f}{\partial z} + \Gamma_j \beta_j \frac{\partial I_m}{\partial \Phi} = 0 \quad (2.17)$$

### Thermodynamic Relations

$$i_f = i_f (t_f, w_f) \quad (2.19)$$

$$I_m = I_m (t_f, W_m) \quad (2.20)$$

$$W_m = W_m (t_f, w_f) \quad (2.21)$$

The conservation laws and the thermodynamic state property relations are still coupled but can be expressed as a pair of uncoupled kinematic wave equations. The derivation described below essentially follows Van den Bulck [30] and is presented here since the author used other partial derivatives of state property functions as coefficients and a different representation of the wave diagrams.

Using the total differentials of the state property relations in Equations (2.19)-(2.21), the enthalpies and the matrix water content can be eliminated and the conservation laws can be expressed with the temperature and humidity ratio as the

dependent variables:

$$\frac{\partial w_f}{\partial z} + a_1 \Gamma_j \beta_j \frac{\partial t_f}{\partial \Phi} + a_2 \Gamma_j \beta_j \frac{\partial w_f}{\partial \Phi} = 0 \quad (4.16)$$

$$a_3 \frac{\partial t_f}{\partial z} + a_4 \frac{\partial w_f}{\partial z} + a_5 \Gamma_j \beta_j \frac{\partial t_f}{\partial \Phi} = 0 \quad (4.17)$$

where

$$a_1 = \left( \frac{\partial W_m}{\partial t_m} \right)_{w_f}$$

$$a_2 = \left( \frac{\partial W_m}{\partial w_m} \right)_{t_f}$$

$$a_3 = \left( \frac{\partial i_f}{\partial t_f} \right)_{w_f}$$

$$a_4 = \left( \frac{\partial i_f}{\partial w_f} \right)_{t_f} - \left( \frac{\partial I_m}{\partial W_m} \right)_{t_f}$$

$$a_5 = \left( \frac{\partial I_m}{\partial t_m} \right)_{W_m}$$

The coefficients  $a_i$  are derivatives of state property functions and can be computed using Equations (3.5) and the appropriate expressions for the isotherm and matrix enthalpy correlations described in Chapter 3.

The total differentials of the temperature and humidity ratio can be written in terms of the independent variables  $z$  and  $\Phi$ :

$$dt_f = \left( \frac{\partial t_f}{\partial z} \right)_\Phi dz + \left( \frac{\partial t_f}{\partial \Phi} \right)_z d\Phi$$

$$dw_f = \left( \frac{\partial w_f}{\partial z} \right)_\Phi dz + \left( \frac{\partial w_f}{\partial \Phi} \right)_z d\Phi$$

After substitution Equations (4.16)-(4.17) can then be written as

$$\begin{aligned} -a_1 dz \quad \frac{\partial t_f}{\partial z} + (\tau - a_2 dz) \frac{\partial w_f}{\partial z} &= -a_1 dt_f - a_2 dw_f \\ (a_3 d\tau - a_5 dz) \frac{\partial t_f}{\partial z} + a_4 d\tau \frac{\partial w_f}{\partial z} &= -a_5 dt_f \end{aligned} \quad (4.18)$$

where

$$\tau = \frac{\Phi}{\Gamma_j \beta_j}$$

This set of partial differential equations can be considered as a set of two linear algebraic equations with the spatial derivatives of the temperature and humidity ratio as independent variables. The coefficients are functions of the state properties and are non-constant.

The *characteristic lines* are lines in the  $\tau$ - $z$  plane along which property changes propagate and which are defined by the following differential equation:

$$\lambda = \frac{dz}{d\tau} = \Gamma_j \frac{dz}{d(\Phi/\beta_j)} \quad (4.19)$$

If the right hand side of Equation (4.18) is set equal to zero the system becomes homogeneous and has a non-trivial solution if and only if the determinant of the coefficients on the left hand side is equal to zero [31]:

$$\begin{vmatrix} -a_1 dz & d\tau - a_2 dz \\ a_3 d\tau - a_5 dz & a_4 d\tau \end{vmatrix} = 0$$

or

$$a_2 a_5 \lambda^2 + (a_1 a_4 - a_2 a_3 - a_3) \lambda + a_3 = 0 \quad (4.20)$$

The quadratic expression in Equation (4.21) has the real solutions  $\lambda_1$  and  $\lambda_2$  which are functions of derivatives of state property functions and can be considered as new state properties. The solutions  $\lambda_1$  and  $\lambda_2$  describe two lines in the  $\tau$ - $z$  plane and are substituted into equation (4.18). The resulting non-homogeneous linear system has only a solution if and only if the determinant of one column of the left hand side and the vector on the right hand side is equal to zero [31]:

$$\begin{vmatrix} -a_1 dz & -(a_1 dt_f + a_2 dw_f) \\ a_3 d\tau - a_5 dz & -a_5 dt_f \end{vmatrix} = 0$$

or

$$a_1 a_3 dt_f + (a_3 - a_5 \lambda_i) a_2 dw_f = 0 \quad i = 1,2 \quad (4.21)$$

Banks [32] introduced new state properties for the equilibrium system air-water-desiccant and called them *combined heat and mass transfer potentials* or *F-potentials*. The idea of the F-potentials is to separate the enthalpy and humidity into independent variables. They can be expressed using the total differentials:

$$dF_i = \left( \frac{\partial F_i}{\partial t_f} \right)_{w_f} dt_f + \left( \frac{\partial F_i}{\partial w_f} \right)_{t_f} dw_f \quad i = 1,2 \quad (4.22)$$

Comparison of Equation (4.22) with the left hand side of Equation (4.21) yields the differential expression

$$dF_i = a_1 a_3 dt_f + (a_3 - a_5 \lambda_i) a_2 dw_f \quad i = 1,2 \quad (4.23)$$

Equation (4.23) is *not* the total differential of the combined potentials since the second derivatives depend on the order of differentiation. The rigorous proof is presented in Appendix B. Therefore Equation (4.23) cannot be used to compute the F-potentials since the integrated values depend on the path of integration. However, the differential expression becomes a total differential by introducing an integrating factor [33]:

$$dF_i = G(t_f, w_f) a_1 a_3 dt_f + G(t_f, w_f) (a_3 - a_5 \lambda_i) a_2 dw_f \quad i = 1,2 \quad (4.24)$$

Due to the difficulties in determining the integrating factor, Equation (4.24) is not used in this study to compute differences of the combined heat and mass transfer potentials.

Along the characteristic lines Equation (4.21) holds and therefore Equation (4.23)

can be written as

$$dF_i = 0 \quad i = 1,2$$

or

$$F_i = \text{constant} \quad i = 1,2$$

Therefore integration of Equation (4.23) yields lines in a psychrometric chart of constant  $F_1$  or  $F_2$ , depending on which solution of Equation (4.20) is substituted into Equation (4.23). Lines of constant  $F_1$ -potential resemble lines of constant enthalpy whereas lines of constant  $F_2$ -potential are similar to lines of constant relative humidity. The most important feature of the new state properties is that they can be computed independently of each other and are uncoupled.

The left side of Equation (4.23) can be expressed in terms of the independent variables:

$$dF_i = \frac{\partial F_i}{\partial z} dz + \frac{\partial F_i}{\partial \tau} d\tau$$

or

$$\frac{dF_i}{d\tau} = \frac{\partial F_i}{\partial z} \frac{dz}{d\tau} + \frac{\partial F_i}{\partial \tau} = \frac{\partial F_i}{\partial z} \lambda_i + \frac{\partial F_i}{\partial \tau} \quad i = 1,2$$

If  $\lambda_i$  is computed as the solution of Equation (4.20) the left hand side becomes zero since  $F_i$  is constant along the characteristic lines:

$$\frac{\partial F_i}{\partial z} \lambda_i + \frac{\partial F_i}{\partial \tau} = 0$$

This equation has the form of a first order kinematic wave equation [21] and  $\lambda_i$ , as defined in Equation (4.19) and computed by solving the quadratic expression in Equation (4.20), can be interpreted as the speed at which the property  $F_i$  propagates through a regenerative heat and mass exchanger.

#### Kinematic Wave Equations in the $\tau$ - $z$ Plane

$$\lambda_1 \frac{\partial F_1}{\partial z} + \frac{\partial F_1}{\partial \tau} = 0$$

$$\lambda_2 \frac{\partial F_2}{\partial z} + \frac{\partial F_2}{\partial \tau} = 0$$

The  $\tau$ - $z$  plane illustrating the dynamics of the combined heat and mass transfer process is called wave diagram. In this study, the wave diagrams are used to illustrate the effect of the dimensionless parameter  $\Gamma_j$  and the matrix characteristics on the performance of a regenerative heat and mass exchanger. The author found it more convenient to use  $\Phi/\beta_i$  as the independent time coordinate since the dimensionless parameter  $\Gamma$  becomes uncoupled from the time axis.

### Kinematic Wave Equations in the $\Phi/\beta_j$ -z Plane

$$\frac{\lambda_1}{\Gamma_j} \frac{\partial F_1}{\partial z} + \frac{\partial F_1}{\partial(\Phi/\beta_j)} = 0 \quad (4.25)$$

$$\frac{\lambda_2}{\Gamma_j} \frac{\partial F_2}{\partial z} + \frac{\partial F_2}{\partial(\Phi/\beta_j)} = 0 \quad (4.26)$$

Equations (4.25)-(4.26) are uncoupled because the combined potentials  $F_1$  and  $F_2$  can be computed independently of each other. Therefore the dynamics of a regenerative heat and mass exchanger with infinite transfer coefficients can be described following the two independent waves of the combined potentials.

The propagation speed of the  $F_i$ -potential in the  $\Phi/\beta_j$ -z plane can be expressed as

$$\frac{dz}{d(\Phi/\beta_j)} = \frac{\lambda_i}{\Gamma_j} \quad i = 1,2 \quad (4.27)$$

For the solid desiccants used in this investigation,  $\lambda_1$  is much larger than  $\lambda_2$  such that  $F_1$  changes propagate much faster than  $F_2$  changes through the matrix. Therefore the  $F_1$  and  $F_2$ -waves are also referred to as first and second wave, respectively. Since  $\lambda_i$  is function of the state properties, the wave speed varies along the flow length and rotation angle of the regenerator. Therefore two different kinds of waves propagate through the matrix.

Van den Bulck [30] investigated the wave speeds for the system air-water-silica

gel and showed that for a period where a warm and humid air stream is dehumidified by a dry matrix expansion waves propagate through the system. In the case where a moist matrix is regenerated by a hot and dry air stream shock waves occur. These combinations of air inlet and matrix conditions are the conditions for a regenerative heat and mass exchanger used in a desiccant cooling cycle, as described in Figure 1.1.

Since the inlet conditions in air conditioning cycle applications are within a defined range [9], a model based on the distinct waves which occur during the two periods has been developed by Van den Bulck [14] to predict the outlet states of an regenerative dehumidifier with infinite transfer coefficients. In energy recovery applications of enthalpy exchangers, as shown in Figure 1.5, the inlet conditions depend on the ambient conditions and vary from hot and humid to cold and dry. Therefore, depending on the ambient conditions, either expansion or shock waves can occur and it was not found as convenient to use the wave theory to develop a model to predict the outlet states of an enthalpy exchanger for any inlet conditions.

Nevertheless, the wave theory provides the background to understand the performance differences between regenerative dehumidifiers and enthalpy exchangers. In order to simplify the analysis the variation of  $\lambda_i$  with the state properties of the air-water-desiccant system is neglected here such that two constant wave speeds at each period characterize the performance.

#### 4.2.2 $F_1$ - $F_2$ Charts and Wave Diagrams

Figure 4.2 shows two air inlet states which represent a typical set of inlet conditions for a regenerative dehumidifier in a solid desiccant cycle as described in Section 1.2.1. The intersections of the lines of constant F-potential through the inlet

states are called *intersection points*. The points of low and high humidity ratio are called the *intermediate states*. The target of a regenerative dehumidifier is dehumidification of stream 1 with regeneration of the matrix provided by stream 2, i.e. the desired outlet of period 1 is the intersection point at low humidity ratio.

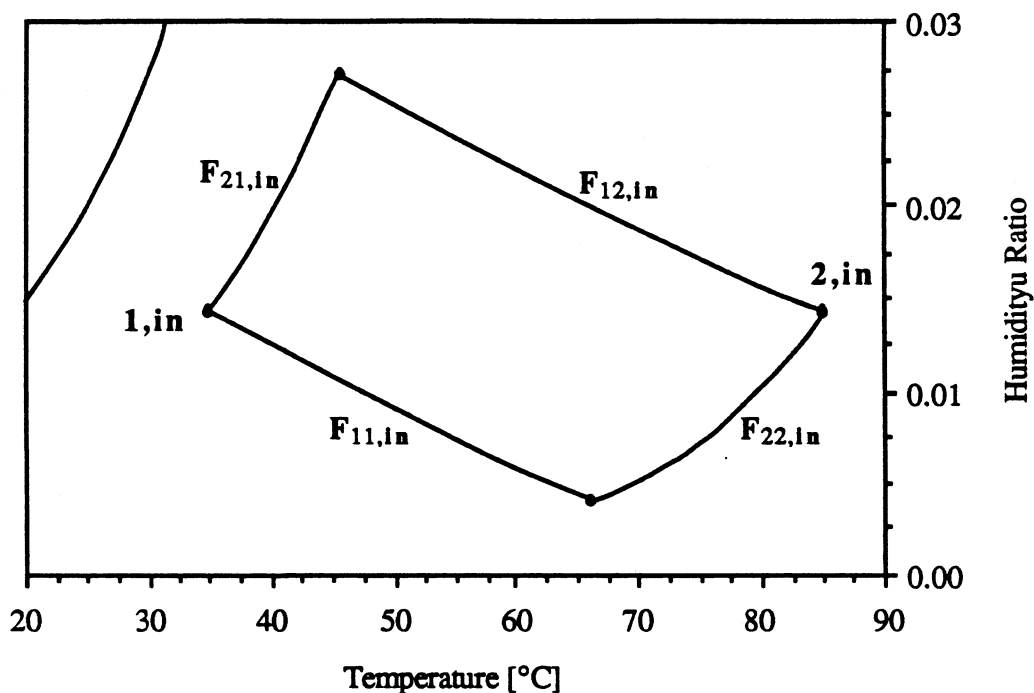


**Figure 4.2** Dehumidifier Inlet States with Lines of Constant F-Potential

The dehumidification process for the process stream (1,in) can be illustrated in a wave diagram shown in Figure 4.3. It is assumed that the matrix is completely regenerated when entering period 1, i.e., the matrix is in equilibrium with the regeneration stream (2,in). The slopes of the lines which separate the different transfer zones are described by Equation (4.27). Assuming that  $\lambda_1$  and  $\lambda_2$  are constant, the

slopes are determined by the dimensionless parameter  $\Gamma_1$  which is the ratio "matrix flow rate" to air flow rate. If the mass of the matrix and the air flow rate are fixed,  $\Gamma_1$  is essentially determined by the rotation speed. Therefore, the rotation speed specifies the ratio of dark-shaded, un-shaded and lightly-shaded areas. Each area represent a distinct transfer zone with certain state properties, indicated in the diagram.

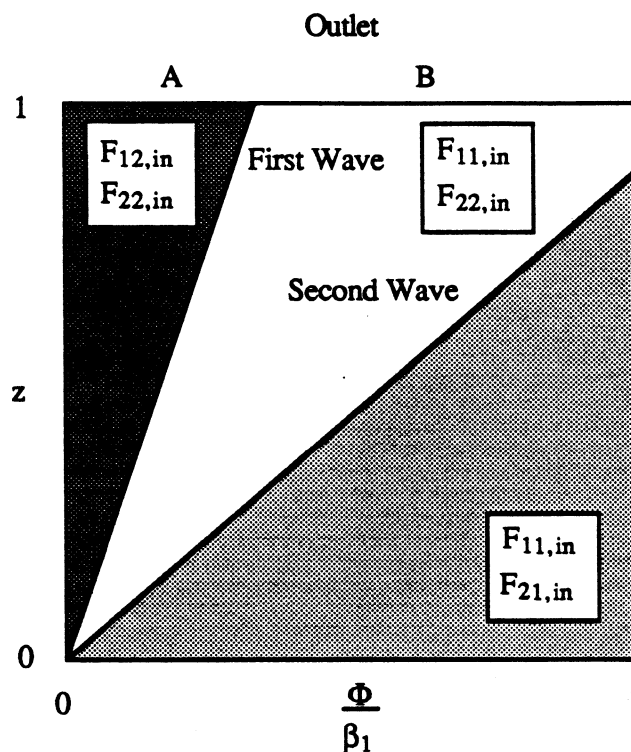


**Figure 4.3** Wave Diagram for Period 1 of a Regenerative Dehumidifier

- lightly-shaded = inlet state of stream 1, warm and humid
- un-shaded = intersection point at low humidity ratio, hot and dry
- dark-shaded = inlet state of stream 2, hot and humid

In the wave diagram shown in Figure 4.3 the ratio of the length A to the length B represents the composition of stream 1 at the regenerator outlet:

$$\frac{A}{B} = \frac{\text{percentage of inlet state stream 2}}{\text{percentage of intermediate state}}$$

This ratio can be increased somewhat by reducing the rotation speed such that the percentage of the intermediate state is increased. Smaller rotation speed increases the slopes of the wave fronts such that the dark-shaded area is reduced. If the speed becomes too slow, however, the second wave "breaks through" which reduces the efficiency of the dehumidification, as shown in Figure 4.4.

In order to achieve a high degree of dehumidification, the rotation speed has to be controlled such that  $\Gamma_1$  is in the range of 0.1 to 0.2 [30]. The outlet of a regenerative dehumidifier is close to the intersection point of low humidity ratio and therefore close to the line of constant  $F_1$ -potential through the inlet state of stream 1. As mentioned above, lines of constant  $F_1$ -potential resemble lines of constant enthalpy in a psychrometric chart and the dehumidification process is close to a process where the enthalpy of the streams do not change.

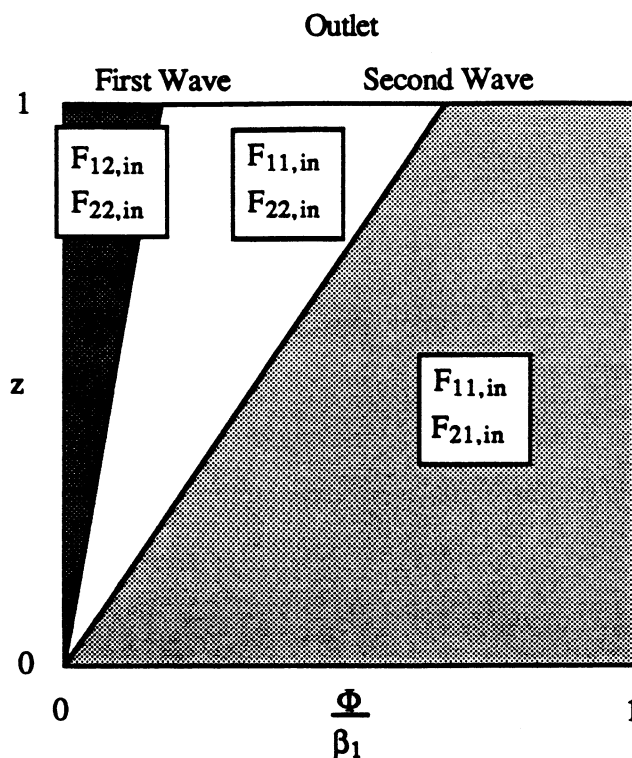


**Figure 4.4** Wave Diagram with Breakthrough of the Second Wave

Figure 4.5 shows the wave diagram of a regenerative heat and mass exchanger operating as an enthalpy exchanger. The objective now is to have the outlet state of stream 1 approach the inlet state of stream 2. This can be achieved only by changing both the  $F_1$  and  $F_2$ -potential of stream 1 as it passes through the regenerator. Since lines of constant  $F_1$ -potential resemble lines of constant enthalpy a change of the  $F_1$ -potential is equivalent to an exchange of the enthalpies between the two fluid streams. The rotation speed and therefore  $\Gamma_1$  is increased in order to decrease the slopes of the wave fronts in a manner that none of the waves breaks through and enthalpy exchange occurs. This can be interpreted as a "reflection" of both the first and second wave

before they reach the outlet of the enthalpy exchanger.

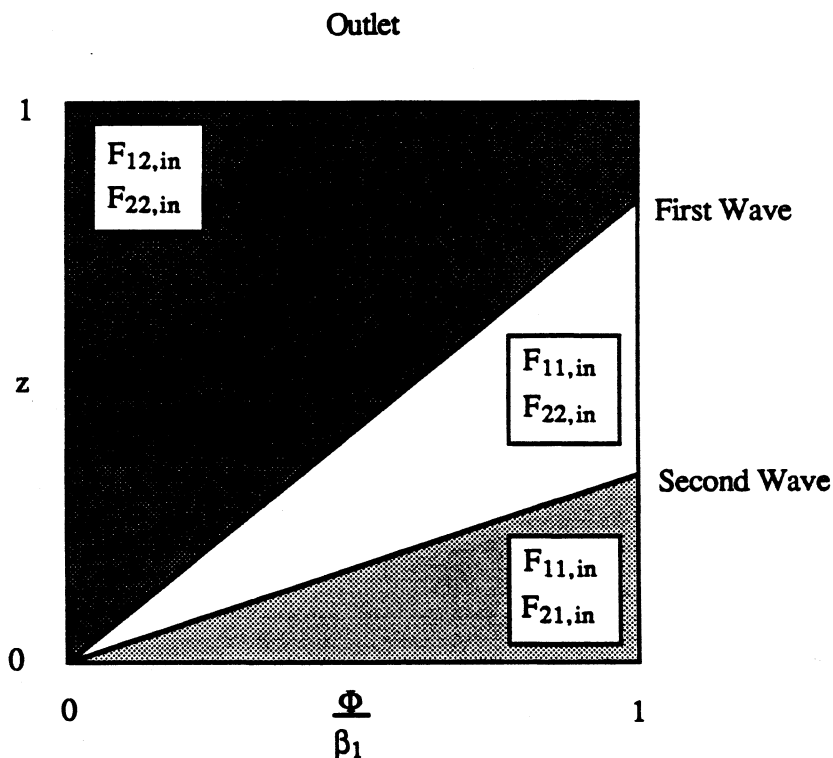


**Figure 4.5** Wave Diagram for Period 1 of an Enthalpy Exchanger

In the case of equilibrium exchange systems with reflected first wave, the outlet state of stream 1 is the same as the inlet of stream 2. The rotation speed of an enthalpy exchanger must be high enough to avoid the breakthrough of the first wave. Beyond that limit a further increase of the rotation speed does not improve the performance of the device but the degree of enthalpy exchange is determined solely by the number of transfer units for both heat and mass transfer.

The equilibrium analysis described above is exact for ideal regenerators with equilibrium between the fluid streams and the matrix and holds approximately for regenerators with high transfer coefficients. Non-equilibrium systems with finite transfer coefficients tend to smear the transfer zones.

### 4.3 ANALOGY METHOD

The analogy of momentum, heat and mass transfer [34] is useful in the analysis of systems with coupled transport phenomena. The coupled set of conservation and transfer rate equations can be transformed to approximately uncoupled form by using the same combined heat and mass transfer potentials presented in Chapter 4.2. Maclaine-cross [13] derived the *combined potentials* and *combined capacitance ratios* using methods of linear algebra and he transformed Equations (2.15)-(2.18) without the assumption of infinite transfer coefficients. The transformed equations are the conservation laws and transfer rate equations of the combined potentials.

#### Conservation Laws

$$\frac{\partial F_{1f}}{\partial z} + \gamma_1 \Gamma_j \beta_j \frac{\partial F_{1m}}{\partial \Phi} = 0 \quad (4.28)$$

$$\frac{\partial F_{2f}}{\partial z} + \gamma_2 \Gamma_j \beta_j \frac{\partial F_{2m}}{\partial \Phi} = 0 \quad (4.29)$$

### Transfer Rate Equations

$$\frac{\partial F_{1f}}{\partial z} = NTU_{1j} (F_{1m} - F_{1f}) \quad (4.30)$$

$$\frac{\partial F_{2f}}{\partial z} = NTU_{2j} (F_{2m} - F_{2f}) \quad (4.31)$$

where

- $F_{if}$  =  $F_i$ -potential at fluid state
- $F_{im}$  =  $F_i$ -potential at matrix state
- $\gamma_i$  = combined capacitance ratio of the  $F_i$ -potential
- $NTU_{ij}$  = number of transfer units of the  $F_i$ -potential at period  $j$

The transformation to uncoupled form requires the following assumptions:

$$\frac{\partial F_{if}}{\partial i_f} = \frac{\partial F_{im}}{\partial i_f}$$

$$Le = 1$$

The first assumption is true for equilibrium systems, i.e the transformation is accurate for systems with high transfer coefficients. In the case of equilibrium between the air stream and the matrix, the transfer rate equations disappear whereas Equations (4.28)-(4.29) become the same as the expressions for the kinematic waves in Equations (4.25)-(4.26). The combined capacitance ratios can be computed as the inverse of the

dimensionless wave speed:

$$\gamma_i = \frac{1}{\lambda_i} \quad i = 1,2 \quad (4.32)$$

The approximately uncoupled Equations (4.28)-(4.31) are analogous to Equations (2.3)-(2.4) for a rotary sensible heat exchanger. The combined potentials correspond to temperatures whereas the combined capacitance ratio is the analogous parameter to the ratio of the heat capacities of the matrix and humid air.

The superposition of two independent  $F_i$ -exchangers is referred to as *analogy method* and is used in this study to compute the outlet of a regenerative heat and mass exchanger. The  $F_i$ -effectiveness is defined as

$$\epsilon_{ij} = \frac{F_{if j,out} - F_{if j,in}}{F_{if 3-j,in} - F_{if j,in}} \quad i = 1,2 \quad j = 1,2 \quad (4.33)$$

Since there is no overall conservation of the combined potentials, the transfer rates of the F-potentials vary from one period to the other and therefore an effectiveness for both periods has to be defined. The computation of the integrating factor introduced in Chapter 4.1 is omitted in this study and therefore the F-potentials cannot be computed as a function of the temperature and humidity. Hence, equation (4.33) is not directly usable.

Jurinak [9] developed curve fits for lines of constant F-potential in a psychrometric chart for the system air-water-silica gel. The author could not find any data for other solid desiccants. Therefore, a simpler approach with the assumption of

linear variation of the potentials with temperature and humidity leads to the *linear analogy solution* [9]. The outlet states of a regenerative heat and mass exchanger can be calculated using the definitions in Equation (4.33) and the states of the intersection point at low absolute humidity:

$$w_{f1,out} = w_{f1,in} + \epsilon_{11} (w_{f2,in} - w_{IP}) + \epsilon_{21} (w_{IP} - w_{f1,in}) \quad (4.34)$$

$$i_{f1,out} = i_{f1,in} + \epsilon_{11} (i_{f2,in} - i_{IP}) + \epsilon_{21} (i_{IP} - i_{f1,in}) \quad (4.35)$$

where

$w_{IP}$  = humidity ratio of the intersection point

$i_{IP}$  = enthalpy of the intersection point

$\epsilon_{i1}$  = effectiveness of  $F_i$  exchanger based on period 1

The intersection points are illustrated in Figure 4.2. In Equations (4.34)-(4.35) the intersection point at low humidity ratio must be used and the temperature at the outlet is computed as a function of humidity and enthalpy.

For the rotary sensible heat exchanger it is assumed that  $\sigma$ , the ratio of the specific heat capacity of the matrix and humid air, does not vary within the temperature range used in this study. The analogous parameter for a regenerative heat and mass exchanger is the combined capacitance ratio  $\gamma_i$  which is the inverse of the non-dimensional wave speed and therefore a function of the state properties. Maclaine-cross [13] describes the proper choice of average values dependent on the rotation speed of the regenerator. Then Equation (2.9) can be used to compute the effectiveness

of the  $F_i$  exchanger using the following parameter instead of  $C_r^*$ :

$$C_{ij} = \bar{\gamma}_{ij} \Gamma_j \quad (4.36)$$

where

$\bar{\gamma}_{ij}$  = average combined capacity ratio

$\Gamma_j$  = ratio of "matrix flow rate" to minimum air flow rate

For low values of  $C_{ij}$ , Equation (2.14) may be used to compute the effectiveness of the  $F_i$ -exchanger.

In the case of a regenerative dehumidifier, it is desirable to have a high  $F_2$  effectiveness and low values for the  $F_1$ -effectiveness in order to produce an outlet state of stream 1 close to the intersection point at low humidity. This can be achieved at medium values of  $\Gamma_j$ . The values of the combined capacitance ratio are the inverse of the wave speeds. Since the  $F_1$  wave is much faster than the  $F_2$  wave,  $\gamma_1$  is much smaller than  $\gamma_2$ . This results in high value of  $C_{2j}$  whereas the values of  $C_{1j}$  are less than one. For equilibrium exchange systems, the inverse of  $C_{ij}$  is the slope of the  $F_i$  wave in a wave diagram as shown in Figure 4.3. Therefore, for medium rotation speeds only the fast wave breaks through resulting in an outlet state close to the intersection point at low humidity ratio. For high values of  $\Gamma_j$ , both  $C_{1j}$  and  $C_{2j}$  become greater than one and therefore none of the waves breaks through. This results in enthalpy exchange between the two air streams.

The linearized analogy method provides a powerful tool to compute the outlet

stream of a regenerative dehumidifier as well as an enthalpy exchanger. The accuracy of the method was studied extensively by Jurinak [9] for the case of medium rotation speed with the desired outlet of stream 1 close to the intersection point at low humidity. The transformation to uncoupled form becomes far more complicated for the case of variable Lewis number and is omitted here. In this study, the number of transfer units are corrected as suggested by Maclaine-cross in order to take into account non-unity Lewis numbers [13]. The accuracy of the linearized analogy method as well the Lewis number correction for enthalpy exchangers is presented in Chapter 5.

#### **4.4 METHOD BASED ON UNCOUPLED TRANSFER RATE EQUATIONS**

The introduction of the F-potentials as new state properties eliminated the coupling of the equations due to coupled thermodynamic equilibrium relationships. Whereas the humidity ratio can change only by mass transfer, energy changes are due to both sensible heat and mass transfer. Hence, the energy transfer rate in Equation (2.18) is the sum of two terms. In the case of fast rotating regenerative heat and mass exchangers, the outlet states can be computed using the approximation of uncoupled transfer rate equations.

##### **4.4.1 The Case of Infinite Rotation Speed**

Infinite rotation speed is equivalent to an infinitely high value of the dimensionless parameter  $\Gamma_j$ . After rearranging Equation (2.15) and (2.17), the conservation laws for infinite rotation speed can be written as follows:

$$\frac{\partial W_m}{\partial \Phi} = 0$$

$$\frac{\partial I_m}{\partial \Phi} = 0$$

The matrix water content and temperature become independent of the rotation angle and the partial differential equations simplify to a system of ordinary differential equations.

#### Mass Conservation

$$\dot{m}_{f1} \frac{dw_{f1}}{dz} - \dot{m}_{f2} \frac{dw_{f2}}{dz} = 0 \quad (4.37)$$

#### Mass Transfer Rate

$$\frac{dw_{fj}}{dz} = NTU_{wj} (w_m - w_{fj}) \quad (4.38)$$

#### Energy Conservation

$$\dot{m}_{f1} \frac{di_{f1}}{dz} - \dot{m}_{f2} \frac{di_{f2}}{dz} = 0 \quad (4.39)$$

### Energy Transfer Rate

$$\frac{di_{fj}}{dz} = c_A NTU_{tj} (t_m - t_{fj}) + i_{wj} NTU_{wj} (w_m - w_{fj}) \quad (4.40)$$

Equations (4.37)-(4.40) are for counterflow. The humidity ratio in equilibrium with the matrix and the matrix temperature are the only matrix properties in the model equations of an enthalpy exchanger with infinite rotation speed. These properties can be eliminated in the transfer rate expressions whereas the enthalpies in the energy balance are replaced by the fluid temperatures:

$$\frac{dw_{f1}}{dz} - \frac{\dot{m}_{f2}}{\dot{m}_{f1}} \frac{dw_{f2}}{dz} = 0 \quad (4.41)$$

$$\frac{dw_{f1}}{dz} + \frac{\dot{m}_{f2}}{\dot{m}_{f1}} \frac{dw_{f2}}{dz} - NTU_{w1} (w_{f2} - w_{f1}) = 0 \quad (4.42)$$

$$i_{w1} \frac{dw_{f1}}{dz} + c_A \frac{dt_{f1}}{dz} - \frac{\dot{m}_{f2}}{\dot{m}_{f1}} \left( i_{w2} \frac{dw_{f2}}{dz} + c_A \frac{dt_{f2}}{dz} \right) = 0 \quad (4.43)$$

$$\frac{dt_{f1}}{dz} + \frac{\dot{m}_{f2}}{\dot{m}_{f1}} \frac{dt_{f2}}{dz} - NTU_{t1} (t_{f2} - t_{f1}) = 0 \quad (4.44)$$

This new set of ordinary differential equations is still coupled since the enthalpy of the transferred water vapor is a function of both the temperature and humidity ratio.

Equation (4.41)-(4.44) were solved along with Equation (3.4) as the expression

for the enthalpy of the water vapor. The numerical integration was accomplished using the integration and parametric sensitivity analysis package DDASAC<sup>2</sup> [35,36]. The counterflow arrangement causes a two point boundary value problem and an iterative integration scheme was required. The *sensitivity coefficients* are the partial derivatives of state properties with respect to one model parameter and are defined as follows:

$$W_{11} = \frac{\partial t_{f1}}{\partial NTU_{t1}}$$

$$W_{12} = \frac{\partial t_{f2}}{\partial NTU_{t1}}$$

$$W_{21} = \frac{\partial t_{f1}}{\partial NTU_{w1}}$$

$$W_{22} = \frac{\partial t_{f2}}{\partial NTU_{w1}}$$

Table 4.1 shows the results obtained using DDASAC for one particular set of parameters and a pair of inlet states.

---

<sup>2</sup>DDASAC stands for Double Precision Differential Algebraic Sensitivity Analysis Code

**Table 4.1** Parametric Sensitivity Coefficients at the Outlet of an Enthalpy Exchanger with Infinite Rotation Speed

Coefficient	Values Computed by DDASAC
$W_{11}$	-0.571
$W_{12}$	-0.571
$W_{21}$	-0.00108
$W_{22}$	-0.00251

The sensitivities of the air outlet temperatures to the number transfer units for mass transfer ( $W_{21}, W_{22}$ ) are two orders of magnitude less than the sensitivities to the number of transfer units for heat transfer ( $W_{11}, W_{12}$ ). This indicates that only about one percent of the total energy is latent energy transferred with the water vapor stream. This led to the assumption that all energy is transferred via temperature gradients. The change of the latent term of the air enthalpy in Equation (4.43) is neglected and the equations become uncoupled:

$$\frac{dt_{f1}}{dz} - \frac{\dot{m}_{f2}}{\dot{m}_{f1}} \frac{dt_{f2}}{dz} = 0 \quad (4.45)$$

$$\frac{dt_{f1}}{dz} + \frac{\dot{m}_{f2}}{\dot{m}_{f1}} \frac{dt_{f2}}{dz} - NTU_{t1} (t_{f2} - t_{f1}) = 0 \quad (4.44)$$

The approximation of uncoupled heat and mass transfer simplifies the analysis of enthalpy exchangers with infinite rotation speed. Both Equations (4.41)-(4.42) and (4.44)-(4.45) are a set of independent equations each analogous to the balance and transfer rate expressions of a counterflow direct type heat exchanger. The outlet states of the air streams can be computed conveniently using the humidity and temperature effectiveness:

$$\epsilon_w = \frac{w_{fj,out} - w_{fj,in}}{w_{f3-j,in} - w_{fj,in}} \quad (4.46)$$

$$\epsilon_t = \frac{t_{fj,out} - t_{fj,in}}{t_{f3-j,in} - t_{fj,in}} \quad (4.47)$$

In the case of infinite rotation speed and balanced flow arrangement, the humidity effectiveness can be computed using the correlation of the counterflow direct heat exchanger along with the appropriate number of transfer units [2]:

$$\epsilon_w = \frac{NTU_0}{1 + NTU_0} \quad (4.48)$$

where

$$NTU_0 = \frac{NTU_w}{2}$$

The number of transfer units for heat transfer can be expressed in terms of the overall

Lewis number and the number of transfer units for mass transfer:

$$\varepsilon_t = \frac{NTU_0}{1 + NTU_0} \quad (4.49)$$

where

$$NTU_0 = Le \frac{NTU_w}{2}$$

#### 4.4.2 Wave Diagram and Infinite Rotation Speed

The computational simplicity of the method described above led to the idea of predicting the outlet states of an enthalpy exchanger using Equations (4.48)-(4.49). For equilibrium systems the performance of a regenerative heat and mass exchanger can be illustrated in wave diagrams introduced in Section 4.2.2. Equation (4.27) determines the slope of the two transfer waves propagating through the matrix:

$$\frac{dz}{d(\Phi/\beta_j)} = \frac{\lambda_i}{\Gamma_j} \quad i = 1,2 \quad (4.27)$$

In the case of infinite rotation speed the slopes of both the first and second wave fronts become zero as shown in Figure 4.6. None of the wave fronts moves through the matrix and can be considered to be stagnant. The axial flow position of the wave fronts depend on the initial conditions. The outlet of stream 1 is equal to the inlet state of stream 2 which is equivalent to a humidity and temperature effectiveness in

Equations (4.46)-(4.47) of one.

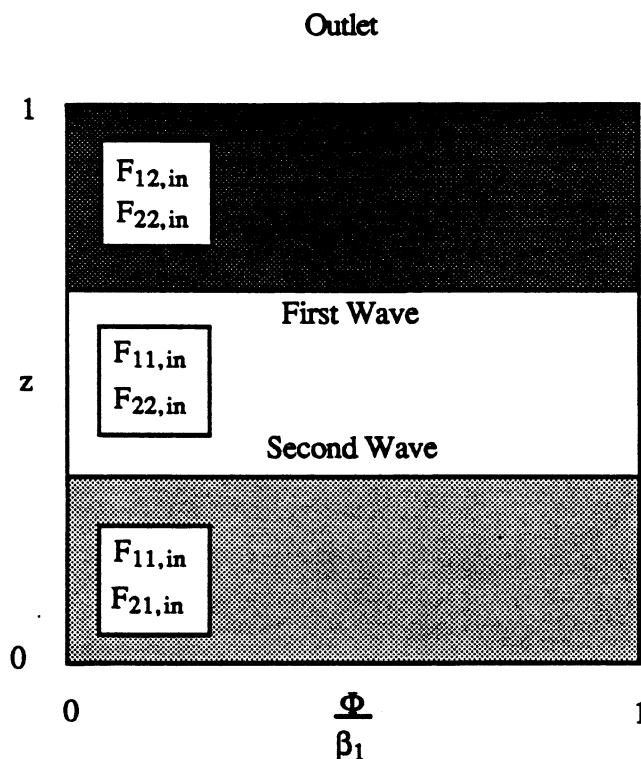


**Figure 4.6** Wave Diagram for Period 1 of an Enthalpy Exchanger with Infinite Rotation Speed

Comparison with Figure 4.5 indicates that the outlet state of regenerators with infinite transfer coefficients reaches the inlet of the other stream even for finite rotation speed, as long as the second wave does not break through. In Chapter 5 the range where Equations (4.46)-(4.49) can be used to predict the outlet of an enthalpy exchanger with finite rotation speed and finite transfer coefficients is investigated by using the finite difference solution described in Chapter 4.1 as a reference solution.

---

Chapter 5

**Model Comparison and Parametric Studies**

---

The performance of regenerative dehumidifiers and enthalpy exchangers is determined by the system parameters and the inlet states and mass flow rates of the two air streams. This chapter presents a comparison of the solution methods described in Chapter 4 for a wide range of system parameters. Two pairs of inlet conditions were chosen in order to represent typical air inlet states of a regenerative dehumidifier and an enthalpy exchanger, respectively.

### 5.1 MODEL PARAMETERS AND INLET CONDITIONS

The case of balanced flow streams is important for energy recovery applications. In contrast the performance of a regenerative dehumidifier in a solid desiccant cooling cycle is improved if the flow rates of the two air streams entering the regenerator are different [30]. In this study, only balanced flows are considered which reduces the number of model parameters. Furthermore, it is assumed that the two period fractions,  $\beta_1$  and  $\beta_2$ , are equal such that both the areas for heat and mass transfer and the transfer coefficients are the same for both periods. With these assumptions the following parameters determine the performance characteristics of a regenerative heat and mass exchanger:

$\Gamma$	ratio of "matrix flow rate" to air flow rate
$NTU_t$	overall number of transfer for heat transfer
$Le = \frac{NTU_t}{NTU_w}$	overall Lewis number
$c_m$	specific heat capacity of the matrix

#### Adsorption isotherm correlation of the solid desiccant

Adsorption hysteresis is excluded in this study and therefore the matrix parameters described above are sufficient to model the thermodynamic behavior of a sorptive matrix<sup>1</sup>, as illustrated in Chapter 3.2. The analysis is limited to humid air streams and therefore thermodynamic quantities such as specific heat capacity of dry air and water vapor or the heat of vaporization of liquid water are not model parameters.

Two pairs of inlet states used in this parametric study were chosen and are referred to as pair 1 and pair 2. The temperatures and humidity ratios were taken as follows:

---

<sup>1</sup>Parameters such as maximum water content and differential heat of adsorption are determined by the isotherm correlation whereas heat conductance and moisture diffusivity are considered in the overall number of transfer units.

$$\begin{aligned}
 \text{Pair 1} \quad t_{f1,in} &= 35 \text{ }^\circ\text{C} \\
 w_{f1,in} &= 0.0142 \text{ kgW/kgDA} \\
 t_{f2,in} &= 85 \text{ }^\circ\text{C} \\
 w_{f2,in} &= 0.0142 \text{ kgW/kgDA}
 \end{aligned}$$

$$\begin{aligned}
 \text{Pair 2} \quad t_{f1,in} &= 25 \text{ }^\circ\text{C} \\
 w_{f1,in} &= 0.010 \text{ kgW/kgDA} \\
 t_{f2,in} &= 35 \text{ }^\circ\text{C} \\
 w_{f2,in} &= 0.020 \text{ kgW/kgDA}
 \end{aligned}$$

Pair 1 represents typical inlet conditions of a regenerative dehumidifier operating in a ventilation cycle shown in Figure 1.1 [9]. Pair 2 is an example for inlet conditions of an enthalpy exchanger used as a energy recovery unit as illustrated in Figure 1.5. The colder stream represents indoor conditions which are within the thermal comfort range specified by ASHRAE [27], whereas the hotter stream is typical for outdoor conditions in a hot and humid summer climate such as Jacksonville, Florida [37]. Outdoor conditions which represent typical cold winter climates are discussed in Chapter 6.

## 5.2 EFFECT OF ROTATION SPEED AND NUMBER OF TRANSFER UNITS

In Chapter 4, two methods were derived to uncouple the set of partial differential equations introduced in Chapter 2. The assumption of infinite transfer coefficients was

required to introduce new uncoupled state properties called combined heat and mass transfer potentials. In the case of infinite rotation speed, the partial differential equations simplify to a set of ordinary differential equations which can be solved using the  $\epsilon$ -NTU correlations for a counterflow direct type heat exchanger [2]. Both methods are idealizations and the validation of models based on these approximations can be obtained only by comparison with either experimental data or with a numerical solution of the complete set of uncoupled Equations (2.15)-(2.22).

The finite difference solution described in Chapter 4.1 and implemented in the MOSHMX program was used as a reference solution throughout this chapter. Figure 5.1 shows the outlet states of stream 1 in a psychrometric chart as predicted by MOSHMX for a regenerative heat and mass exchanger with a high number of transfer units and various rotation speeds.

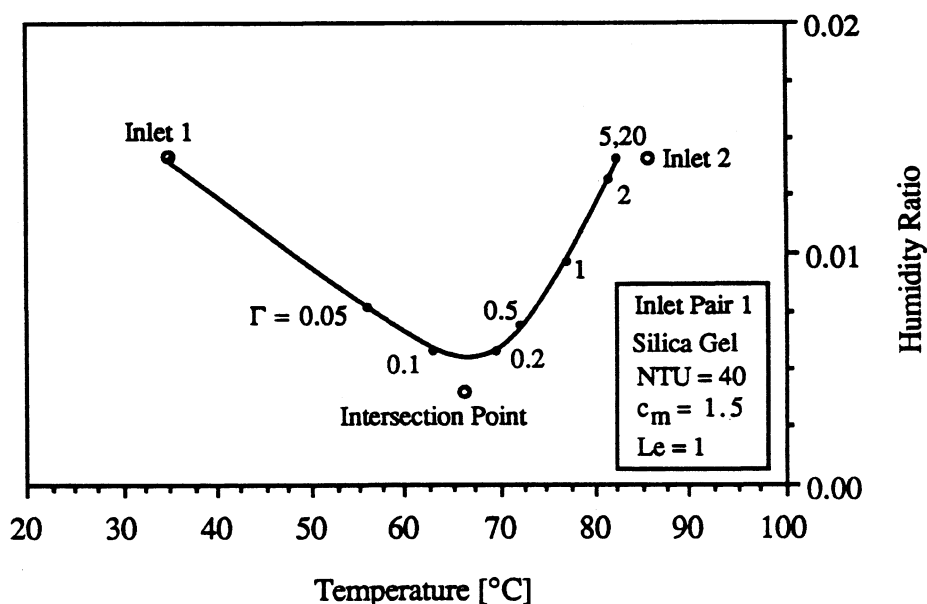


Figure 5.1 Outlet States of Stream 1 as Computed by MOSHMX for High NTU

It can be seen that at medium rotation speeds, equivalent to values of  $\Gamma$  between 0.1 and 0.2, the highest degree of dehumidification can be achieved. The regenerator is operating as a regenerative dehumidifier with a breakthrough of the first wave and a reflection of the second wave, as described in Chapter 4.2. At higher values of  $\Gamma$ , the outlet of stream 1 approaches the inlet of stream 2 and the device is operating as an enthalpy exchanger. The simulations were done for values of  $\Gamma$  up to 20 since the predicted outlet states do not change for higher values of  $\Gamma$ .

A regenerative heat and mass exchanger with NTU equals 40 can be considered as a system which is close to thermodynamic equilibrium. Simulations using higher values for the number of transfer units were omitted in this study since an increase in the number of transfer units requires smaller discretization of the finite difference grid in order to maintain the same accuracy.

Figure 5.1 indicates that the outlet of stream 1 at medium rotation speed does not reach the intersection point at low humidity. This is due to the fact that, for a small portion of the dehumidifier outlet, the air state is determined by the breakthrough of the first wave which carries the hot inlet state of stream 2.

Figures 5.2 and 5.3 show the variation of the outlet state of stream 1 with  $\Gamma$  for lower values of NTU. The effect of the rotation speed is the same as described above, but both the degree of dehumidification and enthalpy exchange are reduced due to decreased heat and mass transfer ratios between the air streams and the matrix.

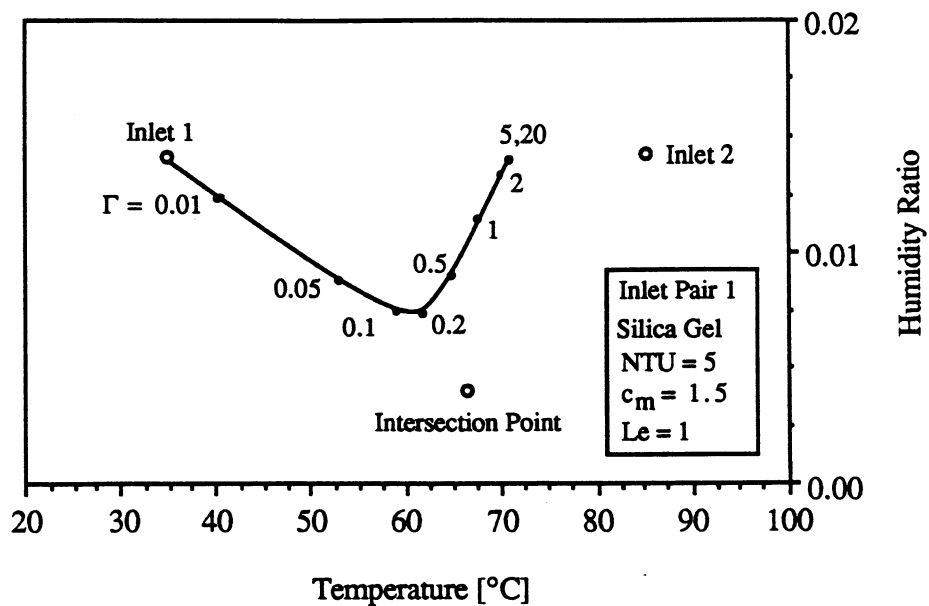


Figure 5.2 Outlet States of Stream 1 as Computed by MOSHMX for Medium NTU

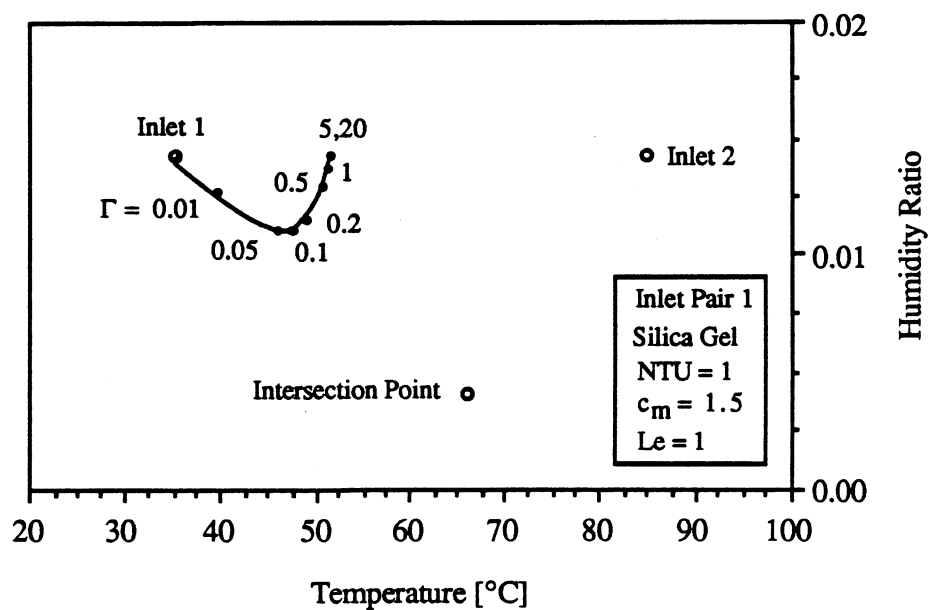
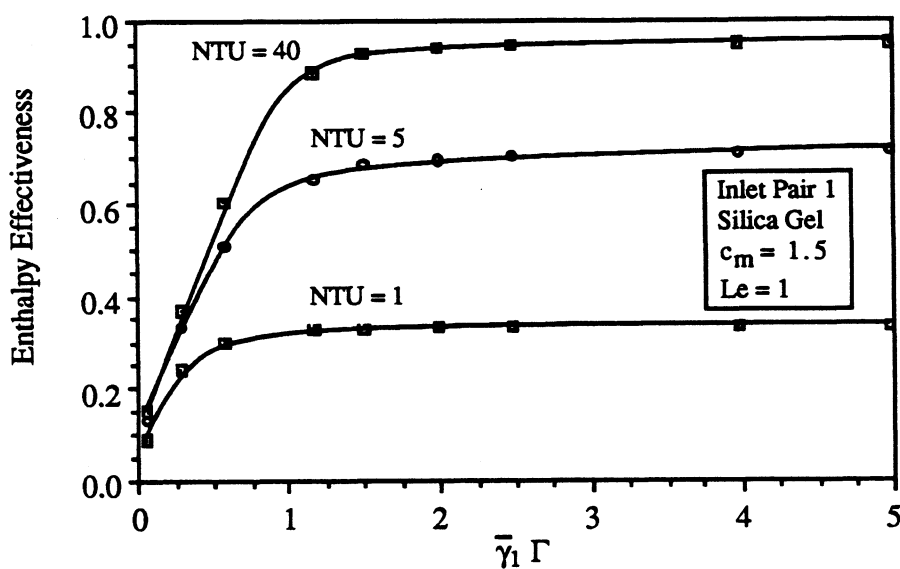


Figure 5.3 Outlet States of Stream 1 as Computed by MOSHMX for Low NTU

A convenient measure for the approach of the outlet of stream 1 to the inlet of stream 2 is the enthalpy effectiveness which can be expressed as

$$\epsilon_i = \frac{\dot{i}_{f1,out} - \dot{i}_{f1,in}}{\dot{i}_{f2,in} - \dot{i}_{f1,in}}$$

Figure 5.4 shows the enthalpy effectiveness computed by MOSHMX as a function of the rotation speed and the number of transfer units.



**Figure 5.4** Enthalpy Effectiveness as Computed by MOSHMX as a Function of  $\bar{\gamma}_1 \Gamma$  and the Number of Transfer Units

The product  $\bar{\gamma}_1 \Gamma$  was chosen as the independent axis. The average combined capacity ratio,  $\bar{\gamma}_1$ , was computed as the reciprocal of the non-dimensional wave speed  $\lambda_1$  of the

first wave at the average state of the two inlet streams, as suggested by Maclaine-cross [13]. Therefore, a value of the independent axis can be interpreted as the reciprocal of the slope of the first wave front in a wave diagram described in Chapter 4.2.

For the ideal case of sharp wave fronts in equilibrium exchange systems, the first wave is reflected if the slope of the first wave front is smaller than one. Therefore the enthalpy effectiveness becomes independent of the rotation speed if  $\bar{\gamma}_1 \Gamma > 1.0$ .

Figure 5.4 indicates that for  $\bar{\gamma}_1 \Gamma > 1.5$  the enthalpy effectiveness can be considered to be a function of the number of transfer units only. This is consistent with the wave theory for equilibrium exchange systems. The wave diagrams shown in Chapter 4.2 are based on the assumption of constant  $\lambda_1$  and  $\lambda_2$  at each period. The values of the dimensionless wave speeds, however, depend on the thermodynamic state properties of the air-water-desiccant system and must be computed by solving the quadratic expression in Equation (4.20). Therefore, the two wave fronts propagating through the system are broadened, as illustrated in Figure 5.5. Van den Bulck [14] considered the case of broadened wave fronts in order to compute the outlet states of a regenerative dehumidifier and called the broadened wave fronts  $F_{1\text{-fan}}$  and  $F_{2\text{-fan}}$ . For the combination of inlet states in desiccant cooling cycle applications the wave theory shows that at the regeneration period shock waves with sharp wave fronts occur. The broadening of these wave fronts is due to the finite number of transfer units.

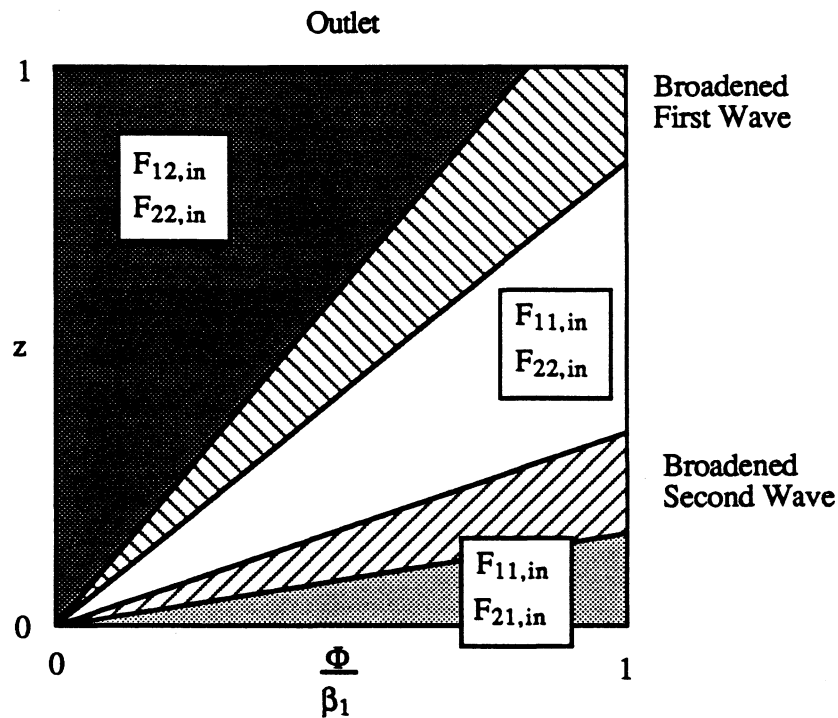


**Figure 5.5** Wave Diagram with Broadened Wave Fronts

The average combined capacity ratio is fixed by the inlet states and the thermodynamic behavior of the system air-water-desiccant. In order to achieve optimal enthalpy exchange between the two air streams, the operating parameter  $\Gamma$  has to be determined such that the product  $\bar{\gamma}_1 \Gamma$  exceeds the value where the curves in Figure 5.4 becomes a horizontal line and independent of the abscissa, which is about 1.5.

The curves in Figure 5.4 were obtained using inlet pair 1 and a specific heat capacity of the matrix of 1.5 kJ/kg°C. The parameters result in a value for the average combined capacity ratio of about 0.5. Thus, the value of the non-dimensional parameter  $\Gamma$  must be at least 3.0 in order to achieve an enthalpy effectiveness which is

determined solely by the number of transfer units and the Lewis number.

It was shown in Chapter 4.4 that the outlet of an enthalpy exchanger with infinite rotation speed can be computed using the effectiveness correlations for a counterflow direct type heat exchanger. Figure 5.6 shows the error of the predicted outlet temperatures and humidities computed with the counterflow heat exchanger effectiveness correlations compared to the finite difference solution. The errors are very large for low and medium rotation speeds but decrease rapidly as the reciprocal of the slope of the first wave front approaches the range where the regenerator is operating as an enthalpy exchanger. Therefore, the counterflow effectiveness correlations can be used to predict the outlet states of enthalpy exchangers if they are designed and operated at high rotational speeds.

The analysis of an enthalpy exchanger with given values for the number of transfer units, the Lewis number and the specific heat capacity of the matrix as well as a known adsorption isotherm correlation for the desiccant is a twofold problem:

1. Determination of the average combined capacity ratio

$$\bar{\gamma}_1 = \frac{1}{\lambda_1}$$

where  $\lambda_1$  is the larger of the two solutions of Equation (4.20) using the average of the inlet states. Then the non-dimensional operating parameter  $\Gamma$  can be determined such that  $\bar{\gamma}_1 \Gamma > 1.5$ . The values of  $\bar{\gamma}_1$  are in the range of 0.5 to 1.0, depending on the inlet conditions.

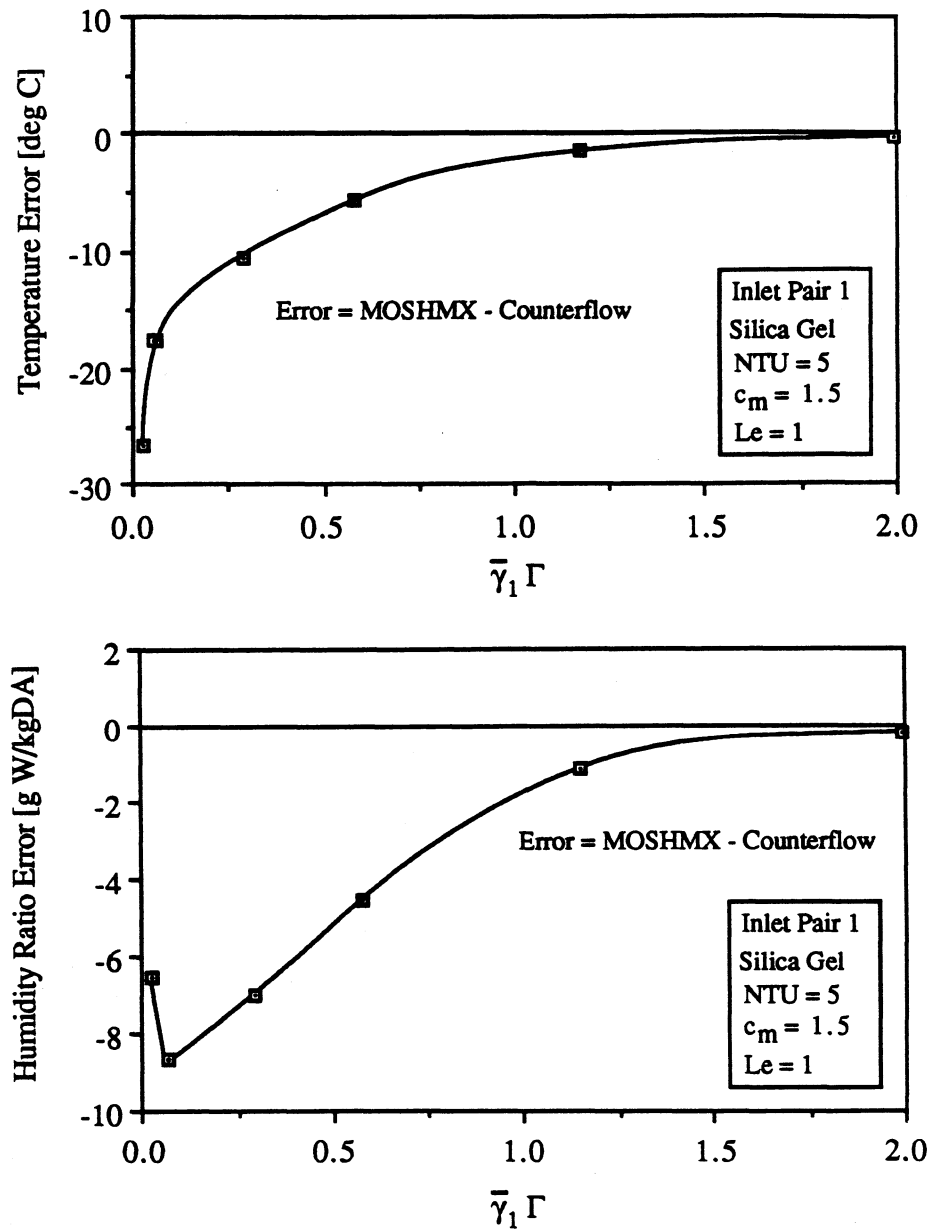


**Figure 5.6** Absolute Errors in Outlet States Computed with Counterflow Heat Exchanger Correlations Compared to MOSHMX

2. Determination of the temperature and humidity effectiveness using Equations (4.48)-(4.49) and computation of the outlet states using Equations (4.46)-(4.47).

Figure 5.7 illustrates the variation of the outlet states of stream 1 of an enthalpy exchanger with the number of transfer units in a psychrometric chart.

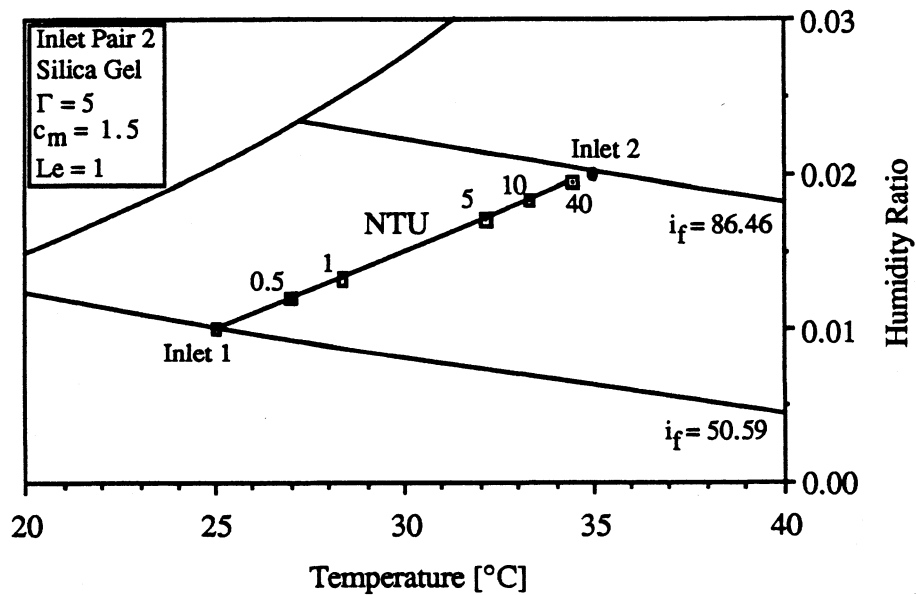


**Figure 5.7** Outlet States of an Enthalpy Exchanger Computed Using Counterflow Heat Exchanger Correlations

The average capacity ratio  $\bar{\gamma}_1$  was computed using the average of the inlet states of inlet Pair 2 (30°C and 0.015 kgW/kgDA). For a silica gel matrix with a specific heat capacity of 1.5 kJ/kg°C the value for  $\bar{\gamma}_1$  was computed to be 0.62. In the simulations

used to construct Figure 5.7, a value of 5 was chosen for the dimensionless parameter  $\Gamma$  which results in value of  $\bar{\gamma}_1 \Gamma$  of 3.1. This value of  $\bar{\gamma}_1$  can be considered to be in the range where the degree of enthalpy exchange depends on the number of transfer units only. Thus, the  $\epsilon$ -NTU correlations for counterflow heat exchangers were used to compute the outlet states of the system. The computed outlet states lie on a straight line connecting the two inlet states if the Lewis number is one. The effect of the Lewis number is discussed in Chapter 5.4.

The approach to thermodynamic equilibrium for increasing number of transfer units is shown in Figure 5.8.

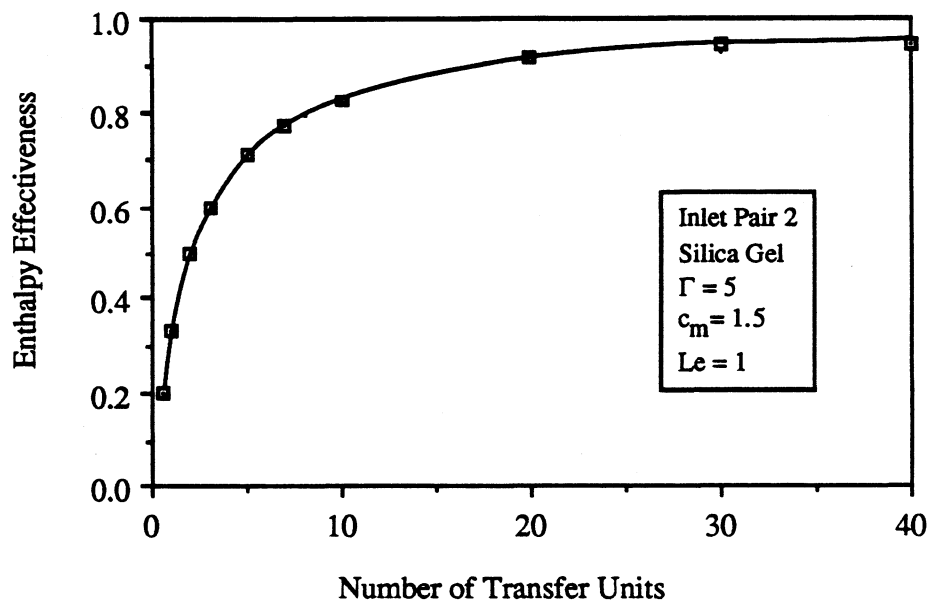


**Figure 5.8** Enthalpy Effectiveness as a Function of the Number of Transfer Units

Whereas the counterflow direct type heat exchanger correlations provide a powerful tool to compute the outlet states of a regenerative heat and mass exchanger

operating as an enthalpy exchanger, the method fails at rotation speeds where the first wave breaks through and dehumidification occurs. The counterflow heat exchanger analogy assumes that the outlet states lie on a straight line between the inlet states, which is not the case for dehumidifier applications.

The linear analogy solution described in Chapter 4.3 assumes the outlet states on straight lines between the inlet states and the intersection points. Therefore, this method is also applicable for systems operating as a regenerative dehumidifier. Figure 5.9 shows the outlet states of stream 1 computed by the finite difference solution and the linear analogy method.

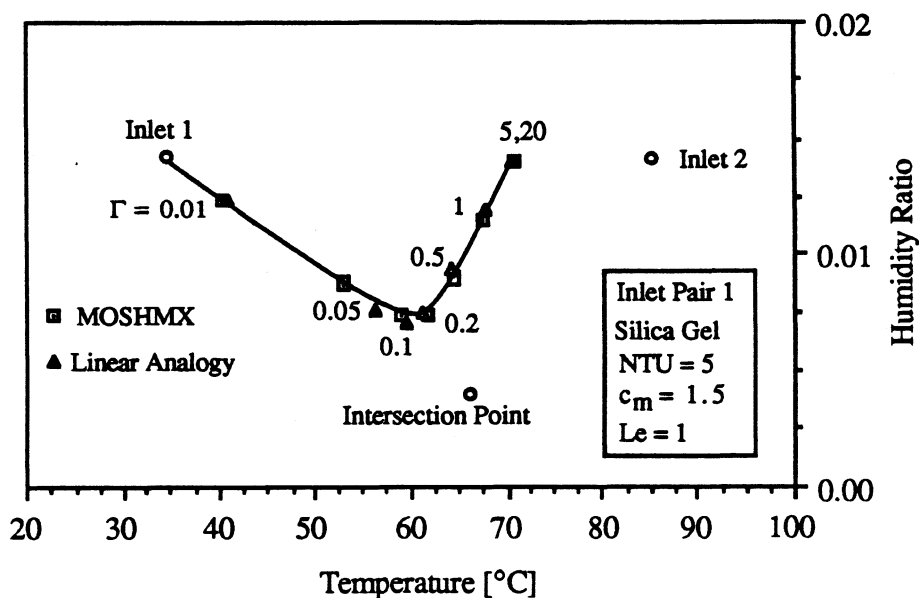


**Figure 5.9** Comparison of MOSHMX and the Linear Analogy Solution

Tables 5.1 and 5.2 show the CPU times required for simulations using the different solution methods. The simulations were done on a Micro VAX computer.

**Table 5.1** Comparison of Required CPU Times for the Solution Methods Used in this Study for Medium Number of Transfer Units

Inlet Pair 1    Silica Gel    NTU = 5 $c_m = 1.5 \text{ kJ/kg}^\circ\text{C}$ Le = 1			
$\Gamma$	MOSHMX	Linear Analogy Solution	Counterflow Heat Exchanger Correlations
0.2	34.01 sec	1.55 sec	-
5	15.60 sec	1.44 sec	0.05 sec

**Table 5.2** Comparison of Required CPU Times for the Solution Methods Used in this Study for High Number of Transfer Units

Inlet Pair 1    Silica Gel    NTU = 40 $c_m = 1.5 \text{ kJ/kg}^\circ\text{C}$ Le = 1			
$\Gamma$	MOSHMX	Linear Analogy Solution	Counterflow Heat Exchanger Correlations
0.2	2:43.20 sec	1.46 sec	-
5	1:00.66 sec	1.37 sec	0.05 sec

The finite difference solution includes algorithms to determine the number of space and time steps, as described in Chapter 4.1. Therefore, the CPU time varies with the rotation speed and the number of transfer units. The number of required time steps can be considered to be proportional to the slope of the first wave front in a wave diagram. Thus, the computation time is reduced if the first wave is reflected and the regenerative heat and mass exchanger is operating as an enthalpy exchanger. Increasing number of transfer units causes an increase of the CPU time due to higher heat and mass transfer ratios and steeper property profiles at the inlet faces of the regenerator.

The linear analogy solution computes the outlet states using the algebraic expressions in Equations (4.34)-(4.35). Numerical integration of Equation (4.21) yields the two intersection points. A fourth order Runge-Kutta method was used in this study to integrate the ordinary differential equation starting at the two inlet states. This integration method reduces the computational effort compared to the two dimensional integration of the partial differential equations performed in the finite difference scheme.

Finally, the use of the counterflow heat exchanger correlations does not require any numerical integration. The method was not used to compute the outlet of the regenerative dehumidifier ( $\Gamma = 0.2$ ) since the error becomes too big. For enthalpy exchangers, however, the method is accurate and reduces the requires the least CPU time of the three methods.

### 5.3 EFFECT OF MATRIX PARAMETERS

The effect of the matrix properties on the outlet states of a regenerative heat and mass exchanger is not as apparent as the influence of the rotation speed or the number of transfer units. The finite difference solution is affected by the adsorption characteristics and thermal capacity of the matrix since several coefficients of the matrix  $A$  in Equation (4.12) depend on the derivatives of desiccant properties. In the equilibrium theory, the non-dimensional wave speeds  $\lambda_1$  and  $\lambda_2$  are computed as the solutions of Equation (4.20) and are functions of the matrix parameters. Thus, the slopes of the wave fronts in a wave diagram are determined by both the rotation speed and the thermodynamic properties of the system air-water-desiccant.

#### 5.3.1 Specific Heat Capacity

Figure 5.10 illustrates the dependence of the wave speeds on the specific heat capacity of the matrix. The wave speeds were computed as a function of the specific heat capacity  $c_m$  by solving Equation (4.20). All other parameters were kept constant. The temperature and humidity ratio were taken at the average of the inlet pair 2. For increasing specific heat capacities,  $\lambda_2$  decreases moderately, but  $\lambda_1$  is significantly lowered. This behavior can be visualized by interpreting  $c_m$  as the "resistance" of the matrix against the propagation of the transfer waves.

In the case of sensible heat transfer only, the coefficients  $a_1$ ,  $a_2$  and  $a_4$  become zero and Equation (4.20) simplifies to a linear equation which has only one solution for the wave speed:

$$\lambda = \frac{c_A}{c_m}$$

i.e., the transfer mechanism is determined by only one wave front which is propagating through the matrix at speed  $\lambda$ .

The wave speed of the first wave in a regenerative heat and mass exchanger does not become infinite for  $c_m$  approaching zero since the first wave is not a heat transfer wave but a wave carrying the  $F_1$ -potential. Lines of constant  $F_1$  do resemble lines of constant enthalpy but are not exactly the same.

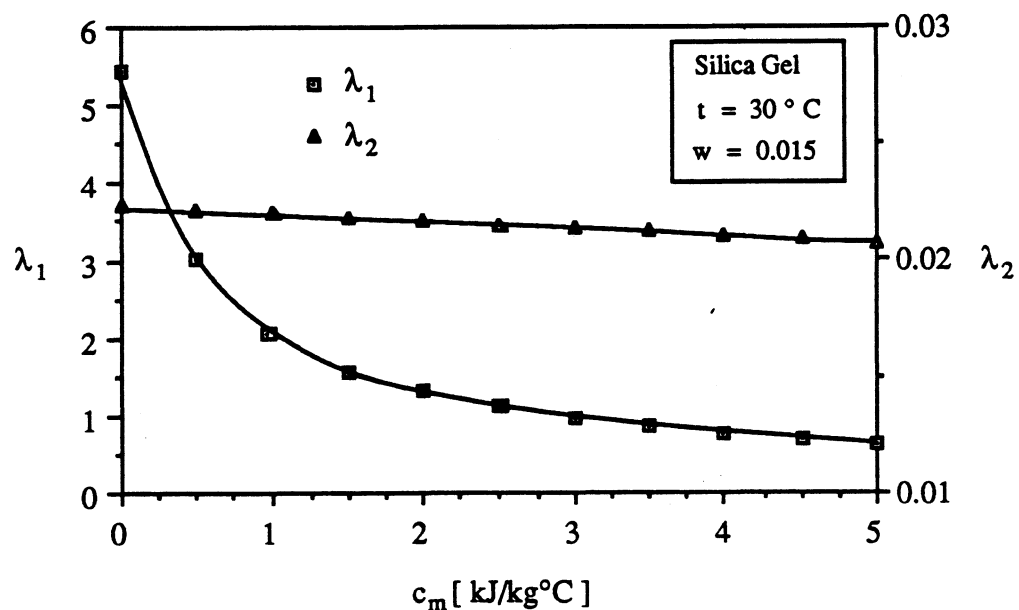


**Figure 5.10** Dimensionless Wave Speeds as a Function of the Specific Heat Capacity of the Matrix

The wave speed  $\lambda_1$  of the first wave is about two orders of magnitude greater than the wave speed  $\lambda_2$  of the second wave. The slope of the  $i^{\text{th}}$  wave front in a wave diagram can be computed as a function of the wave speed  $\lambda_i$  and the dimensionless parameter  $\Gamma$ :

$$m_i = \frac{dz}{d(\Phi/\beta)} = \frac{\lambda_i}{\Gamma} \quad i = 1,2 \quad (5.1)$$

The derivative of the slope with respect to the specific heat capacity is a convenient measure to describe the effect of  $c_m$  on the performance of a regenerative heat and mass exchanger:

$$\frac{\partial m_i}{\partial c_m} = \frac{1}{\Gamma} \frac{\partial \lambda_i}{\partial c_m} \quad i = 1,2 \quad (5.2)$$

Explicit expressions for the derivatives could be obtained from the solutions of Equation (4.20). In this study, however, the ratio  $\psi$  is used along with the following approximation:

$$\psi = \left( \frac{\frac{\partial m_1}{\partial c_m}}{\frac{\partial m_2}{\partial c_m}} \right) = \frac{\partial m_1}{\partial m_2} \approx \frac{\Delta m_1}{\Delta m_2} = \frac{\Delta \lambda_1}{\Delta \lambda_2} \quad (5.3)$$

It can be seen from Figure 5.10 that the variation of the second wave speed with the specific heat capacity is much smaller than the variation of the speed of the first wave.

For the range between 0.5 and 1.5 kJ/kg°C the following values were obtained:

$$\Delta\lambda_1 = 1.41$$

$$\Delta\lambda_2 = 0.0003$$

$$\psi = 4700$$

The slope of the first wave is much more sensitive to the specific heat capacity of the matrix than the second wave, consistent to the fact that the first wave is frequently referred to as *heat transfer wave* whereas the slower second wave is called *mass transfer wave* [29].

In the case of a regenerative dehumidifier the breakthrough of the first wave and the reflection of the second wave can be achieved with high values for  $\lambda_1$  and low values for  $\lambda_2$ . Since the wave speed of the second wave is less sensitive to the specific heat capacity of the matrix, low values of  $c_m$  minimize the part of the outlet which is determined by the breakthrough of the hot first wave without having a breakthrough of the second wave. Therefore, low values for the specific heat capacity are required for high performance regenerative dehumidifiers. Figure 5.11 shows that the degree of dehumidification is reduced if the specific heat capacity of the matrix is increased from 1.5 to 3.0 kJ/kg°C whereas the curves superimpose for higher rotation speeds.

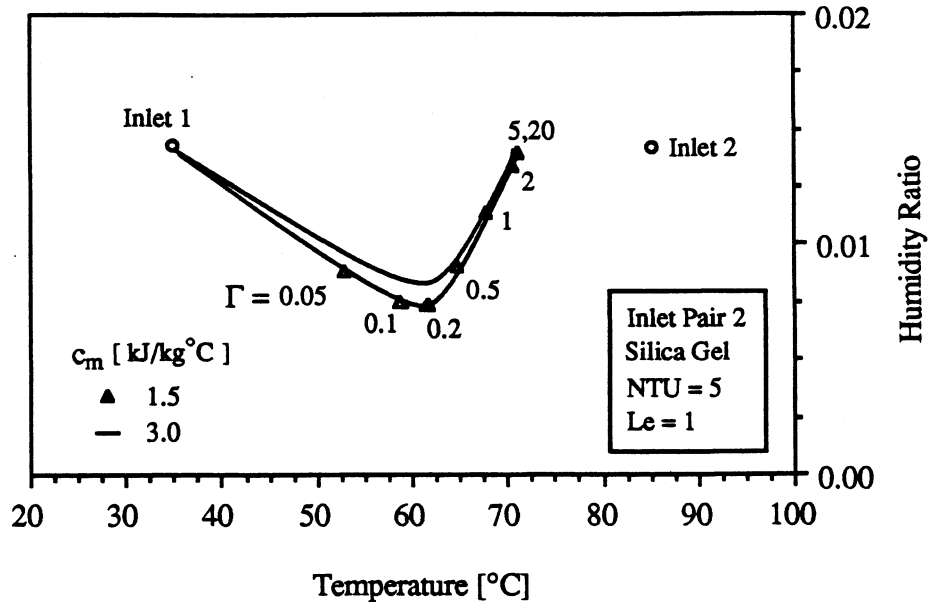


**Figure 5.11** Outlet States of Stream 1 as Computed by MOSHMX for Different Specific Heat Capacities of the Matrix

Enthalpy exchange occurs if both the fast and the slow waves are reflected. Hence, low values for  $\lambda_1$  and  $\lambda_2$  are advantageous for regenerators operating as enthalpy exchangers. Figure 5.12 depicts the effect of the specific heat capacity of the matrix on the enthalpy effectiveness. The non-dimensional parameter  $\Gamma$  was chosen as the independent axis. For lower values of  $c_m$ , the regenerator must be rotating at higher speed in order to avoid a breakthrough of the first wave which would reduce the enthalpy effectiveness. Decreasing values of  $c_m$  cause higher values of the wave speed of the first wave. This must be compensated by increased values of  $\Gamma$  such that the slope of the wave front decreases and the wave is reflected back before a breakthrough occurs.

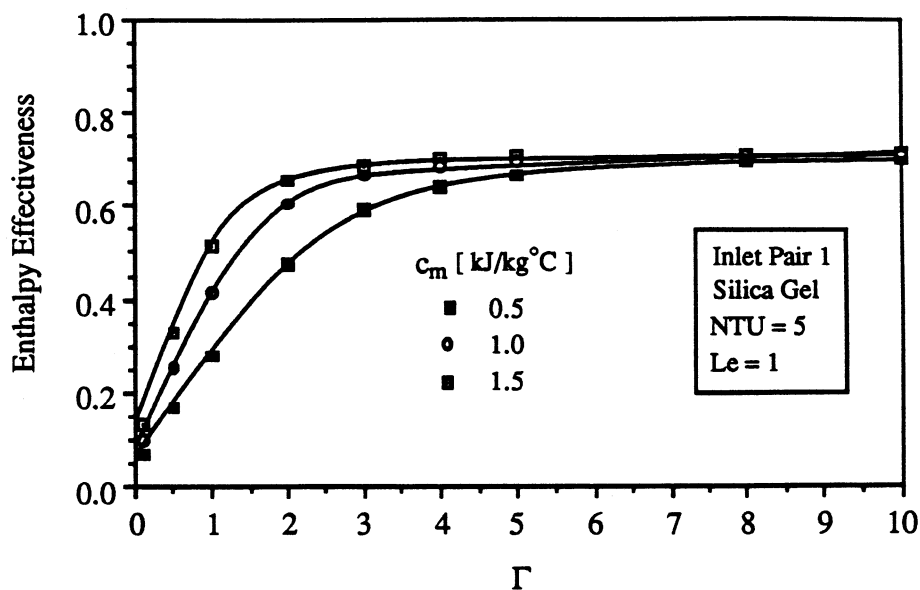


**Figure 5.12** Enthalpy Effectiveness as Computed by MOSHMX as a Function of  $\Gamma$  and the Specific Heat Capacity of the Matrix

If the reciprocal of the slope of the first wave front in Equation (5.1) is chosen as the independent axis the computed data points superimpose, as indicated in Figure 5.13. The product of the average combined capacity ratio and the dimensionless parameter  $\Gamma$  depend on the specific heat capacity of the matrix such that the enthalpy effectiveness can be considered to be a function of  $\bar{\gamma}_1 \Gamma$  and the number of transfer units only. At higher rotation speeds, the curve becomes a horizontal line which indicates that the counterflow heat exchanger correlations can be used to compute the outlet of the enthalpy exchanger as described in Chapter 5.2.

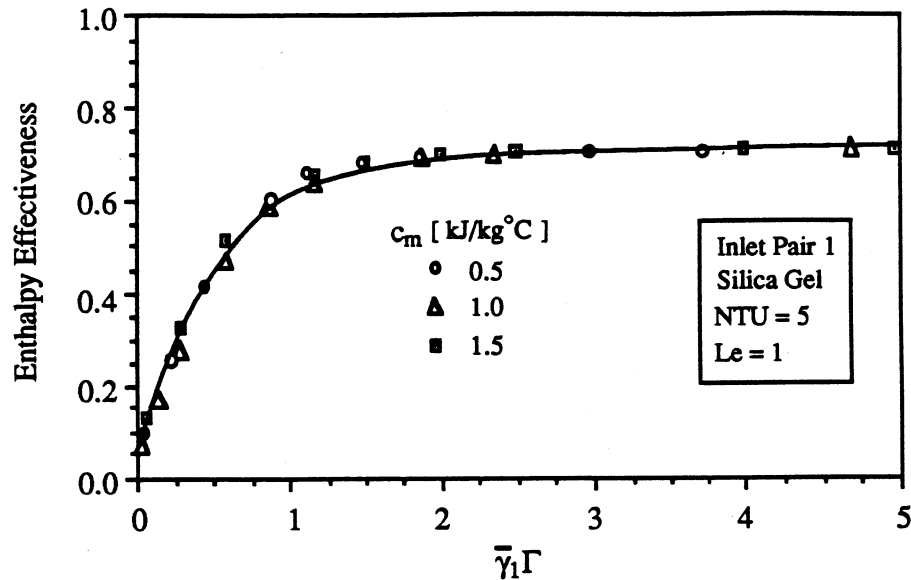


Figure 5.13 Enthalpy Effectiveness as Computed by MOSHMX as a Function of  $\bar{\gamma}_1 \Gamma$  and the Specific Heat Capacity of the Matrix

### 5.3.2 Adsorption Isotherm Correlation

Whereas the thermal capacity of the matrix can be characterized using a constant specific heat capacity, the water uptake of the solid desiccant cannot be described with an equivalent single "mass capacity" parameter due to the non-linear equilibrium relationship between the humidity ratio of the air and the water content of the matrix. The effect of the adsorption isotherm correlation on the non-dimensional wave speeds is far more complicated than the effect of the specific heat capacity of the matrix. The only parameter in Equation (4.20) which is affected by the specific heat capacity is  $a_5$ , the derivative of the matrix enthalpy with respect to the temperature. The nature of the desiccant and therefore the isotherm correlation influences the non-dimensional wave

speeds through at least four parameters. The value of  $a_1$  determines the dependence of the isotherm on the temperature and can be considered as a measure how close the adsorption equilibrium curves for different temperatures lie together. The shape of the isotherm is characterized by the derivative of the matrix water content with respect to the humidity ratio and therefore the isotherm shape affects the wave speed through the value of  $a_2$ . Since the enthalpy of the matrix is determined by both the temperature and the water content of the desiccant the derivatives  $a_4$  and  $a_5$  depend also on the isotherm correlation.

In Chapter 3 the isotherm correlations for silica gel, a molecular sieve and a Brunauer Type 3 isotherm were presented. Since the values of the parameters  $a_i$  vary with the temperature and water concentrations of the air and the matrix, the effect of the solid desiccant depends also on the inlet condition of the air streams. In this study, the two inlet pairs presented in Chapter 5.1 were used to investigate which desiccant is advantageous for applications in energy recovery enthalpy exchangers.

Figure 5.14 shows the outlet states computed by MOSHMX for various rotation speeds. Whereas the predicted outlet states for silica gel and the molecular sieve as adsorbent are very close, the degree of dehumidification is reduced significantly using the Brunauer Type 3 isotherm correlation. Figure 5.14 also indicates that the value of the dimensionless parameter  $\Gamma$  is higher at the point where maximal dehumidification for the Type 3 isotherm occurs, consistent with the results of Jurinak who investigated the region of best dehumidification extensively [9]. At higher values of  $\Gamma$ , the outlet states become independent of the desiccant and the system operates as an enthalpy exchanger.

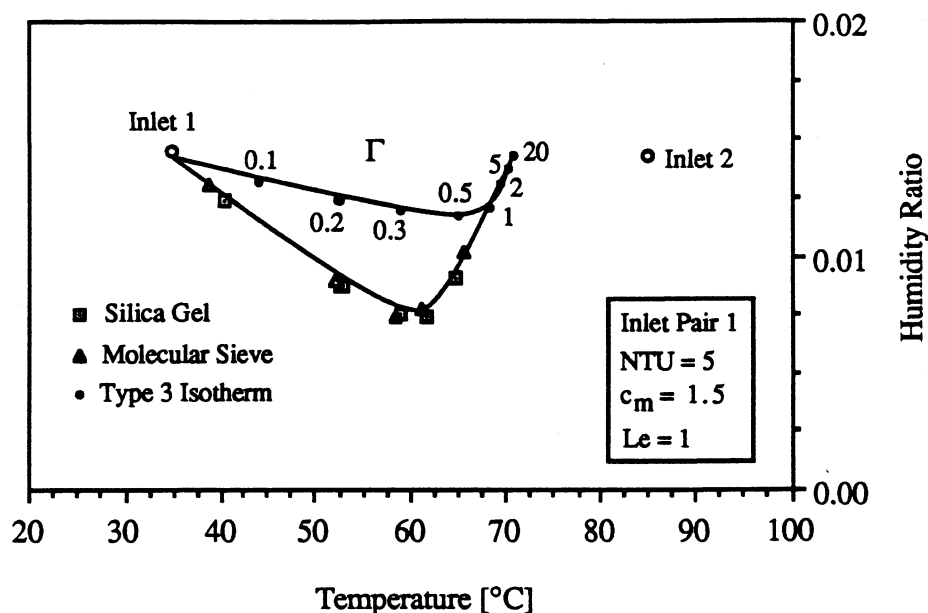


**Figure 5.14** Outlet States of Stream 1 as Computed by MOSHMX for Different Isotherm Correlations

A characteristic feature of the Type 3 isotherm is the low slope of the isotherm, i.e., the values for  $a_2$  are low. Banks investigated the thermodynamic constraints of the slopes of lines of constant  $F$ -potential in a psychrometric chart [32]. It can be shown that, in the limit of negligible matrix adsorption (which is equivalent to  $a_2$  equals zero) the lines of constant  $F_1$  become horizontal lines of constant humidity ratio. Compared to silica gel or a molecular sieve the lines of constant  $F_1$  are less steep for the Type 3 isotherm. The outlet states using silica gel or a molecular sieve lie close to the line of constant enthalpy through the inlet of stream 1 at low and medium values of  $\Gamma$ , whereas using the Type 3 isotherm results in enthalpy exchange even at low and medium rotation speeds and the degree of dehumidification is reduced.

Figure 5.15 illustrates the effect of  $\Gamma$  on the enthalpy effectiveness for silica gel and a molecular sieve.

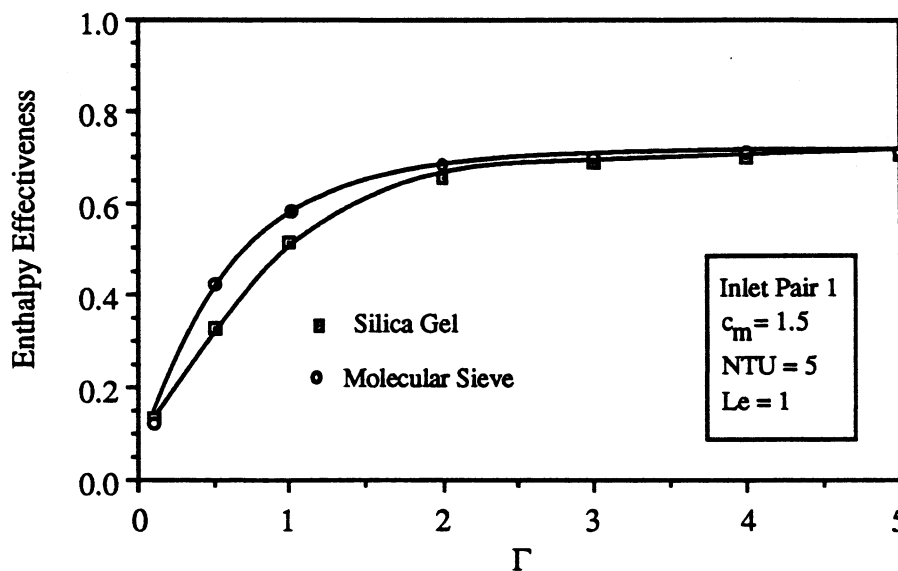


**Figure 5.15** Enthalpy Effectiveness as Computed by MOSHMX as a Function of  $\Gamma$  for Silica Gel and a Molecular Sieve

The regenerator carrying silica gel as adsorbent must be rotating at higher speeds in order to achieve the optimum enthalpy exchange with the reflection of the first wave. This can be explained using the equilibrium theory along with wave analysis. Table 5.3 shows the non-dimensional wave speeds evaluated at the average of the two inlet states.

**Table 5.3** Dimensionless Wave Speeds and Slope of the Isotherm for Silica Gel and a Molecular Sieve Evaluated at the Average of Inlet Pair 1

$$t = 60 \text{ }^\circ\text{C} \quad w = 0.0142 \text{ kgW/kgDA} \quad \phi = 0.113 \quad c_m = 1.5 \text{ kJ/kg}^\circ\text{C}$$

Isotherm Correlation	$\lambda_1$	$\lambda_2$	$a_2$
Silica Gel	1.858	0.1056	2.708
Molecular Sieve	1.780	0.0976	3.609

The range of operation is a range of low relative humidity. A comparison of Figure 3.1 and 3.3 shows that the isotherm of the molecular sieve is steeper than the equilibrium curve of silica gel. This results in a lower speed of the first wave for the molecular sieve. Thus, the silica gel wheel must be rotating faster to avoid the breakthrough of the first wave.

If the reciprocal of the slope of the first wave front is chosen as the independent variable the computed data points for the enthalpy effectiveness are independent of the adsorption isotherm correlation. Figure 5.15 shows the enthalpy effectiveness of silica gel and the molecular sieve as a function of  $\bar{\gamma}_1 \Gamma$ .

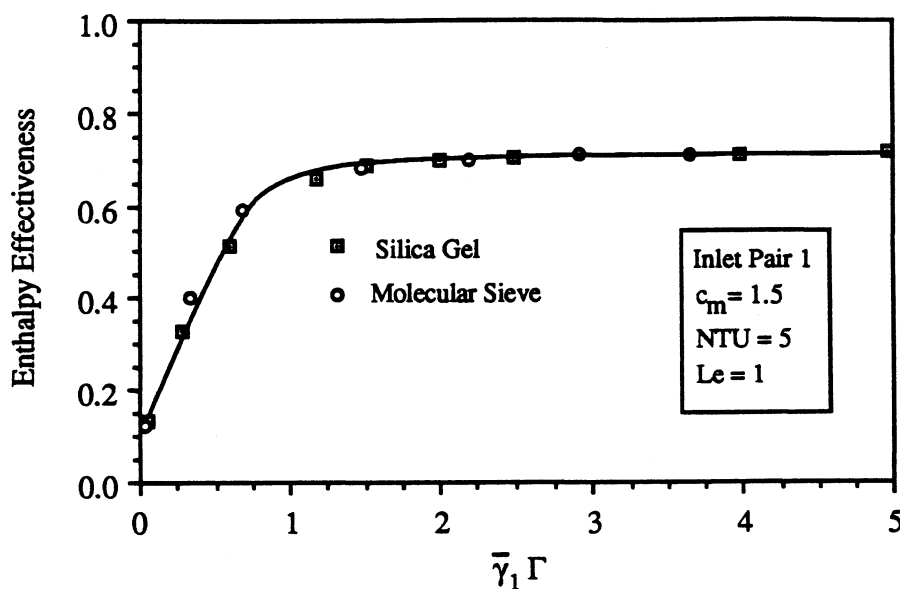


**Figure 5.16** Enthalpy Effectiveness as Computed by MOSHMX as a Function of  $\bar{\gamma}_1 \Gamma$  for Silica Gel and a Molecular Sieve

In order to show the dependence of the desiccant parameters on the state properties, simulations using inlet pair 2 were also done in this study. Figure 5.17 depicts the outlet streams for various rotation speeds and the three different isotherm relations. Whereas the predicted outlet states of the silica gel and Type 3 isotherm exchanger are on the same line in a psychrometric chart, the system using the molecular sieve as adsorbent shows a different behavior which can be explained taking the intersection points under consideration. The intersection points depend on the lines of constant F-potential and therefore vary from one desiccant to another and are shown in Figure 5.18.

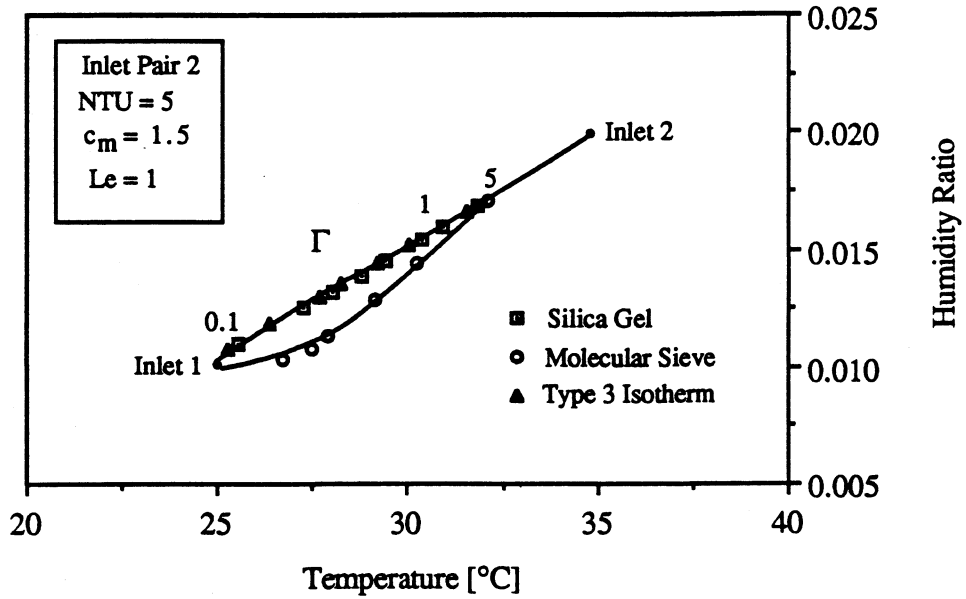


**Figure 5.17** Outlet States of Stream 1 as Computed by MOSHMX for Different Isotherm Correlations

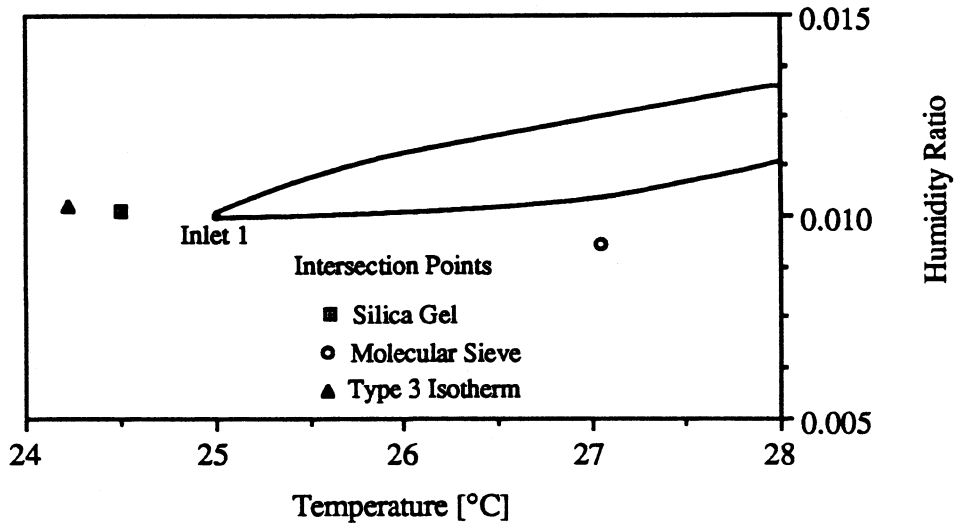


**Figure 5.18** Enlargement of Figure 5.17 Showing the Intersection Points

For low and medium rotation speeds, the transfer process in a regenerative heat and mass exchanger can be interpreted as a "pulling" of the outlet states towards the intersection points whereas at higher rotational speeds the outlet states are closer to the inlet state of the other stream.

Figure 5.19 shows the enthalpy effectiveness as a function of the rotation speed for silica gel and a Brunauer Type 3 isotherm.

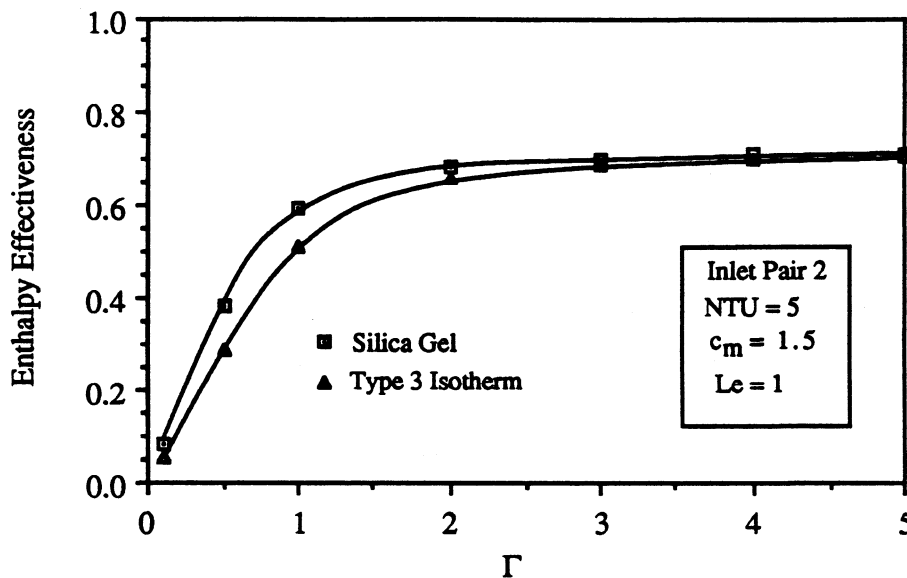


**Figure 5.19** Enthalpy Effectiveness as Computed by MOSHMX as a Function of  $\Gamma$  for Silica Gel and the Type 3 Isotherm

For increasing  $\Gamma$ , the system using silica gel reaches the point of optimum enthalpy exchange earlier than a desiccant wheel carrying a Brunauer Type 3 adsorbent, due to the wave speed,  $\lambda_1$ , which varies from one desiccant to the other. Table 5.4 shows the values computed at the average of the inlet pair 2.

**Table 5.4** Dimensionless Wave Speeds and Slope of the Isotherm for Silica Gel and a Type 3 Isotherm Evaluated at the Average of Inlet Pair 2

$$t = 30 \text{ }^\circ\text{C} \quad w = 0.015 \text{ kgW/kgDA} \quad \phi = 0.562 \quad c_m = 1.5 \text{ kJ/kg}^\circ\text{C}$$

Isotherm Correlation	$\lambda_1$	$\lambda_2$	$a_2$
Silica Gel	1.62	0.0219	13.80
Type 3 Isotherm	4.70	0.1820	2.298

Using inlet pair 2 as inlet states, the relative humidity of the entire process is higher than for inlet pair 1. In this operating range of increased relative humidity the values of  $a_2$  are higher for silica gel than for the Type 3 isotherm. This fact is consistent with Figures 3.2 and 3.3 which indicate a flatter curve for the Type 3 isotherm. Thus, the non-dimensional wave speeds are smaller for silica gel which decreases the rotation speed required to avoid the breakthrough of the first wave.

Finally, Figure 5.20 illustrates the same dependence of the reciprocal of the slope of the first wave front for both isotherms. Again, for  $\bar{\gamma}_1 \Gamma > 1.5$ , the enthalpy effectiveness can be considered to be a function of the number of transfer units only. This behavior is consistent with the statement of desiccant independent properties if the regenerative heat and mass exchanger is rotating fast enough such that the first wave cannot break through.

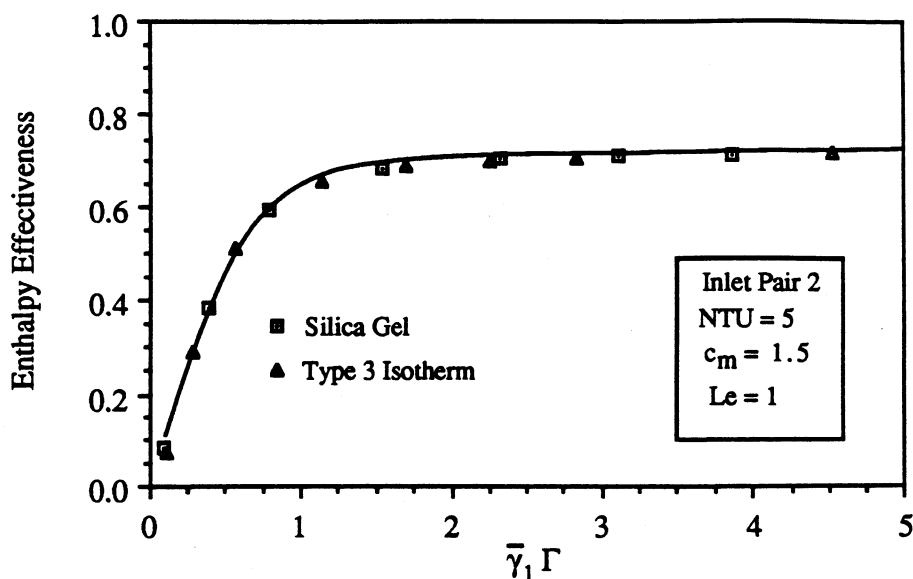


**Figure 5.20** Enthalpy Effectiveness as Computed by MOSHMX as a Function of  $\bar{\gamma}_1 \Gamma$  for Silica Gel and the Type 3 Isotherm

#### 5.4 EFFECT OF NON-UNITY LEWIS NUMBER

The Lewis number used in the matrix A in Equation (4.12) is defined as the ratio of the number of transfer units for heat transfer to the number of transfer units for mass transfer and is a measure for the resistance to water vapor diffusion into the porous solid desiccant matrix. One of the model assumptions in Chapter 2 was that the combined heat and mass transfer process can be described by constant convective transfer coefficients. With the assumption of negligible heat conduction into the matrix, the Lewis number can be used to model a solid side resistance to water vapor diffusion. The value of the Lewis number for the solid desiccants used in this study is uncertain. Schultz [20] states that the Lewis number of dehumidifiers is unity, while experimental

studies of Van den Bulck indicate that there might be a diffusive resistance of the adsorbent resulting in Lewis numbers of 3 to 4 [15].

The finite difference model is not limited to unity Lewis number. It was used to validate the range where the linear analogy method and the counterflow effectiveness correlations can be used to predict the outlet of a regenerative heat and mass exchanger with Lewis numbers greater than one. Figure 5.21 shows the predicted outlet of an enthalpy exchanger for varying Lewis number.

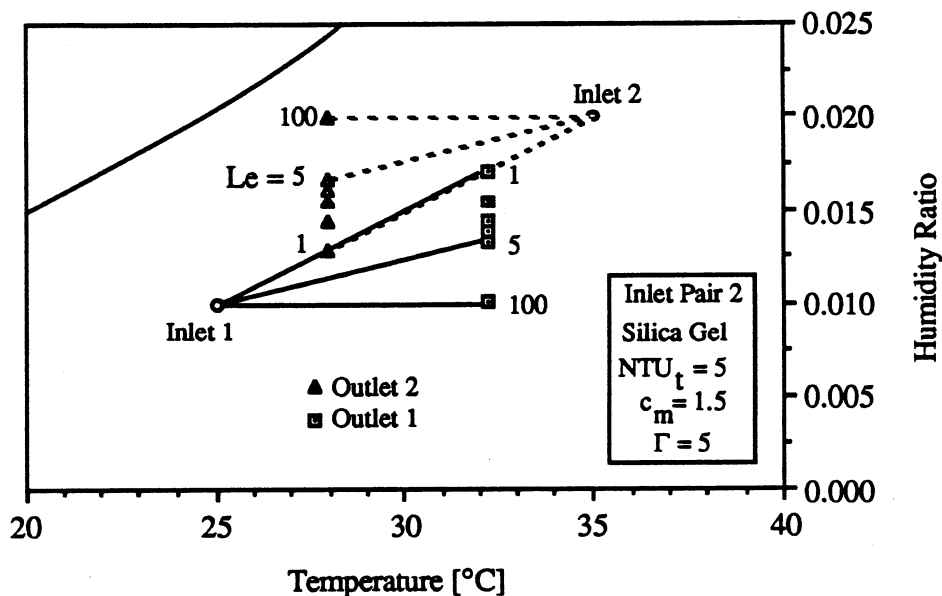


**Figure 5.21** Outlet States of Streams 1 and 2 as Computed by MOSHMX for Different Lewis Numbers

The rotation speed for the simulation to construct Figure 2.21 was taken to be high enough such that for unity Lewis number, the outlet states lie on a straight line connecting the two inlet states. For increasing mass transfer resistance into the

desiccant matrix, the outlet states are no longer on this line due to a reduced mass transfer rate. For the case of very large Lewis numbers the enthalpy exchanger operates as a rotary sensible heat exchanger where no mass is transferred between the flow streams and the humidity ratios at the outlet are equal to the one at the inlet.

The linear analogy method described in Chapter 4.3 was derived by Maclaine-cross using the assumption of unity Lewis number [13]. However, for the analysis of regenerators with Lewis number greater than one, Maclaine-cross recommends using corrected values for the number of transfer units to account for non-unity Lewis number effects:

$$NTU_1 = NTU_w \left( \frac{Le - \frac{\alpha_1}{\alpha_2}}{1 - \frac{\alpha_1}{\alpha_2}} \right) \quad (5.4)$$

$$NTU_2 = NTU_w \left( \frac{Le - \frac{\alpha_2}{\alpha_1}}{1 - \frac{\alpha_2}{\alpha_1}} \right) \quad (5.5)$$

where

$$-\frac{1}{\alpha_i} = \left( \frac{\partial w_f}{\partial t_f} \right)_{F_i} = - \frac{a_1 a_3}{(a_3 - a_5 \lambda_i) a_2}$$

The negative reciprocal of  $\alpha_i$  is the slope of a lines of constant  $F_i$ -potential in a psychrometric. The correction takes into account both the Lewis number and the adsorption characteristics of the desiccant.

As described in Chapter 5.2, the counterflow heat exchanger correlations can be used to compute the outlet of an enthalpy exchanger where the first wave is reflected. Using this model to predict the outlet states the number of transfer units for heat mass transfer must be corrected using the following expression:

$$NTU_w = \frac{NTU_t}{Le} \quad (5.6)$$

Figure 5.22 shows the absolute errors involved in the two Lewis number corrections described above. The errors are very small using the counterflow heat exchanger correlations with the correction for the non-unity Lewis number presented in Equation (5.6). The linear analogy, along with the corrections in Equations (5.4)-(5.5), shows an increasing error for increasing Lewis numbers. Therefore, the use of counterflow heat exchanger correlation is more accurate for enthalpy exchangers with varying Lewis numbers. The linear analogy method, however, can be used also for rotation speeds where the first wave breaks through and the counterflow heat exchanger correlations fail.

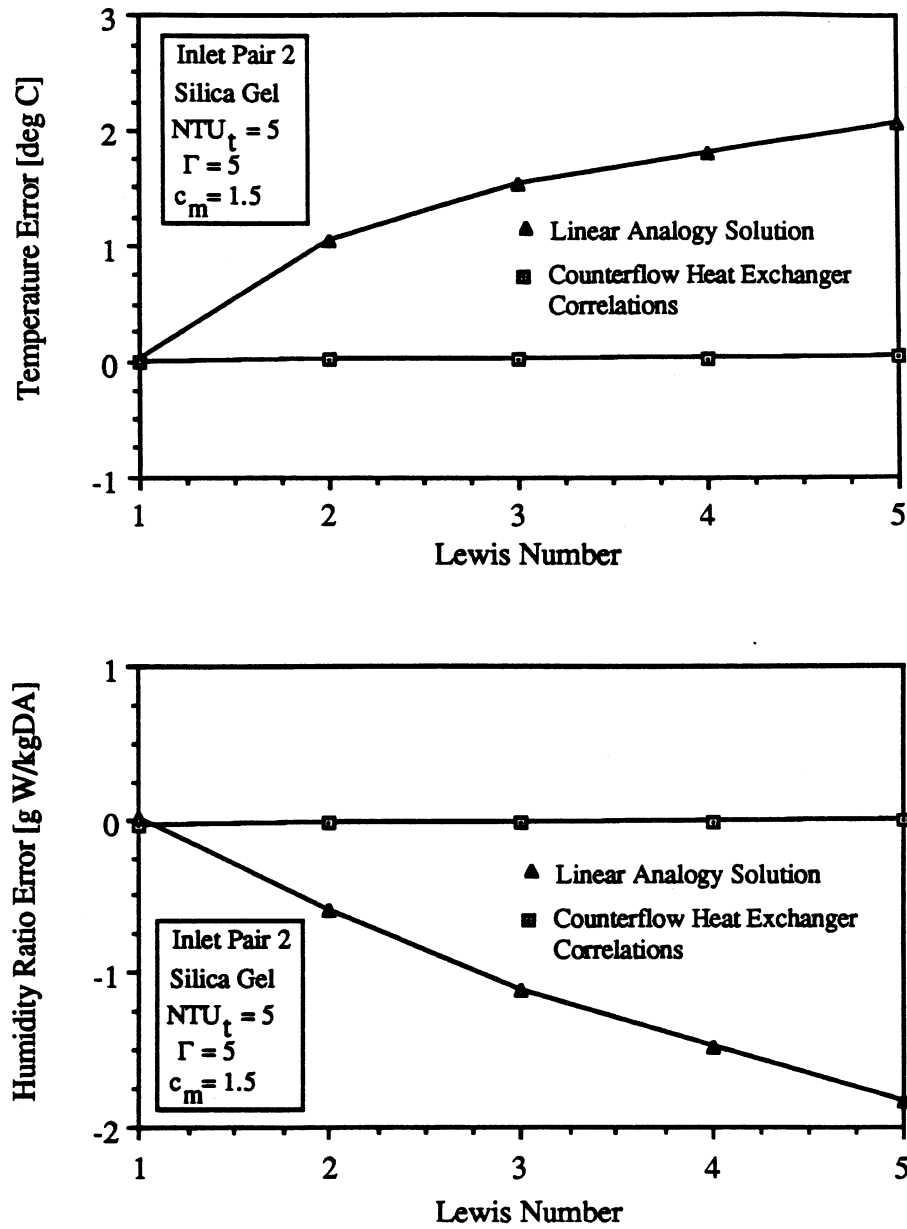


**Figure 5.22** Errors in the Outlet States Using the Linear Analogy Method and the Counterflow Heat Exchanger Correlations

---

## Chapter 6

# Condensation and Freezing in Rotary Regenerators

---

This chapter presents the analysis of both hygroscopic and non-hygroscopic rotary regenerators with water vapor transfer in adsorbed and/or condensed phase. The fundamental conservation and transfer rate equations are presented along with the thermodynamic relationships which may vary from one point of the regenerator to another. The finite difference method described in Chapter 4.1 was used to compute the outlet states as well as temperature and humidity profiles for a given set of inlet conditions and system parameters. For certain combinations of inlet states, the algorithm does not converge to a steady state solution. This observation led to the conclusion that there are cases where steady state operation of the regenerator is not possible.

### 6.1 MASS TRANSFER IN NON-HYGROSCOPIC ENERGY RECOVERY REGENERATORS

A rotary regenerator with non-hygroscopic matrix usually transfers only sensible heat from the hot to the cold stream. For some combinations of inlet states and system parameters, however, water vapor may condense on the matrix during one period and evaporate into the other air stream.

Figure 6.1 shows a pair of inlet conditions where the dew point temperature of the hot and humid air stream is higher than the dry bulb temperature of the cold and dry stream.

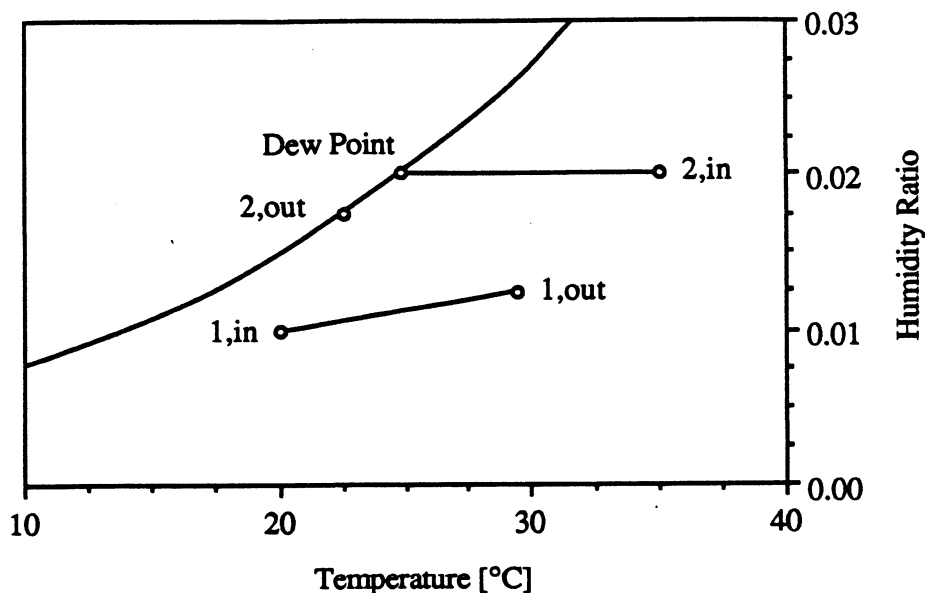


**Figure 6.1** Inlet Conditions with Condensation on a Non-Hygroscopic Matrix

The heat exchanger effectiveness is high enough such that stream 2 approaches the saturation line and water vapor condenses on the matrix. The thin film of liquid water rotates with the matrix to the other period and evaporates into stream 1. The regenerator operates as a regenerative heat and mass exchanger and removes both heat and mass moisture from stream 2.

Whereas condensation as described above can be advantageous in energy recovery applications of rotary regenerators, the formation of ice on the matrix results in poor performance since the flow channels of the regenerator are blocked and the

device cannot be operated anymore at a high heat transfer effectiveness. An example for a combination of air inlet states where freezing may occur is given in Figure 6.2.

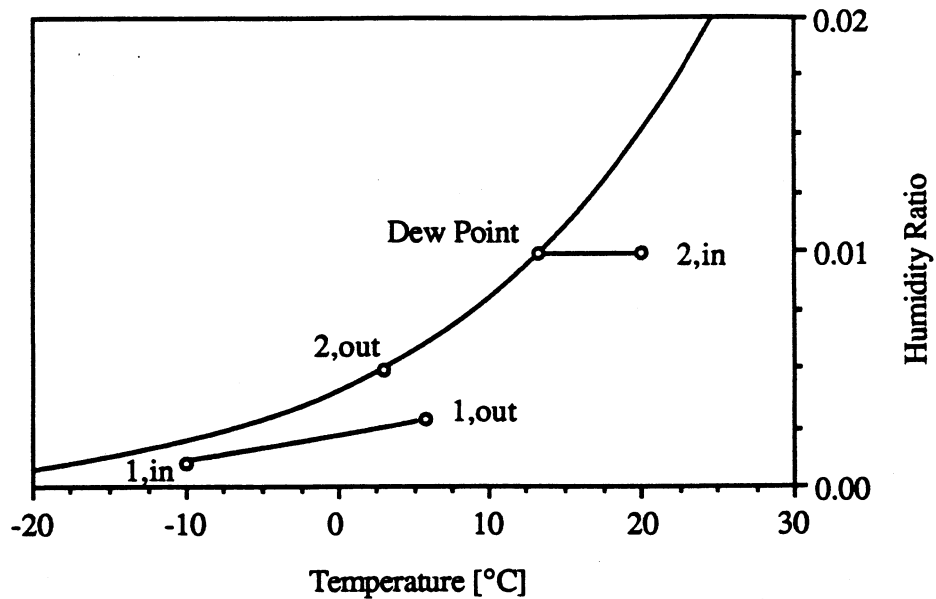


**Figure 6.2** Inlet Conditions with Freezing on a Non-Hygroscopic Matrix

The heat exchanger effectiveness shown in Figure 6.2 is kept low to avoid freezing on the matrix. If the effectiveness is increased, the outlet state of stream 2 moves down along the saturation line and below 0 °C ice starts to build up.

### 6.1.1 Van Leersum's Model of Combined Heat and Mass Transfer

Regenerators with non-hygroscopic matrices and water vapor transfer in condensed phase have been investigated by Van Leersum [17,18]. He used two different sets of differential equations and developed a finite difference scheme called

REGENCOND. In steady state operation of the regenerator, parts of the matrix are covered with liquid bulk phase water whereas other parts are still dry. For the dry part, the equations for the sensible heat exchanger described in Chapter 2.2 apply and the humidity of the air does not change:

Dry Part

$$\frac{\partial t_f}{\partial z} + \sigma \Gamma_j \beta_j \frac{\partial t_m}{\partial \Phi} = 0 \quad (6.1)$$

$$\frac{\partial t_f}{\partial z} = NTU_{t,j} (t_m - t_f) \quad (6.2)$$

After the air is cooled and the saturation line is reached at the dewpoint temperature of the air-water mixture, water vapor condenses on the matrix and the humidity ratio of the air decreases. The matrix water content becomes greater than zero since a thin layer of liquid water covers the non-hygroscopic matrix. Therefore, the wet part of the regenerator requires conservation and transfer rate equations for both heat and mass in order to describe the combined heat and mass transfer. In the case of a hygroscopic matrix, the matrix water content is a measure of the amount of adsorbed water by the solid desiccant whereas for a non-hygroscopic matrix, the matrix water content describes the amount of liquid water covering the matrix surface.

Wet Part

$$\frac{\partial w_f}{\partial z} + \Gamma_j \beta_j \frac{\partial W_m}{\partial \Phi} = 0 \quad (6.3)$$

$$\frac{\partial w_f}{\partial z} = NTU_{w_j} (w_m - w_f) \quad (6.4)$$

$$\frac{\partial i_f}{\partial z} + \Gamma_j \beta_j \frac{\partial I_m}{\partial \Phi} = 0 \quad (6.5)$$

$$\frac{\partial t_f}{\partial z} = NTU_{t_j} (t_m - t_f) \quad (6.6)$$

Equations (6.3)-(6.6) are the same as for a regenerator with hygroscopic matrix described in Chapter 2.3. The difference between the performance of a hygroscopic and a wet non-hygroscopic matrix is due to the different thermodynamic behavior of the matrix surface:

$$i_f = c_{pA} t_f + w_f (i_v + c_{pw} t_f) \quad (6.7)$$

$$I_m = c_m t_m + c_{Lw} t_m W_m \quad (6.8)$$

$$w_m = w_{sat} (t_m) \quad (6.9)$$

The expression for the enthalpy of humid air is not affected by the matrix characteristics. An important feature of non-hygroscopic matrices is that the expression for the matrix enthalpy in Equation (6.8) does not contain the integral heat of wetting. In the case of hygroscopic matrices, the equilibrium relationship between water vapor in the air and adsorbed water in the desiccant is determined by the non-linear adsorption isotherm correlation. If there is liquid water on a non-hygroscopic matrix, the air in equilibrium with the matrix is saturated and can be determined using the water vapor pressure curve as described in Chapter 3.1.

The two sets of finite difference equations of REGENCOND are identical to that used by Lambertson [24] and Maclaine-cross [13], respectively. The determination of the grid size is similar to that used in MOSHMX as described in Chapter 4.1, however, the solution procedure was modified by Van Leersum to take into account that there are wet and dry parts of the matrix. Usually, the inlet states of the air streams are not saturated such that the matrix can be assumed to be dry and the finite difference equations based on Equations (6.1)-(6.2) for the dry part are used to start the integration at the inlet of the air streams. At each grid, a check is done to determine whether the air state reaches the saturation line. In this case, the finite difference equations based on Equation (6.3)-(6.9) for the wet part must be used for the next grid. Van Leersum [17] developed special finite difference equations for the grids where the matrix changes from dry to wet to consider the fact that the transition usually occurs within the grid and not at the boundaries. The convergence criteria in REGENCOND compares the enthalpy effectiveness computed for two consecutive numerical cycles, as described in Equation (4.13). In order to achieve high accuracy, an extrapolation to zero grid size as suggested by Maclaine-cross [13] was implemented in the FORTRAN code of

## REGENCOND.

Van Leersum compared the performance of REGENCOND with experimental results and obtained agreement within the experimental limitations [17]. If one regenerator inlet stream is very wet (46 °C, 0.051 kgW/kgDA), the method did not converge to a steady state solution and led to the conclusion that the regenerator operates in a unstable manner which is consistent with the experimental results.

The unstable operation is due to the fact that, at one period, more water vapor condenses on the matrix than can be evaporated at the other period. This behavior violates the *deposit condition* postulated by Hausen [4] which requires that the water vapor deposited during one period must be evaporated before the end of the other period.

## 6.2 FREEZING IN HYGROSCOPIC ENTHALPY EXCHANGERS

As shown in Chapter 5, the outlet states of an enthalpy exchanger with unity Lewis number lie on a straight line connecting the inlet states, due to the fact that the temperature and water vapor effectiveness are equal. Therefore, condensation and freezing usually do not occur since the water vapor is transferred in an adsorbed rather than condensed phase. Only in cases where the line between the two inlet states intersects the saturation line, these phenomena must be taken under consideration. An example for the case where water vapor transfer might occur in other than adsorbed phase is shown in Figure 6.3. The inlet conditions are for an energy recovery application of an enthalpy exchanger as illustrated in Figure 1.5. The warm stream represents indoor conditions which are within the thermal comfort range specified by

ASHRAE [27], whereas the cold stream is typical for outdoor conditions in very cold winter climates, such as Chicago, IL [37].

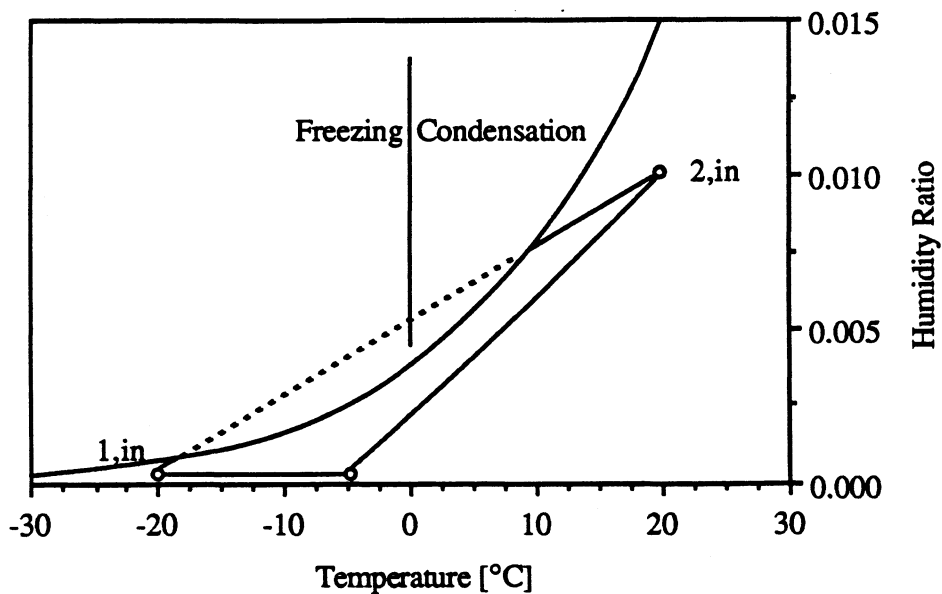


**Figure 6.3** Inlet Conditions with Freezing on a Hygroscopic Matrix

For inlet conditions shown in Figure 6.3, the finite difference method implemented in the version of MOSHMX available to the author would not converge. After personal communication with Maclaine-cross [38] the author decided to modify the MOSHMX code and to use the ideas in REGENCOND to model water vapor transfer in condensed<sup>1</sup> phase in the combination with a hygroscopic matrix.

---

<sup>1</sup>Condensed phase in this context stands for liquid water or ice, depending on the temperature of the system.

### 6.2.1 Modification of the Finite Difference Method for Hygroscopic Matrices

As described in Section 6.1.2, two sets of partial differential equations are necessary to describe regenerators with a non-hygroscopic matrix and susceptibility of condensation which is due to the fact that the matrix is partially dry and wet. If a hygroscopic material is, however, exposed to humid air, the matrix water content equilibrium is always greater than zero. Therefore, a set of conservation and transfer rate equations for heat and mass transfer is required to describe a hygroscopic system, no matter if condensation occurs or not. For the sake of completeness, these equations are presented below:

$$\frac{\partial w_f}{\partial z} + \Gamma_j \beta_j \frac{\partial W_m}{\partial \Phi} = 0 \quad (6.3)$$

$$\frac{\partial w_f}{\partial z} = NTU_{w_j} (w_m - w_f) \quad (6.4)$$

$$\frac{\partial i_f}{\partial z} + \Gamma_j \beta_j \frac{\partial I_m}{\partial \Phi} = 0 \quad (6.5)$$

$$\frac{\partial t_f}{\partial z} = NTU_{t_j} (t_m - t_f) \quad (6.6)$$

The term *saturated matrix* is used in this section to refer to a matrix which has adsorbed water up to its maximum water content. If the matrix is saturated, further

water uptake results in a film of liquid water or solid ice on the adsorbent, depending on the temperature of the system. The thermodynamic behavior of the matrix depends on whether the matrix water content is below or above the saturated matrix state. Therefore, two different sets of thermodynamic equilibrium relationships are required in order to describe a hygroscopic system with matrix water contents below and above saturation.

Matrix below Saturation ( $W_m \leq W_{max}$ )

$$w_m = w_m(t_m, W_m) \quad (6.10)$$

$$I_m = c_m t_m + c_{Lw} t_m W_m + \int_0^{W_m} (i_v - i_s) dW \quad (6.11)$$

Matrix above Saturation ( $W_m > W_{max}$ )

$$w_m = w_{sat}(t_m) \quad (6.12)$$

$$I_m = c_m t_m + c_{Lw} t_m W_m + \int_0^{W_{max}} (i_v - i_s) dW \quad (6.13)$$

Equation (6.10) is the inverse form of the isotherm correlation as required by MOSHMX and depends on the nature of the solid desiccant described in Chapter 3.

The air inlet states are usually below saturation such that the enthalpy of the air

can be expressed independently of the matrix state using the ideal gas relation.

#### Enthalpy of Humid Air

$$i_f = c_{pA} t_f + w_f (i_v + c_{pw} t_f) \quad (6.14)$$

After implementation of the new thermodynamic relations into the property support routines of MOSHMX, the question of modifying the system parameters for the parts where the matrix is covered with water arose. In the derivation of the model equations in Chapter 2, it was assumed that the heat and mass transfer between the air and the matrix can be described by convective film transfer coefficients. Hausen [4] describes the condensed water on the matrix: "...the layer of water or ice deposited upon the heat storing mass is rarely thicker than about 1/100 mm". The fact that the condensed phase is very thin led to the assumption of negligible conductive or diffusive resistance such that the overall transfer coefficients can be kept constant.

The author did not find any reference concerning isotherm correlations at temperatures below freezing. It is believed that at these low temperatures, adsorption still can be considered as a process with the transition of water vapor from gaseous phase to an adsorbed phase which is different from bulk phase liquid water or ice [39]. In this study, it was assumed that the isotherm correlation presented in Chapter 3 can be used at low temperatures. The adsorption potential in the Dubinin-Polanyi theory for silica gel becomes the difference between the differential heat of adsorption and the heat of sublimation at temperatures below the freezing point.

### 6.2.2 Simulations of Transient Behavior

The transient iteration method described in Chapter 4.1 uses successive substitution of the matrix states and essentially follows the changing matrix states from the initial values to the steady state solution. The modified version of MOSHMX allows the user to specify the initial conditions of the system. Steady state operation is reached as soon the enthalpy effectiveness of two consecutive numerical cycles is within a specified limit:

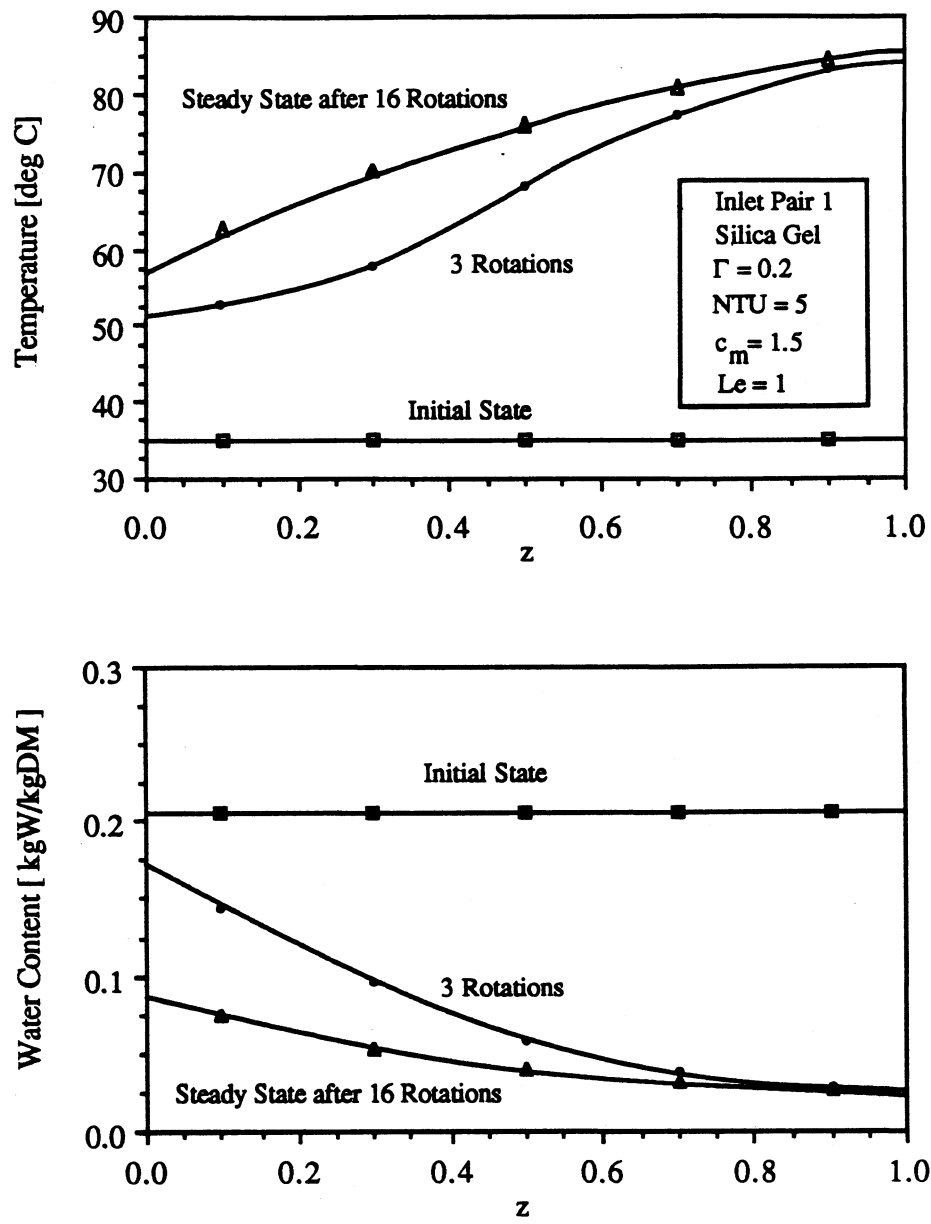
$$|(\epsilon_i)^n - (\epsilon_i)^{n+1}| \leq 10^{-6} \quad (4.13)$$

where

$$\epsilon_i = \frac{i f_{j,out} - i f_{j,in}}{i f_{3-j,in} - i f_{j,in}}$$

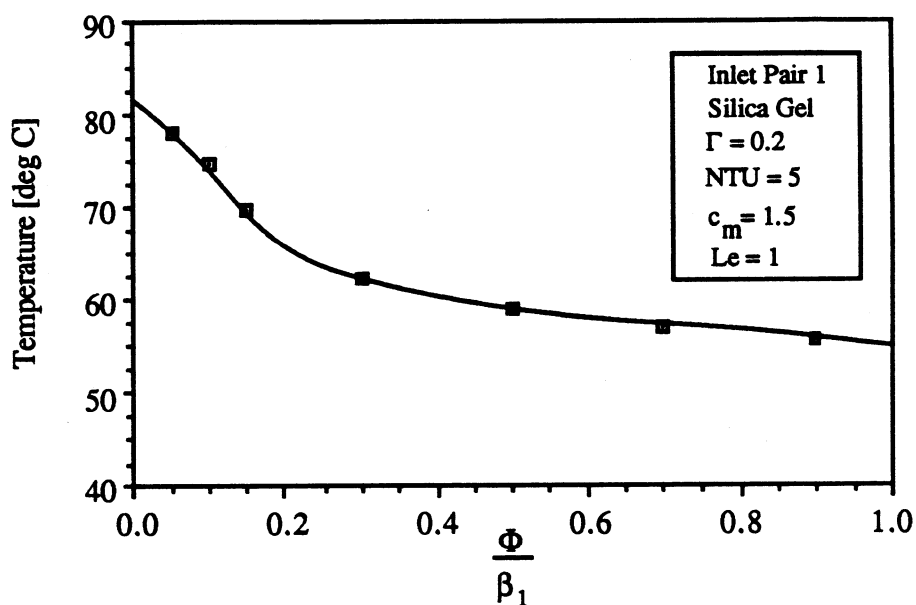
enthalpy effectiveness using the stream  
with the minimum flow rate

Figure 6.4 shows the transient behavior of a regenerative heat and mass exchanger operating as a regenerative dehumidifier. Inlet pair 1 of Chapter 5 was used to represent typical inlet conditions of the device in a solid desiccant cooling cycle.



**Figure 6.4** Transient Matrix Profiles of a Regenerative Dehumidifier at the Beginning of the First Period with Convergence to Steady State

Initially, the matrix was set to be in thermodynamic equilibrium with stream 1 (35°C, 0.0142 kgW/kgDA). After 16 rotations, the regenerator operates at steady state. The profiles in Figure 6.4 show the matrix states at the beginning of the first period after switching from the hot regeneration period (85°C, 0.0142 kgW/kgDA). Since the dehumidifier is rotating at medium speed ( $\Gamma = 0.2$ ), the air outlet states are highly non-uniform with the rotation angle even after steady state is reached. Figures 6.5 and 6.6 show the variation of the air temperature and humidity ratio at the outlet of the regenerator.



**Figure 6.5** Variation of the Air Outlet Temperature of Stream 1 with the Rotation Angle

At low angles, the outlet temperature is determined by the breakthrough of the first

wave whereas at higher, angles the intermediate state at low humidity determines the outlet as shown in Figure 6.6.

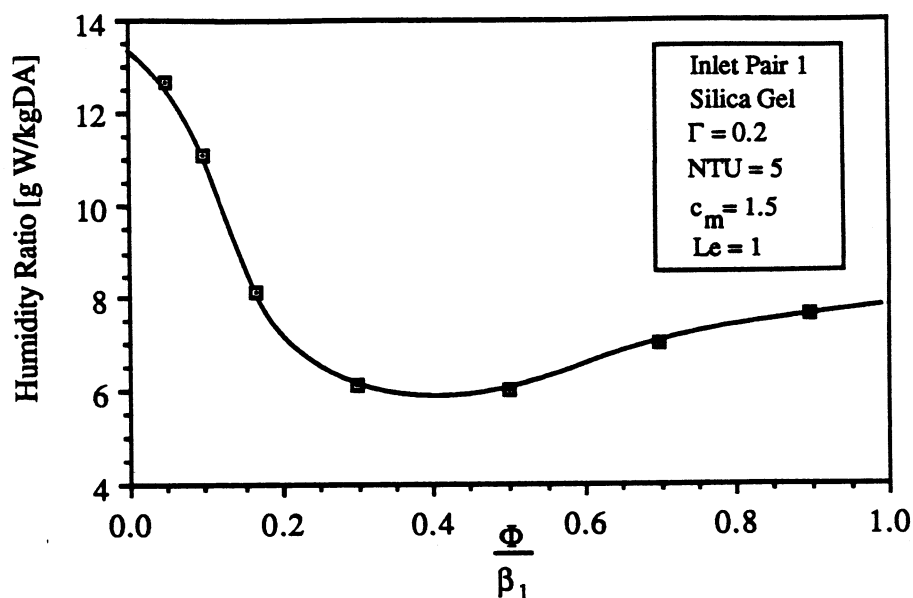


**Figure 6.6** Variation of the Air Outlet Humidity Ratio of Stream 1 with the Rotation Angle

Fast rotating enthalpy exchangers require more rotations before reaching steady state operation. Figure 6.7 illustrates the dynamic behavior of an enthalpy exchanger matrix used as an energy recovery unit with inlet pair 2. The matrix was set to be initially in equilibrium with the exhaust stream at indoor conditions (25 °C, 0.010 kgW/kgDA).

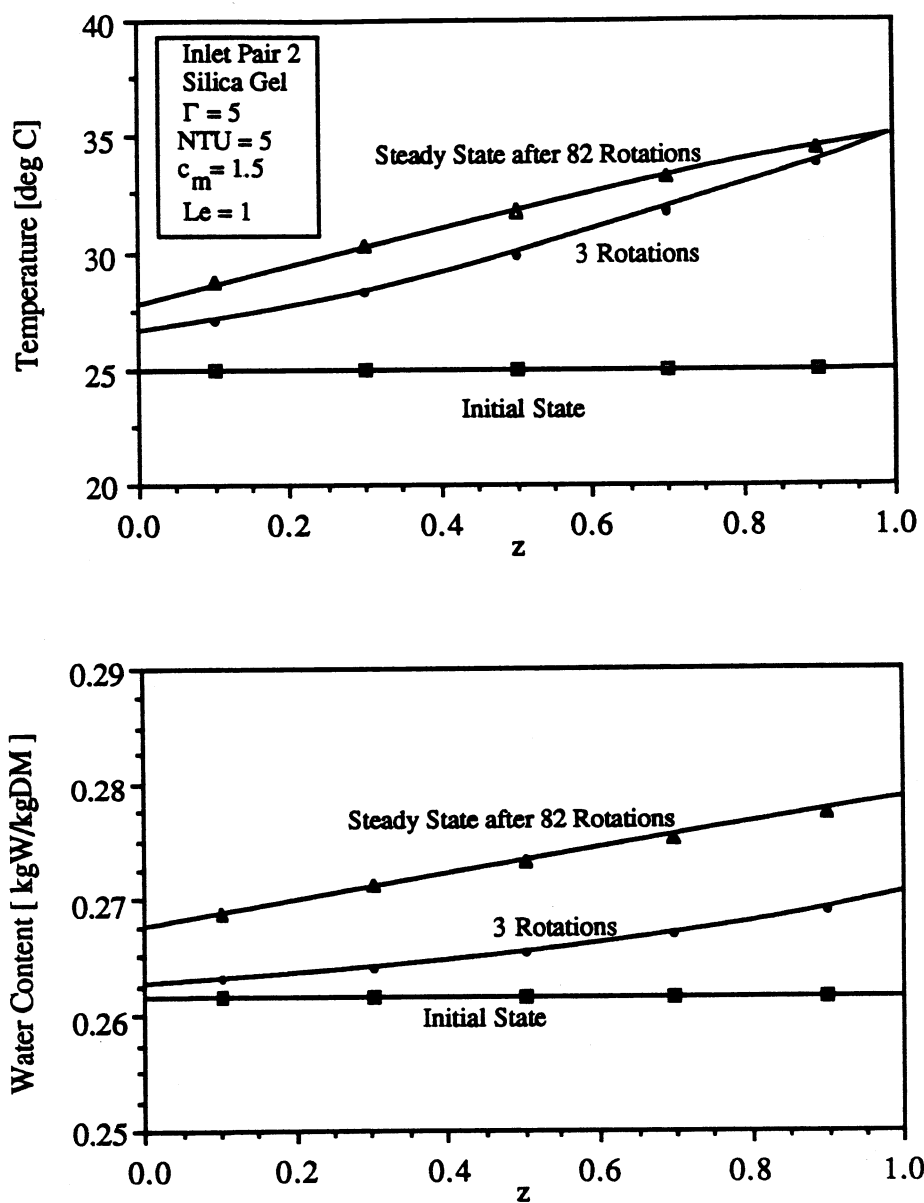


**Figure 6.7** Transient Matrix Profiles of an Enthalpy Exchanger at the Beginning of the First Period with Convergence to Steady State

After 82 rotations, the enthalpy exchanger operates at steady state and the matrix and air outlet states do not change with the time anymore. However, the outlet temperature and humidity ratio depend on the rotation angle as shown in Figures 6.8 and 6.9.

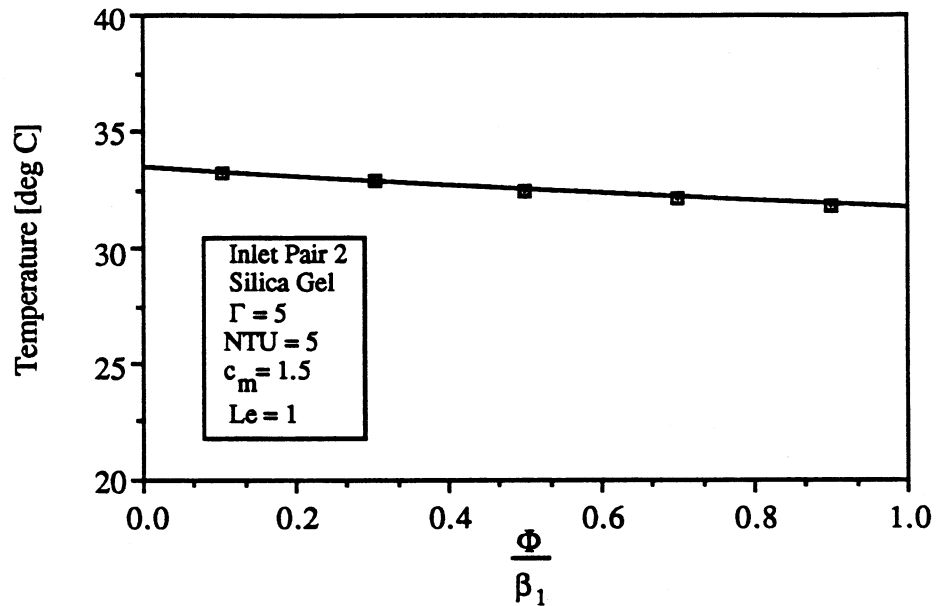


**Figure 6.8** Variation of the Air Outlet Temperature of Stream 1 with the Rotation Angle for an Enthalpy Exchanger

The dependence of the temperature on the rotation angle for an enthalpy exchanger is less than for a regenerative dehumidifier due to both lowered rotational speed and less difference between the two inlet temperatures.

The variation of the humidity ratio at the outlet stream 1 is shown in Figure 6.9. Since neither wave breaks through, the profile is fairly linear.

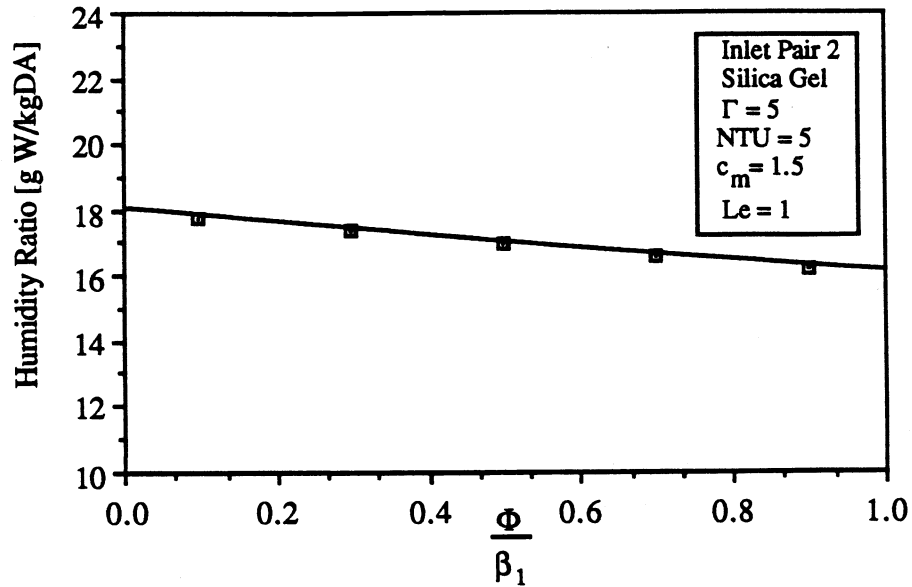


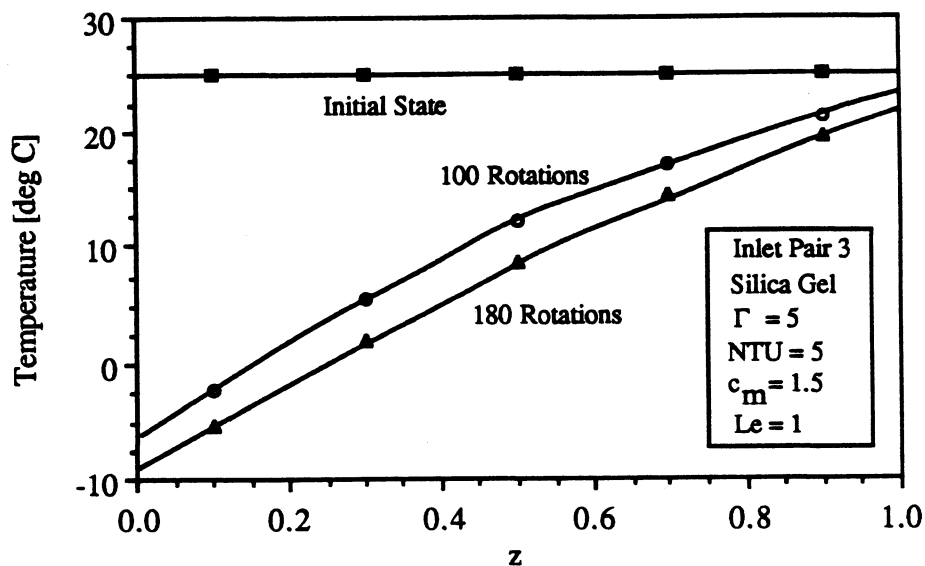
**Figure 6.9** Variation of the Air Outlet Humidity Ratio of Stream 1 with the Rotation Angle for an Enthalpy Exchanger

A third pair of inlet conditions was considered in this study in order to investigate the behavior when a straight line connecting the two inlet states in a psychrometric chart intersects the saturation line. The combination of inlet conditions is referred to as inlet pair 3 and is defined as follows:

$$\begin{aligned}
 \text{Pair 3} \quad t_{f1,\text{in}} &= -20 \text{ }^\circ\text{C} \\
 w_{f1,\text{in}} &= 0.0006 \text{ kgW/kgDA} \\
 t_{f2,\text{in}} &= 25 \text{ }^\circ\text{C} \\
 w_{f2,\text{in}} &= 0.010 \text{ kgW/kgDA}
 \end{aligned}$$

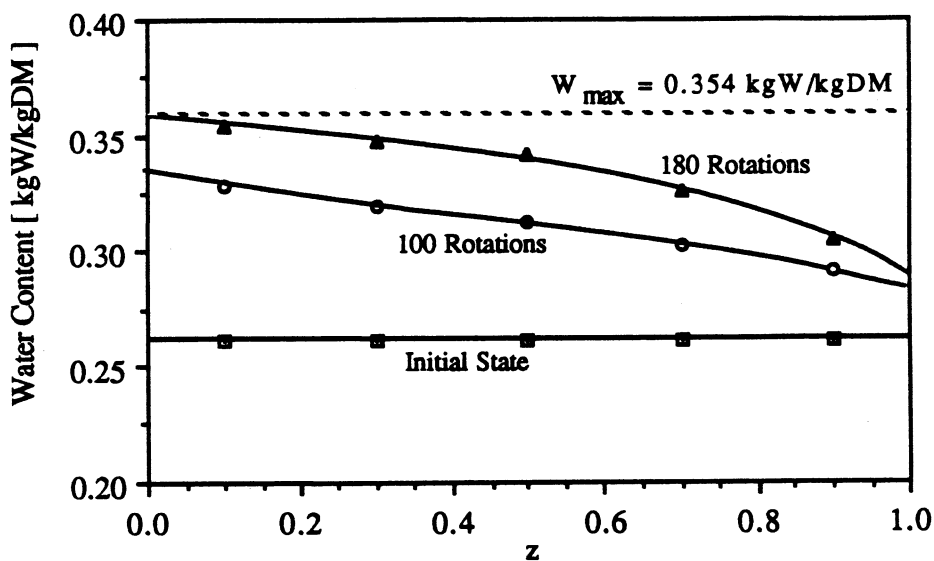
The modified version of MOSHMX was used in order to account for mass transfer in both adsorbed and condensed phase. If the matrix water content becomes larger than its value for the maximum water uptake, condensed water or ice covers part of the desiccant. The susceptibility to ice formation is high at the cold side of the regenerator where the dry and cold air cools a matrix which has dehumidified the warm and humid exhaust air. Simulations are terminated if ice is on the matrix at the cold inlet for all angular positions which is equivalent to having all flow channels partially blocked and the regenerator cannot be operated anymore.

Figure 6.10 illustrates the transient temperature profiles of an enthalpy exchanger matrix using inlet pair 3 just after the matrix switches from the warm to the cold stream.



**Figure 6.10** Transient Matrix Temperature Profiles of an Enthalpy Exchanger with One Cold Inlet Stream at the Beginning of the First Period

Initially, the matrix is in equilibrium with the warm and humid stream (25°C, 0.010 kgW/kgDA). The cold air stream cools the matrix below the freezing point of water. Figure 6.11 shows the water content profiles of the matrix.



**Figure 6.11** Transient Matrix Water Content Profiles of an Enthalpy Exchanger with One Cold Inlet Stream at the Beginning of the First Period

After 160 rotations, ice starts building up at the inlet of the cold stream when the matrix is rotating from the warm to the cold period. For other angular positions, the matrix water content is still below its maximum value and ice formation does not occur. Finally, after 180 rotations, the matrix water content reaches the value for the maximum water uptake, which depends on the characteristics of the adsorbent. The entire matrix is covered with ice at the inlet of the cold stream and the simulation was terminated.

MOSHMIX did not converge to a steady state solution since the amount of water

vapor in the warm air stream and adsorbed by the desiccant cannot be removed from the enthalpy exchanger by the cold and dry air stream. Therefore, the matrix water content increases steadily until the maximum value is reached and water vapor is transferred from period to the other in condensed phase. If the matrix temperature is below 0 °C, the water freezes on the matrix and blocks the flow channels of the regenerator.

These results are consistent with Van Leersum [17] who did not reach a steady state solution for regenerators with non-hygroscopic matrices and one very humid inlet stream. Hausen [4] did simulations for inlet conditions down to -100 °C and also could not get a solution for steady state.

In Chapter 5.3, the effect of the adsorbents characteristics were discussed. The used inlet conditions were in the range of low to medium relative humidities. Hence, the slope of the adsorption isotherm was the most important matrix parameter. The influence of the matrix characteristics decreased if the the enthalpy exchanger operates at higher rotational speed. The cold inlet stream used in this chapter is very dry in terms of absolute humidity ratio. However, the relative humidity of the air is very high such that the maximum water content becomes the most important parameter of the desiccant. Table 6.1 shows the comparison between silica gel and a molecular sieve as solid desiccant. Taking the inlet state of stream 1 as the initial state of the matrix the table shows the number of rotation after which the simulation was terminated since ice has built up at the cold inlet side of the enthalpy exchanger.

**Table 6.1 Simulation Summary Using Inlet Pair 3 and Different Isotherm Correlations**

Isotherm Correlation	$W_{\max}$ [ kgW/kgDM]	Number of Performed Rotations
Silica Gel	0.354	180
Molecular Sieve	0.230	6

The initial matrix state is close to the maximum water uptake of the molecular sieve such that ice formation starts after a few rotations already whereas the enthalpy exchanger using silica gel as adsorbent can be operated a longer time period due to the higher value of the maximum water content of the desiccant.

If the inlet temperature of the cold stream is increased to  $-10\text{ }^{\circ}\text{C}$  the finite difference algorithm converges to a steady state solution due to the fact that the line connecting the two inlet states does not intersect the saturation line a psychrometric chart. Therefore, after preheating the cold outdoor air stream an enthalpy exchanger can be operated without ice formation on the matrix whereas in the case of a non-hygroscopic matrix water vapor condenses or freezes as soon the exhaust air stream is cooled down to the dewpoint of the air water mixture, as shown in Figure 6.2.

---

Chapter 7

**Conclusions and Recommendations**

---

### 7.1 CONCLUSIONS

The objective of this study was to develop a computational simple model of a solid desiccant air-to-air enthalpy exchanger. Partial differential equations in two spatial domains are required to describe the combined heat and mass transfer in the thermodynamic system air-water-desiccant. These coupled equations must be solved numerically. The finite difference method MOSHMX was available to the author and extensively used to predict the outlet states for a set of given inlet conditions and system parameters.

The theory of equilibrium exchange systems was used to show the operating conditions where enthalpy exchange between the two flow streams can be accomplished. The hyperbolic differential equations can be transformed to a set of uncoupled kinematic wave equations. To achieve optimum enthalpy exchange between the two air streams, the regenerator must be operated at conditions such that neither of the two transfer waves reaches the outlet of the regenerator. Comparison with the numerical solution of the coupled set of equations and finite transfer coefficients shows that the product of two non-dimensional parameters,  $\bar{\gamma}_1 \Gamma$ , must be greater than 1.5 in order to operate the enthalpy exchanger at a point where the enthalpy exchange

effectiveness is determined only by the number of transfer units and the Lewis number. Since the value of the combined capacitance ratio is fixed by thermodynamics of the air-water vapor-solid desiccant system, the parameter  $\Gamma$  must be computed such that the degree of enthalpy exchange is maximized.  $\Gamma$  increases as the rotation speed of the enthalpy exchanger increases.

The case of infinite rotation speed was investigated. The outlet states can be computed using the counterflow direct type heat exchanger  $\epsilon$ -NTU correlations. It was found that these correlations are accurate enough at operating conditions where enthalpy exchange occurs. The errors in the predicted outlet states were less than 0.5 °C and 0.5 gW/kgDA, compared to the finite difference solution. Therefore, the counterflow heat exchanger correlations can be used to compute the outlet states of a well designed enthalpy exchanger. The predicted outlet states lie, in the case of unity Lewis number, on a straight line connecting the outlet states.

A wide range of system parameters was investigated. If the line connecting the two inlet states does not intersect the saturation line in a psychrometric chart the matrix parameters are not important since reduced adsorptive capabilities of the matrix can be eliminated by rotating the enthalpy exchanger faster. The degree of performance in terms of enthalpy effectiveness is determined by the number of transfer units for heat transfer and the Lewis number.

The use of the counterflow heat exchanger correlations is based on the uncoupling of the transfer rate equations. The linear analogy method introduces new states properties in order to uncouple the thermodynamic equilibrium relationships. The analogy method shows an increasing error in the predicted outlet states if the Lewis number increases whereas using the counterflow  $\epsilon$ -NTU correlations maintains the

same accuracy for high Lewis numbers. It is believed that the solid desiccant particles show a solid side resistance to water vapor diffusion which results in Lewis numbers greater than one.

Since enthalpy exchangers transfer water vapor in adsorbed phase, they are less susceptible to freezing than sensible heat exchangers in energy recovery applications in cold winter climates. The line between the inlet states intersects the saturation line if the exhaust air is within the thermal comfort range (25 °C, 0.010 kgW/kgDA) and the supply air stream is very cold and dry in terms of absolute humidity ratio (-20 °C, 0.0006 kgW/kgDA). The finite difference solution was modified in order to investigate the behavior of enthalpy exchangers at very cold outdoor conditions. It was found that the enthalpy exchanger performance at extreme conditions depends on the solid desiccant characteristics. The maximum water content of the matrix was not important in cases where condensation or freezing does not occur. In winter applications, however, a silica gel enthalpy exchanger performs better than a regenerator carrying a molecular sieve or an adsorbent with the unfavorable Type 3 isotherm.

## 7.2 UNRESOLVED ISSUES

In this study, carry-over of air to the other period was neglected which might be important for enthalpy exchangers rotating at high speed. The same holds for leakage through the sealing strips attached on the regenerator wheel. Modeling of these effects would help to establish upper limits for the rotation speed since carry-over losses might become too large at higher rotation speeds.

The effect of non-uniform matrix characteristics and the variation of the

convective transfer coefficients could have significant effect of the performance characteristics of an enthalpy exchanger. Experimental studies are necessary in order to get reliable values for the effective desiccant mass, the effective heat capacity of the matrix and the lumped film transfer coefficients. Parameters estimation has been done so far only for regenerative heat and mass exchangers operating as regenerative dehumidifiers.

Adsorption isotherm data is available for a variety of solid desiccants at moderate and high temperature whereas no data was available for this study at very low temperatures. Single blow measurements at extreme conditions would help to validate the results obtained in this study that hygroscopic enthalpy exchangers are less susceptible to freezing than sensible heat exchangers.

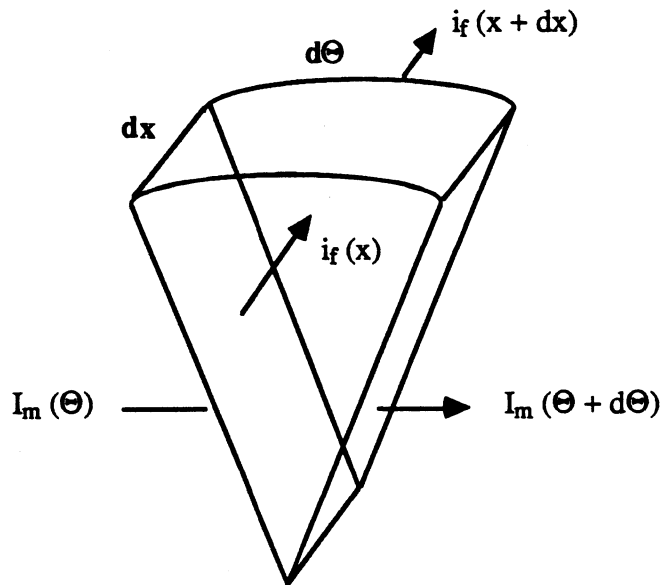
---

Appendix A

**Derivation of the Energy Balance**

---

The matrix is considered to be a homogeneous porous solid with the axial flow length  $L$  and the time  $T$  is required for one complete rotation. The energy balance is derived using the following control element:



Energy Conservation

$$\Delta M_m I_m(\Theta + d\Theta) = \Delta M_m I_m(\Theta) + \Delta \dot{m}_{fj} i_f(x) d\Theta - \Delta \dot{m}_{fj} i_f(x + dx) d\Theta \quad (A.1)$$

where

$\Delta M_m$  = mass of the control element [kg]

$\Delta \dot{m}_{fj}$  = flow rate through the control element [ kgDA/s ]

First Order Taylor Series

$$I_m(\Theta + d\Theta) = I_m(\Theta) + \frac{\partial I_m}{\partial \Theta} d\Theta \quad (\text{A.2})$$

$$i_f(x + dx) = i_f(x) + \frac{\partial i_f}{\partial x} dx \quad (\text{A.3})$$

Substitution into (A.1)

$$\Delta \dot{m}_{fj} \frac{\partial i_f}{\partial x} dx + \Delta M_m \frac{\partial I_m}{\partial \Theta} = 0 \quad (\text{A.4})$$

Geometric Considerations

$$\Delta M_m = M_m \frac{dx}{L} \frac{d\Theta}{T} \quad (\text{A.5})$$

$$\Delta \dot{m}_{fj} = \dot{m}_{fj} \frac{d\Theta}{T\beta_j} \quad (\text{A.6})$$

Substitution into (A.4)

$$L \frac{\partial i_f}{\partial x} + \beta_j \frac{M_m}{\dot{m}_{fj}} \frac{\partial I_m}{\partial \Theta} = 0 \quad (\text{A.7})$$

Dimensionless Coordinates

$$z = \frac{x}{L} \quad \Phi = \frac{\Theta}{T}$$

Energy Balance in Dimensionless Coordinates

$$\frac{\partial i_f}{\partial z} + \beta_j \frac{M_m}{\dot{m}_{fj} T} \frac{\partial I_m}{\partial \Phi} = 0$$

$$\frac{\partial i_f}{\partial z} + \beta_j \Gamma_j \frac{\partial I_m}{\partial \Phi} = 0 \quad (\text{A.8})$$

**Equation (A.8) is the same as Equation (2.1)**

Energy Transfer Rate

$$\Delta \dot{m}_{fj} \frac{\partial i_f}{\partial x} dx = \Delta A_j h_{tj} (t_m - t_f) \quad (\text{A.9})$$

where

$\Delta A_j$  = transfer area of the control element

### Geometric Considerations

$$\Delta A_j = \frac{\Delta \dot{m}_{fj}}{\dot{m}_{fj}} \frac{dx}{L} A_j$$

Substitution into (A.9)

$$\dot{m}_{fj} L \frac{\partial i_f}{\partial x} = A_j h_{tj} (t_m - t_f) \quad (\text{A.10})$$

### Energy Transfer Rate in Dimensionless Coordinates

$$\frac{\partial i_f}{\partial z} = c_A \frac{A_j h_{tj}}{\dot{m}_{fj} c_A} (t_m - t_f)$$

$$\frac{\partial i_f}{\partial z} = c_A \text{NTU}_{tj} (t_m - t_f) \quad (\text{A.11})$$

Equation (A.11) is the same as Equation (2.2)

---

Appendix B

**Analysis of the Combined Potentials**

---

This appendix presents the proof that Equation (4.23) is *not* the total differential of the combined heat and mass transfer potentials.

Since the combined heat and mass transfer potentials are functions of the temperature and humidity ratio of air in equilibrium with the desiccant their total differential can be written as

$$dF_i = \left( \frac{\partial F_i}{\partial t_f} \right)_{w_f} dt_f + \left( \frac{\partial F_i}{\partial w_f} \right)_{t_f} dw_f \quad i = 1,2 \quad (4.22)$$

Assume that the differential expression in Equation (4.23) is the total differential:

$$dF_i = a_1 a_3 dt_f + (a_3 - a_5 \lambda_i) a_2 dw_f \quad i = 1,2 \quad (4.23)$$

Then the derivatives with respect to temperature and humidity can be written as<sup>1</sup>

$$\frac{\partial F_i}{\partial t} = a_1 a_3 \quad \text{and} \quad \frac{\partial F_i}{\partial w} = (a_3 - a_5 \lambda_i) a_2 \quad (B.1)$$

---

<sup>1</sup>The index "f" is omitted in this appendix as well as the specification of the variable which is kept constant in the expressions for the partial derivatives

A differential expression is a total differential if the following condition is satisfied [33]:

$$\frac{\partial^2 F_i}{\partial t \partial w} = \frac{\partial^2 F_i}{\partial w \partial t}$$

In this particular case this can be expressed as

$$\frac{\partial a_1 a_3}{\partial w} = \frac{\partial(a_3 - a_5 \lambda_i) a_2}{\partial t} \quad (\text{B.2})$$

**Left hand side**

$$\frac{\partial a_1 a_3}{\partial w} = a_1 \frac{\partial a_3}{\partial w} + a_3 \frac{\partial a_1}{\partial w}$$

Using the definition of  $a_1$ ,  $a_3$  and  $c_A$  this can be written as

$$\frac{\partial a_1 a_3}{\partial w} = c_{pw} \frac{\partial W_m}{\partial t} + c_A \frac{\partial^2 W_m}{\partial t \partial w}$$

**Right hand side**

$$\frac{\partial(a_3 - a_5 \lambda_i) a_2}{\partial t} = \frac{\partial a_2 a_3}{\partial t} - \frac{\partial a_2 a_5 \lambda_i}{\partial t} \quad i = 1,2$$

Using the definition of  $a_2$ ,  $a_3$  and  $a_5$  this can be written as

$$\frac{\partial(a_3 - a_5 \lambda_i) a_2}{\partial t} = \frac{\partial c_A}{\partial t} \frac{\partial W_m}{\partial w} + c_A \frac{\partial^2 W_m}{\partial w \partial t} - \frac{\partial a_2 a_5 \lambda_i}{\partial t} \quad i = 1,2$$

After substitution into Equation (B.2) the second derivatives of the matrix water content cancel out since it is a state property and the second derivatives are independent of the order of differentiation:

$$c_{pw} \frac{\partial W_m}{\partial t} = \frac{\partial c_A}{\partial t} \frac{\partial W_m}{\partial w} - \frac{\partial a_2 a_5 \lambda_i}{\partial t} \quad i = 1,2 \quad (\text{B.3})$$

The left hand side of Equation (B.3) is independent of  $\lambda_i$  whereas the right hand side contains a term depending on the dimensionless wave speed. Equation (B.2) can only be satisfied if

$$\frac{\partial a_2 a_5 \lambda_1}{\partial t} = \frac{\partial a_2 a_5 \lambda_2}{\partial t} \quad (\text{B.4})$$

If the two dimensionless wave speeds would be equal Equation (B.2) is satisfied and Equation (4.23) would be the total differential of the F-potentials.  $\lambda_1$  and  $\lambda_2$ , however, are the solutions of the quadratic expression in equation (4.20) which can be written as

$$\lambda_{1,2} = \frac{-(a_1 a_4 - a_2 a_3 - a_5) \pm \sqrt{(a_1 a_4 - a_2 a_3 - a_5)^2 - 4 a_2 a_3 a_5}}{2 a_2 a_5}$$

and

$$a_2 a_5 \lambda_i = \frac{-(a_1 a_4 - a_2 a_3 - a_5) \pm \sqrt{(a_1 a_4 - a_2 a_3 - a_5)^2 - 4 a_2 a_3 a_5}}{2}$$

Using the chain rule the derivatives in Equation (B.4) can be written as

$$\begin{aligned} \frac{\partial a_2 a_5 \lambda_i}{\partial t} &= -\frac{1}{2} \frac{\partial (a_1 a_4 - a_2 a_3 - a_5)}{\partial t} \\ &\pm \frac{(a_1 a_4 - a_2 a_3 - a_5) \frac{\partial (a_1 a_4 - a_2 a_3 - a_5)}{\partial t} - 2 \frac{\partial a_2 a_3 a_5}{\partial t}}{2 \sqrt{(a_1 a_4 - a_2 a_3 - a_5)^2 - 4 a_2 a_3 a_5}} \end{aligned} \quad (\text{B.5})$$

In this expression the minus sign is for  $\lambda_1$  and the plus sign for  $\lambda_2$ . To satisfy Equation (B.2) the right hand side of Equation (B.5) must be the same for both dimensionless wave speeds. This can be true only if the numerator of the second term is equal to zero. After using the product rule the numerator can be written as

$$\begin{aligned} &\frac{\partial a_1}{\partial t} (a_1 a_4^2 - a_2 a_3 a_4 - a_4 a_5) \\ &+ \frac{\partial a_2}{\partial t} (a_2 a_3^2 - a_1 a_3 a_4 + a_3 a_5 - 2 a_3 a_5) \\ &+ \frac{\partial a_3}{\partial t} (a_3 a_2^2 - a_1 a_2 a_4 + a_2 a_5 - 2 a_2 a_5) \\ &+ \frac{\partial a_4}{\partial t} (a_4 a_1^2 - a_1 a_2 a_3 - a_1 a_5) \end{aligned}$$

$$+ \frac{\partial a_5}{\partial t} (a_5 - a_1 a_4 + a_2 a_3 - 2 a_2 a_3) \neq 0 \quad (\text{B.6})$$

Since the left hand side of Equation (B.6) is not equal zero Equations (B.2)-(B.4) are not satisfied and therefore Equation (4.23) is not the total differential of the combined heat and mass transfer potentials.

The whole procedure can be done using Equation (4.24) with the integrating factor instead of Equation (4.23):

$$dF_i = G(t_f, w_f) a_1 a_3 dt_f + G(t_f, w_f) (a_3 - a_5 \lambda_i) a_2 dw_f \quad i = 1, 2 \quad (4.24)$$

Using the procedure described above the integrating factor  $G$  can be determined as a function of the temperature and humidity such that Equation (B.2) is satisfied. Then Equation (4.24) is the total differential of the combined heat and mass transfer potentials and the integration is independent of the path, i.e., values of the  $F$ -potentials can be computed if a reference state is defined.

---

## Bibliography

---

1. Treybal, R. E., *Mass Transfer Operations*, Mc Graw Hill, Third Edition, New York, 1980
2. Kays, W. M. and London, A. L., *Compact Heat Exchangers*, Mc Graw Hill, Third Edition, New York, 1984
3. Nußelt, W., "Der Beharrungszustand im Winderhitzer", *VDI-Z*, Vol. 72, 1928
4. Hausen, H., *Wärmeübertragung im Gegenstrom, Gleichstrom und Kreuzstrom*, Springer Verlag, 1. Auflage, Berlin, 1950
5. Mondt, J. R., "Vehicular Gas Turbine Periodic Flow Heat Exchanger Solid and Fluid Temperature Distributions", *ASME Transactions*, Vol. 80, 1964
6. Lightfoot, E. N., Sanchez Palma, R. J. and Edwards, D. O., "Chromatography and Allied Fixed Bed Separation Processes", *New Chemical Separation Techniques*, Interscience, New York, 1962
7. Mitchell, J W., *Energy Engineering*, John Wiley and Sons, First Edition, New York, 1983
8. Stoecker, W. F. and Jones, J. W., *Refrigeration and Air Conditioning*, Mc Graw Hill, Second Edition, New York 1982
9. Jurinak, J. J., "Open Cycle Desiccant Cooling - Component Models and System Simulations", Ph.D. Thesis in Mechanical Engineering, University of Wisconsin-Madison, 1982

10. Duffie, J. A. and Beckman, W. A., *Solar Engineering of Thermal Processes*, John Wiley and Sons, Second Edition, New York, 1980
11. Schultz, K.J. and Mitchell, J.W., "Experimental Analysis of a Rotary Silica Gel Dehumidifier", ASME Winter Annual Meeting of Combined Heat and Mass Transfer in Porous Media, 1987
12. Dunkle, R. V., "A Method of Solar Air Conditioning", Mechanical and Chemical Engineering Transactions, *Institution of Engineers*, Australia, MC 1, 73, 1965
13. Maclaine-cross, I. L., "A Theory of Combined Heat and Mass Transfer in Regenerators", Ph.D. Thesis in Mechanical Engineering, Monash University, Australia, 1974
14. Van den Bulck, E., Mitchell, J. W. and Klein, S. A., "Design Theory for Rotary Heat and Mass Exchangers - I. Wave Analysis of Rotary Heat and Mass Exchangers with Infinite Transfer Coefficients", *Int. J. Heat Mass Transfer*, Vol. 28, 1985
15. Van den Bulck, E., Mitchell, J. W. and Klein, S. A., "Design Theory for Rotary Heat and Mass Exchangers - II. Effectiveness-Number of Transfer Units Method for Rotary Heat and Mass Exchangers", *Int. J. Heat Mass Transfer*, Vol. 28, 1985
16. Holmberg, R. B., "Combined Heat and Mass Transfer In Regenerators with Hygroscopic Materials", *Journal of Heat Transfer, ASME Transactions*, Vol 101, 1979
17. Van Leersum, J. G., "Heat and Mass Transfer in Regenerators", Ph.D. Thesis in Mechanical Engineering, Monash University, Australia, 1975
18. Van Leersum, J. G. and Banks, P. J., "Equilibrium Heat and Mass Transfer in Regenerators in which Condensation Occurs", *Int. J. Heat Mass Transfer*, Vol. 20, 1977

19. Van Leersum, J. G., "Condensation in Regenerators Operating at High Temperatures", *Mechanical Engineering Transactions, Institution of Engineers, Australia*, ME 11, 3, 1986
20. Schultz, J. K., "Rotary Solid Desiccant Dehumidifiers - Analysis of Models and Experimental Investigation", Ph.D. Thesis in Mechanical Engineering, University of Wisconsin-Madison, 1987
21. Brandemuehl, M. J., "Analysis of Heat and Mass Regenerators with Time Varying or Spatially Nonuniform Inlet Conditions", Ph.D. Thesis in Mechanical Engineering, University of Wisconsin-Madison, 1982
22. Hausen, H., "Vervollständigte Berechnung des Wärmeaustausches in Regeneratoren", *VDI-Z Beiheft Verfahrenstechnik*, 1942
23. Verein Deutscher Ingenieure, *VDI Wärmeatlas*, VDI Verlag GmbH, 2. Auflage, Düsseldorf, 1974
24. Lambertson, T. J., "Performance Factors of a Periodic Flow Heat Exchanger", *ASME Transactions*, Vol. 80, 1958
25. Bahnke, G. D. and Howard, C. P., "The Effect of Logitudinal Heat Conduction on Periodic Flow Heat Exchanger Performance", *ASME Transactions*, Vol. 86, 1964
26. Jeffreson, C. P., "Prediction of Breakthrough Curves in Packed Beds -I. Applicability of Single Parameter Models", *AIChE Journal*, Vol. 18, 1972
27. ASHRAE, *Handbook of Fundamentals*, American Society of Heating, Refrigeration and Air Conditioning Engineers, New York, 1985
28. Ruthven, D. M., *Principles of Adsorption and Adsorption Processes*, John Wiley and Sons, First Edition, New York, 1984

29. Van den Bulck, E., "Convective Heat and Mass Transfer in Compact Regenerative Dehumidifiers", Ph.D. Thesis in Mechanical Engineering, University of Wisconsin-Madison, 1987
30. Van den Bulck, E., "Analysis of Solid Desiccant Rotary Dehumidifier", M.S. Thesis in Mechanical Engineering, University of Wisconsin, 1983
31. Bronstein, I. N. and Semendjajew K. A., *Taschenbuch der Mathematik*, Harri Deutsch Verlag, 21. Auflage, 1979
32. Banks, J. P., "Coupled Equilibrium Heat Exchange and Single Adsorbate Transfer in Fluid Flow through a Porous Medium - I. Characteristic Potentials and Specific Capacity Ratios", *Chemical Engineering Science*, Vol 27, 1972
33. Schmidt, E., Stephan, K. und Mayinger, F., *Technische Thermodynamik - Einstoffsysteme*, Springer Verlag, 11. Auflage, Berlin, 1975
34. Bird, R. B., Stewart, W. E. and Lightfoot, E. N., *Transport Phenomena*, John Wiley and Sons, First Edition, First Edition, New York, 1960
35. Stewart, W. E., "Documentation of the Software Package DDASAC", Department of Chemical Engineering, University of Wisconsin-Madison, 1986
36. Caracotsios, M. and Stewart, W. E., "Sensitivity Analysis of Initial Value Problems with Mixed Ordinary Differential and Algebraic Equations", *Computers and Chemical Engineering*, Vol. 9, 4, 1985
37. Bowlen, K. L., "Energy Recovery from Exhaust Air for Year Around Environmental Control"
38. Maclaine-cross, I. L., Oral Communication at the University of Wisconsin Solar Energy Laboratory, June 1988
39. Iler, R. I., *The Chemistry of Silica*, John Wiley and Sons, First Edition, New York, 1979